EASTLAND PORT MAINTENANCE DREDGING AND DISPOSAL PROJECT

Disposal Plume Modelling

Report prepared for Eastland Port

April 2018

MetOcean SOLUTIONS

MetOcean Solutions Ltd: Report P0331-07

April 2018

Report status

Version	Date	Status	Approved by
RevA	07/04/2018	Draft for internal review	Weppe
RevB	10/04/2018	Draft for client review	Beamsley

It is the responsibility of the reader to verify the currency of the version number of this report.

PO Box 441, New Plymouth, New Zealand
T: 64-6-7585035 E: enquiries@metocean.co.nz
www.metocean.co.nz

TABLE OF CONTENTS

LIST OF FIGURES

LIST OF TABLES

1. INTRODUCTION

Eastland Port Ltd are seeking to renew their maintenance dredging and disposal consents at the Port of Gisborne.

Currently, dredged sediment is disposed at an offshore disposal site situated in approximately 18 – 20 m water depth (**Error! Reference source not found.**), with an average annual rate of approximately 73,000 m^3 based on estimates obtained between 2002 and 2019 by Eastland Port.

Maintenance dredging is expected to occur using the Trailing Suction Hopper Dredge (TSHD) “Pukunui” although, if there are significant inflows of sediment due to large storm events, a higher productivity Trailing Suction Hopper Dredge (TSHD) may be required to ensure the required port and channel depths can be maintained. It is likely that some maintenance dredging may also be undertaken using a Backhoe Dredger (BHD) or Cutter Suction Dredger (CSD).

MetOcean Solutions (MOS) has been contracted to provide coastal oceanographic expertise to investigate both physical and morphological effects and associated sediment transport patterns resulting from the dredging and disposal of maintenance dredging material at the current disposal site.

A previous report (MetOcean Solutions, 2017) presented the implementation and validation of the Poverty Bay hydrodynamic modelling at regional and local scales.

This report focuses on the characterisation of the disposal plumes and deposition patterns expected during the disposal operations. Sediment plume dispersal and settling was simulated using a particle-tracking modelling over two different 1-year periods with climatically contrasting historical contexts, namely El Niño/La Niña periods. The applied methodology is provided in Section 2, including a description of the particle-tracking model, sediment distribution and disposal scenarios. Model results are presented and interpreted in Section 3 and a brief summary is provided in Section 4. All references cited within the report a listed in Section 5.

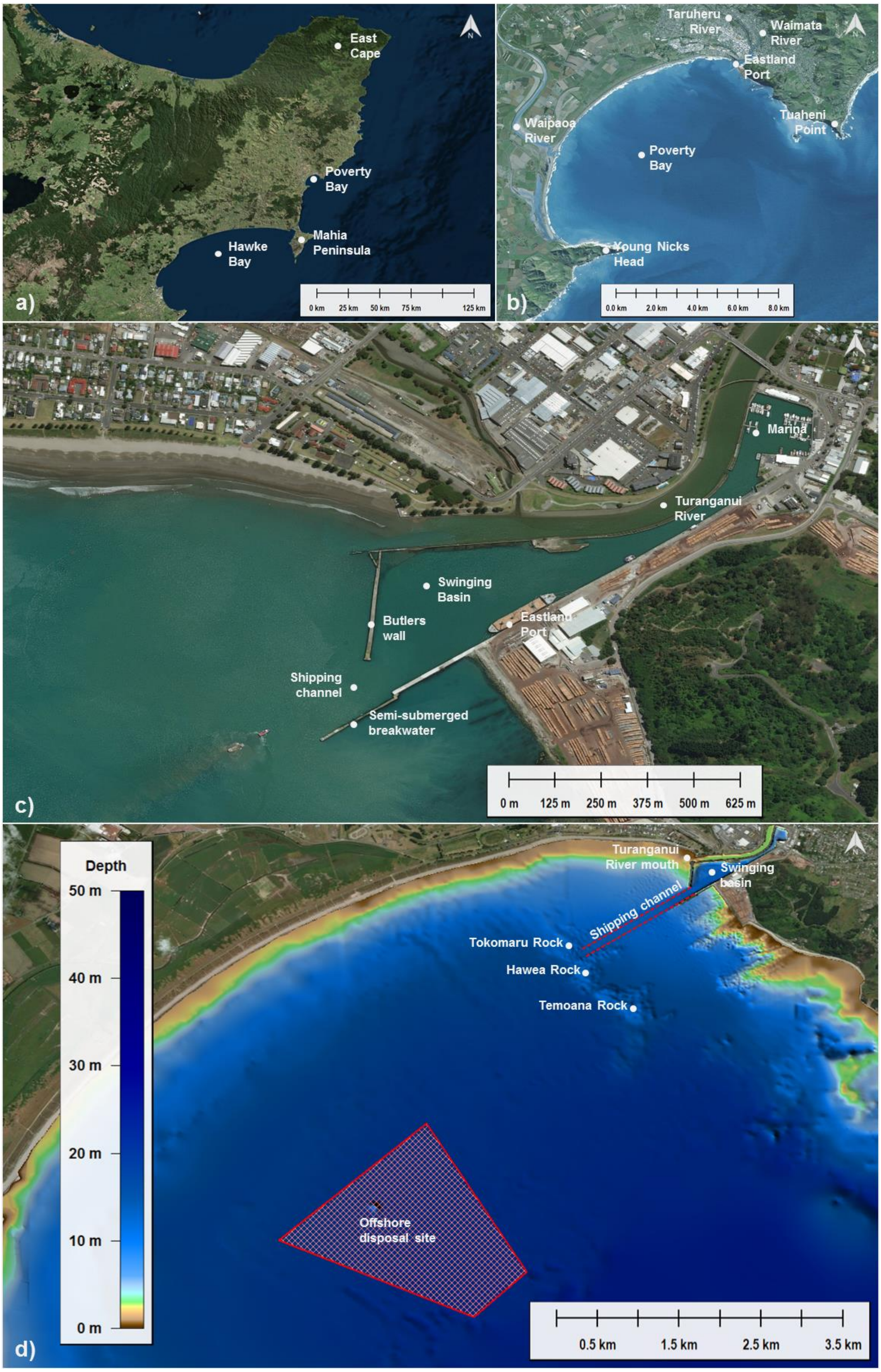

Figure 1.1 Maps showing the location of Poverty Bay (a and b), and Eastland Port (c) with the locations used in the present study. Both offshore disposal and shipping channel are indicated on top of the bathymetry in (d).

2. METHODS

2.1. Approach

An actual release of sediment in the oceanic environment is a process that is finite in time (i.e. occurring at a specific time, over a finite period) and inherently non-deterministic (i.e. controlled by a range of random and unpredictable variables such as currents and turbulences). Since future ocean conditions and exact timing of the disposals are unknown, it is not possible to predict the actual outcomes of a release before the event occurs. However, the probability of future oceanic conditions can be assessed from the historical conditions, thereby allowing “probabilistic” estimations of the geographical dispersion of the suspended sediment plume and deposition patterns.

In the present study, disposal operations were simulated during two 1-year periods with contrasting ambient forcing regimes of La Niña and El Niño (June 1998-June 1999, and June 2002-June 2003, respectively). These long-term simulation allows capturing the variability of current forcing expected on an annual timescale and provide a robust basis to derive probabilistic patterns of dispersions. Annual simulation datasets also form a valuable basis to evaluate statistical characteristics (i.e. mean, extreme, and exceedance) of the suspended sediment concentration plume (*SSC plume* hereafter*)* and deposition footprints.

2.2. Hydrodynamics

The particle-tracking simulations reproducing the disposal operations were undertaken using a 3D hydrodynamic hindcast simulated with the unstructured-grid finite-element SCHISM model[1][2].

SCHISM is a prognostic finite-element unstructured-grid model designed to simulate 3D baroclinic, 3D barotropic or 2D barotropic circulation. The barotropic mode equations employ a semi-implicit finite-element Eulerian-Lagrangian algorithm to solve the shallow-water equations, forced by relevant physical processes (atmospheric, oceanic and fluvial forcing). A detailed description of the SCHISM model formulation, governing equations and numerics, can be found in Zhang and Baptista (2008).

In the present implementation, SCHISM was run in 3D mode using a combination with a vertical discretization using *Localized Sigma Coordinate system with Shaved Cell* (LSC2) which is a type of terrain-following layer vertical grid structure as described in Zhang et al. (2015). The number of vertical layers ranged from 4 in shallow waters to 12 in deep waters near the open boundary. In the horizontal diamension, the finite-element triangular grid structure used by SCHISM has many advantages over the regular or curvilinear grid structure with respect to the representation of complex shoreline and bathymetric features (port channel and structures, reefs and shoals). Here, the horizontal resolution ranged from 150 m at the offshore boundary to 5 m in shallow water. The model domain was also refined around key features, including within Eastland Port, along the shipping channel, within the associated river systems and in areas with complex topography (i.e. Tokomaru, Hawea and Temoana Rocks and the rocky reef shore line). The

[1] http://ccrm.vims.edu/schism/
[2] http://www.ccrm.vims.edu/w/index.php/Main_Page#SCHISM_WIKI

triangular elements of the model domain meshes are shown in Figure 2.1 and associated bathymetries are presented in Figure 2.2.

This high-resolution SCHISM 3D model was nested within a downscaled 3D hydrodynamic hindcast of the wider Poverty Bay region simulated using the Regional Ocean Modelling System (ROMS). This *parent* Poverty Bay ROMS model provided 3D initial and boundary conditions to the SCHISM domain over the two annual periods considered El Niño (2002-2003) and La Niña (1998-1999) periods.

The full details and validation of the 3D ROMS hindcast and downscaling approach from a New Zealand wide domain (resolution 8km) to the Poverty Bay domain (resolution 150m), and the calibration/validation of the SCHISM model are provided in the report MetOcean Solutions (2017).

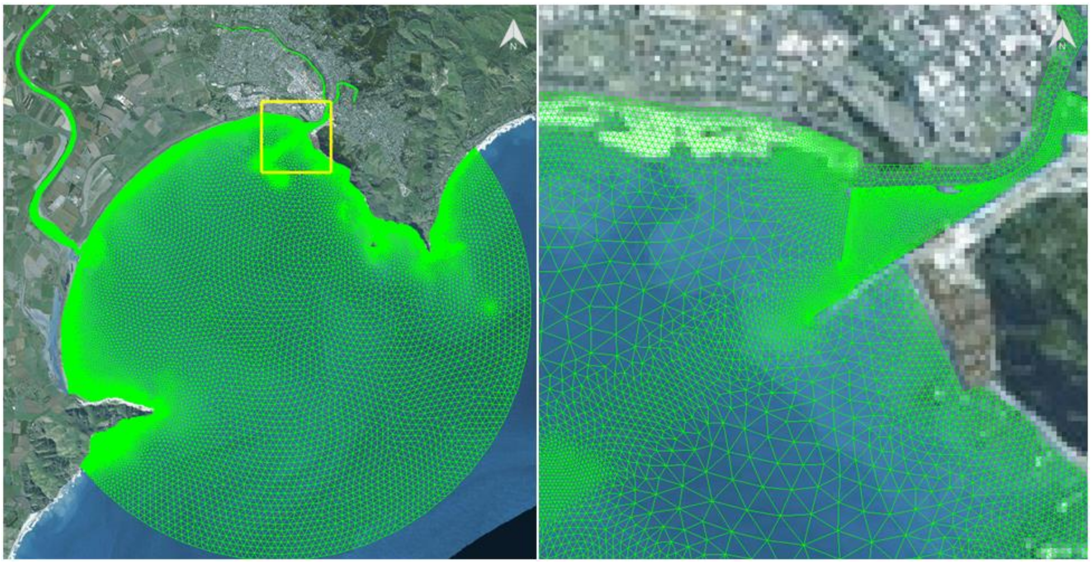

Figure 2.1 Unstructured mesh-grid used in SCHISM to simulate the hydrodynamics over Poverty Bay (left) and Eastland Port (right).

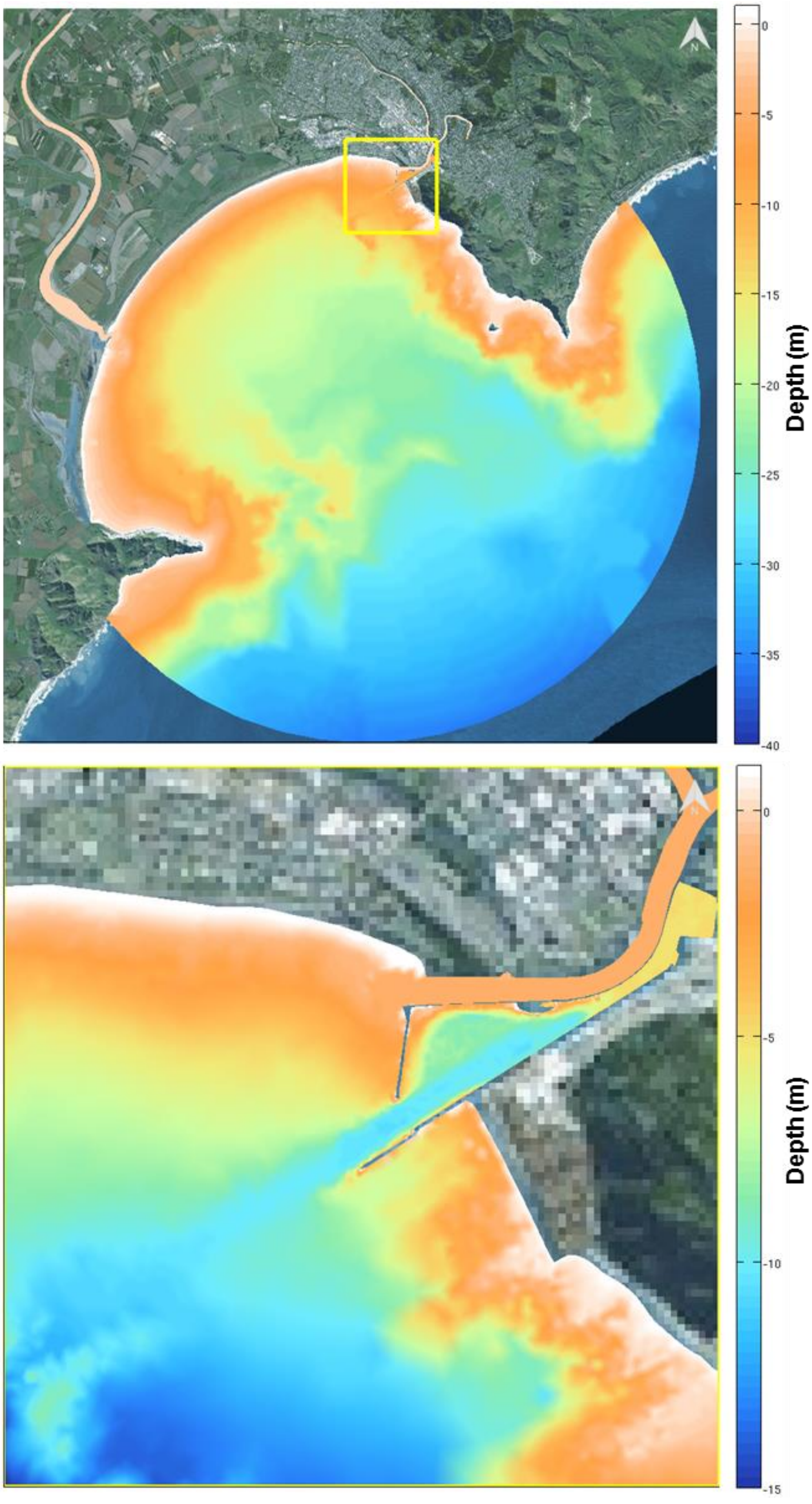

Figure 2.2 Model bathymetries (below mean sea level) over Poverty Bay (left) and Eastland Port (right).

2.3. Trajectory modelling

2.3.1. Particle-tracking model

A Lagrangian model developed by MOS was used to simulate the trajectories of particles released at the disposal site. Here, the particles represent the sediment discharged from the disposal vessel.

The model consists of a trajectory scheme applied to the 3D Eulerian current field $(\tilde{u}, \tilde{v})$, solving the motion of discrete particles.

$$\frac{dx_p}{dt} = \tilde{u}(x, y, z, t) + u_t$$
$$\frac{dy_p}{dt} = \tilde{v}(x, y, z, t) + v_t \qquad (2.1\ a,b,c)$$
$$\frac{dz_p}{dt} = -w_s + w_t$$

where (x_p,y_p,z_p) are the particle coordinates,. (u_t,v_t,w_t) are the diffusion components representing turbulent motions and w_s is the particle settling velocity.

In the horizontal plane, the model uses an Ordinary Differential Equations (ODE) solver, including a 4th order Runge-Kutta method, to calculate the trajectory of a given particle (x_p,y_p) in the time-varying current field.

In the vertical plane, particle motion is controlled by the specified settling velocity w_s, as well as the vertical diffusion component w_t as defined in equation 2.1c.

Horizontal and vertical diffusion motions are treated with the following equation, shown here for the u_t component:

$$\int_t^{t+\Delta t} u_t . dt = \sqrt{6. k_{u,v} . \Delta t} \ . \theta(-1,1) \qquad (2.2)$$

where $\theta(-1,1)$ is a random number from a uniform distribution between -1 and 1, Δt is the time-step of the model in seconds and $k_{u,v}$ is the horizontal eddy diffusivity coefficient in $m^2.s^{-1}$. The same equation is used for the vertical diffusion.

In the absence of specific field data on diffusive processes, the determination of the eddy diffusivity coefficient $k_{u,v}$ is generally based on guidance from empirical relationships. Several relationships are summarised in Fischer et al., 1979 including that of Elder (1956) for simple unidirectional shear flows that estimates the longitudinal diffusion coefficient as a function of the water depth and current velocity of the form.

$$k_{u,v} = 5.93.H.u^* \qquad (2.3)$$

where H and u^* are the water depth and friction velocity respectively.

Transverse mixing can be estimated using a relationship of the same form but with a reduced proportionality factor (with 50% error bound).

$$k_{transverse} \sim 0.6.H.u^* \qquad (2.4)$$

The vertical eddy diffusivity is generally expected to be at least one order or magnitude smaller. Elder's formula suggests a vertically averaged value of:

$$k_{vertical} \sim 0.067 .H.u^{*} \tag{2.5}$$

Here, both depth and mean current velocities vary throughout the region of interest but these equations can still be used to provide a bracketing of reasonable eddy diffusivity coefficient values for the present application.

Assuming generic water depths of order 20.0 metres in the disposal ground region and mean current velocities of ~0.05-0.1 $m.s^{-1}$ as experienced in the disposal ground region, the above equations yield average horizontal coefficients (i.e. average of longitudinal and transverse results) in the range 0.15-0.3 $m^2.s^{-1}$.

Furthermore, in numerical models, the role of the horizontal diffusion coefficient is also to implicitly account for sub-grid scale turbulent processes such as eddies that are not explicitly resolved in the model due to the grid resolution. This means that horizontal diffusion must generally increase as grid size increases since eddies of increasing scale are not represented. Conversely, the reduction of grid size allows explicit resolution of flow patterns and eddies at finer scales, which thereby reduces the required amount of added diffusion.

For dispersion at oceanic scales, Okubo, A., (1971) notably showed that $k_{u,v}$ varies approximately (with wide scatter) as :

$$k_{u,v} = \alpha.L^{4/3} \tag{2.6}$$

where *L* is the horizontal scale of the mixing phenomena and α is an empirical proportionality factor.

The model mesh has fine spatial resolution ranging from ~15-150 m throughout the bay which yields horizontal diffusivities of order 0.01-0.22 $m^2.s^{-1}$.

As a compromise, a generic value of 0.2 $m^2.s^{-1}$ was eventually chosen for the horizontal eddy diffusivity. The vertical eddy diffusivity is expected to be significantly smaller than the horizontal magnitude; it was set to a small generic value of 0.0002 $m^2.s^{-1}$ to ensure that the vertical settling of disposed sediment was not overly altered by the vertical diffusion.

Finally, in the present model implementation, any particle reaching the shoreline or the seabed was removed (i.e. sticky boundaries).

2.3.2. Sediment distribution and settling velocity

The disposal simulations require the definition of a set representative sediment particle classes, which will settle at different velocities, representing the different fractions of the sediment material to be disposed.

Some information on the surficial sediment distribution within the port basin and outer bay are available in Beamsley (2003) and summarized in Table 2.1. These results shows the presence of both fine sand and finer cohesive sediments (i.e. d_{50}<63 µm), with varying distribution throughout the region.

Although general equations are available to compute the settling velocity of individual particles of given sizes (e.g. Stokes Law), it is unrealistic to assume that the sediment consists in single particles in the fine silt range (~63 μm or smaller) because of the cohesive nature of material and associated flocculation effects (i.e. formation of particle aggregates, e.g. Van Rijn, 2007).

In the absence of *in-situ* measurements of the settling of such flocculated cohesive sediment, a “cohesive sediment class” with generic settling rate of 1 $mm.s^{-1}$ was initially applied (Whitehouse R. et al., 2000), which is commonly used in the context of sediment disposal (e.g. Smith and Friedrichs, 2011) to represent the finest sediment grain size fraction. Simulations were then reproduced using a smaller settling rate of 0.1 $mm.s^{-1}$ to sensitivity test the effects of slower sediment settling on the resulting *SSC* plumes and deposition footprints.

The sandy fraction of the material to be disposed was represented using a “sand class” with a settling velocity of 8 $mm.s^{-1}$; equivalent to the theoretical settling velocity associated with the smallest sand median diameter of Table 2.2 (110 microns). Note the smallest sand diameter present was chosen for conservatism; some of the sandy material may indeed be coarser that this generic diameter and thus settle faster.

The relative distribution of cohesive versus sandy material is seen to significantly vary throughout the region of interest (see Table 2.1), from the channel basin (80%-20%) to the outside of the port (20%-80%). The fine cohesive sediment is the most challenging with respect to the produced sediment plumes since it remains longer in suspension in the water column. In that sense, for conservatism, it was primarily assumed the sediment content of the disposal vessel would include 80% fines and 20 % sand i.e. largest fraction of fines measured (see Table 2.2). The *SSC* plume and deposition associated with the disposal of a “sandy” hopper load (i.e. 80% sand and 20% silt) are also presented for comparison purposes (Table 2.3).

Representative sediment densities were defined following sediment sampling analysis by Beamsley (2003). Beamsley (2003) reports a sediment wet bulk density of 1892 $kg.m^{-3}$, with a moisture rate of 40 %, on the outer channel region (site SS) (Table 2.2). This yields a dry bulk density of ~1350 $kg.m^{-3}$. The inner basin region (site SB) includes a much larger fraction cohesive material and has a smaller wet bulk density of 1381 $kg.m^{-3}$, with a high moisture content of 110 %, yielding a dry bulk density of ~650 $kg.m^{-3}$.

Table 2.1 Surficial sediment distribution within the port basin and outer bay (Beamsley, 2003).

	Percentage	**Median diameter d_{50}**
Inner Basin	**[%]**	**[μm]**
sand	20%	180
silt	60%	20
clay	20%	2
Channel Entrance		
sand	80%	170
silt	10%	20
clay	10%	2
Outside of Port		
sand	70%	110
silt	20%	30
clay	10%	2

Table 2.2 Settling velocities, and relative distribution of the representative cohesive and sand sediment classes for a disposal load with a predominant silt fraction. A dry density of 650 $kg.m^{-3}$ was assumed based on samples in Beamsley (2003) (site SB).

	Settling velocity	**Percentage**
Sandy sediment class	8 $mm.s^{-1}$	20 %
Cohesive sediment class	[0.1 and 1] $mm.s^{-1}$	80 %

Table 2.3 Settling velocities, and relative distribution of the representative cohesive and sand sediment classes for a disposal load with a predominant sand fraction. A dry density of 1350 $kg.m^{-3}$ was assumed based on samples in Beamsley (2003) (site SS).

	Settling velocity	**Percentage**
Sandy sediment class	8 $mm.s^{-1}$	80 %
Cohesive sediment class	[0.1 and 1] $mm.s^{-1}$	20 %

2.3.3. Sediment disposal processes and source terms

The processes by which sediment is released and suspended in the water column during disposal operations are briefly outlined here in the context of the choice of the source term magnitudes and release depths for the particle tracking simulations.

In the case of silt to fine sand dredging, the content of loaded dredgers consists of a highly concentrated mixture of sediment and water and the bulk behaviour of that sediment mixture becomes dominant over the individual particle settling processes. When the dredge opens its bottom door for release the content will typically be released as a jet-like sediment flux quickly descending to the seabed. The behaviour of the released sediment can be separated in three main phases (Figure 2.3):

1) Convective descent,
2) Dynamic Collapse, and
3) Passive dispersion

During the convective descent, the dense sediment material quickly descends to the bottom. Ambient water can become entrained around the perimeter of the jet which can strip, or de-entrained, some sediment that eventually becomes suspended in the water column. The proportion lost is expected to be small, commonly cited as 1-5 % of the disposed load (Bokuniewicz, et al., 1978; Gordon, R., 1974; Truitt, C., 1988, USACE-EPA, 1998). That fraction was found to be slightly larger in some recent model simulations by Aarninkhof, S. and Luijendijk, A. (2009) which found that ~10% of the total load was entrained in the water column within the passive plume, while the 90% remaining formed a dynamic plume that settled quickly to the seabed. This slightly larger percentage is consistent with observations in Spearman et al. (2007) as well as the default range suggested for use with the TASS model (5-15%) HR Wallingford (2010), although these concern the overflow discharge rather than discrete full load release.

Following its descent, the dredge material collapses on impact with the seabed; this phase is known as the Dynamic Collapse phase. Note mid column collapse can occur in the specific case of a layer of density similar to that of the descending material but this is not expected in the present case given the limited water depths. The collapse results in a large fraction of the disposed sediment depositing on the seabed and is often coupled to the generation of the density current resulting from the excess energy available following collapsing, whereby a fraction of the disposed sediment is suspended and propagates radially from the point of impact. The density current is expected to be contained within the bottom 15-20% of the water column, with excursion length scales of order 100-500 m (e.g. Aarninkhof, S. and Luijendijk, A., 2009).

These two initial phases relating to the dissipation of the initial plume momentum are also referred to as dynamic plume stage (e.g. Spearman et al., 2007). The Passive dispersion phase relates to the subsequent dispersion of the sediment that became suspended in the water column during the dynamic phase, i.e. de-entrained during descent, and sediment suspension by the density current developing near the seabed by the ambient current.

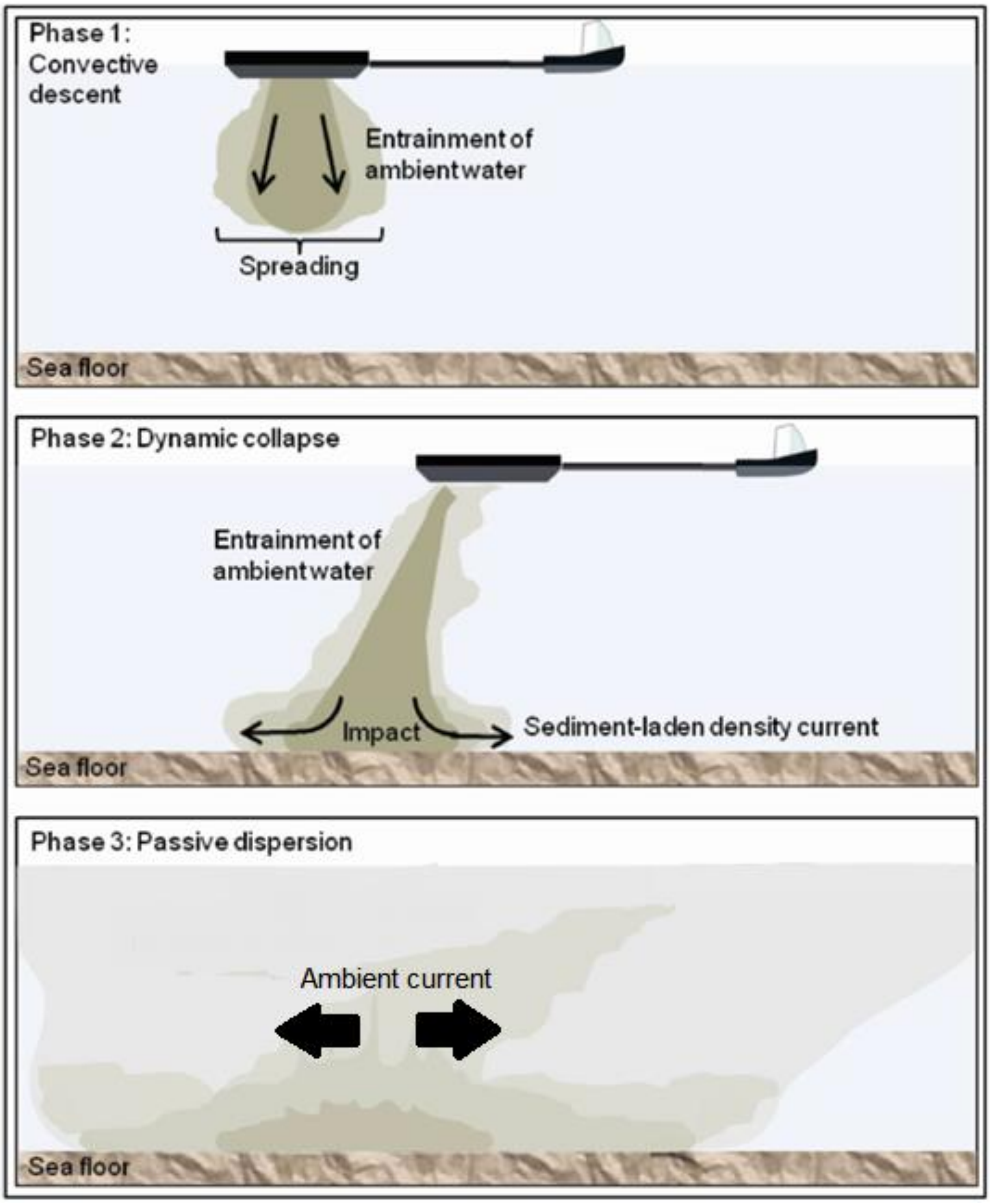

Figure 2.3 Three main phases occurring during the disposal of dredged material: 1) Convective descent, 2) Dynamic Collapse, and 3) Passive plume dispersion.

In the present study, the focus is on characterising the extents and concentrations of the suspended sediment plume resulting from this passive dispersion phase, as these plumes have the potential to effect order of magnitude greater spatial extents than the dynamic plume (which settles quickly). In that respect, the particle tracking simulations considered two main source terms:

1) De-entrained sediment during descent – release through the water column at the disposal location.

2) Density current at the bottom - release within a cylinder near the seabed of given height and radius.

The present simulations also considered an additional sediment source released at near-surface, representative of sediment which, in the unlikely event, is entrained vertically around the hull of the dredger due to turbulence associated with the discharge of sediment.

3) Surface sediment losses - release within the top layer of the water column (from the sea surface to bottom of vessel hull).

The amounts of sediment of each source terms above(i.e.1,2,3) were defined based on recommended ranges and past experiences for the Lyttelton Harbour channel deepening project(e.g. MetOcean Solutions Ltd., 2016); they are provided in Table 2.4.

The convective descent and dynamic collapse processes expected in the present case were evaluated using nearfield simulations under a range of generic ambient conditions. The nearfield modelling consisted in simulating the jet-like descent of the hopper content following disposal using the formulation of Lee. and Cheung, 1990) and subsequent density-current propagation using the model by Drapeau et al. (1992). The two models are coupled so that the final sediment plume momentum upon seabed impact is used to initialize the density current model. Simulations assumed simple case with homogeneous ambient current of varying magnitudes. Details of the Pukunui and Albatros TSHD vessel configuration and parameters used for the nearfield simulation are summarized in Table 2.5, Table 2.6 and Table 2.7, while images of the two TSHD are provided in Figure 2.4.

Predicted plume envelopes for increasing current velocity magnitudes (Figure 2.5) show relatively limited horizontal plume entrainment in the along-current direction of less than 10 m. This indicates the use of single point, with release distributed across the full water column, is reasonable for the source term representing the de-entrained sediment during descent (1).

The envelopes of the resulting density current (Figure 2.6) indicate that most of the sediment remaining in the plume at the seabed impact will settle within ~100 m of the impact point. Note the density current simulation stop when the plume density becomes equal to that of the ambient seawater, taken to be1027 kg.m^{-3}.

For conservatism, and to account for the possible (small) shift in point of impact relative to effective disposal position, it was decided to use a cylinder of 150 m radius, and 2 m height for the source term 2 (i.e. density current at the bottom).

Disposal operations were simulated at the 4 corners of the disposal ground, as well as at the centre in order to capture the flow variability through the region and evaluate outcomes with respect to the sediment plume and deposition. Release sites are shown in Figure 2.7.

Table 2.4 Proportion of total sediment hopper load attributed to each source terms.

Source Term	% of total sediment load	Release depth	Radius
A - Sediment de-entrained during descent	5	water column	point
B - Density current at the bottom	25	bottom 2m	150 m
C - Surface sediment losses	2	surface 2 m	point

Table 2.5 Pukunui Vessel details

Vessel	PUKUNUI
Draft - empty	1.2 m
Draft - full	2.4 m
Hopper Volume	480 m^3
Net Sediment content	220 m^3
Disposal cycle (average)	4 hours

Table 2.6 Albatros vessel details (as define from a daily record)

Vessel	ALBATROS
Draft - empty	3.5 m
Draft - full	3.8 m
Hopper Volume	1860 m^3
Net Sediment content (silty load)	690 m^3
Disposal cycle (average)	4 hours
Net Sediment content (sandy load)	982 m^3
Disposal cycle (average)	7 hours

Table 2.7 Parameters used for the simplified nearfield simulations

Parameter	**Unit**	**Value**	**Notes**
Ambient current	[m.s^{-1}]	[0:0.1:0.5 1 1.5]	
Sea Temperature	deg C	15	
Salinity	ppt	35	
Initial concentration	[-]	1	
Water Depth	[m]	20	
Release depth (above seabed)	[m]	18	
Opening diameter	[m]	7	
Opening area	[m^2]	38.8	Equivalent to Pukunui opening area
Flux	[m^3.sec^{-1}]	8	
in situ density of material (wet)	[kg.m^{-3}]	1892	
in situ density of material (dry)	[kg.m^{-3}]	1350	
Sea water density	[kg.m^{-3}]	1027	
Initial jet density	[kg.m^{-3}]	1423	
phi_jet	[deg]	-90	Angle between the x-axis and jet in the x-z plane (i.e. vertical plane)
theta_jet	[deg]	0	Angle between the x-axis and jet in the x-y plane (i.e. horizontal plane)
tau_crit	[N.m^{-2}]	0.15	Critical shear stress for sediment erosion
ws	[m.s^{-1}]	0.001	Sediment settling velocity

Figure 2.4 Images of the Pukunui (top) and Albatros TSHD (bottom).

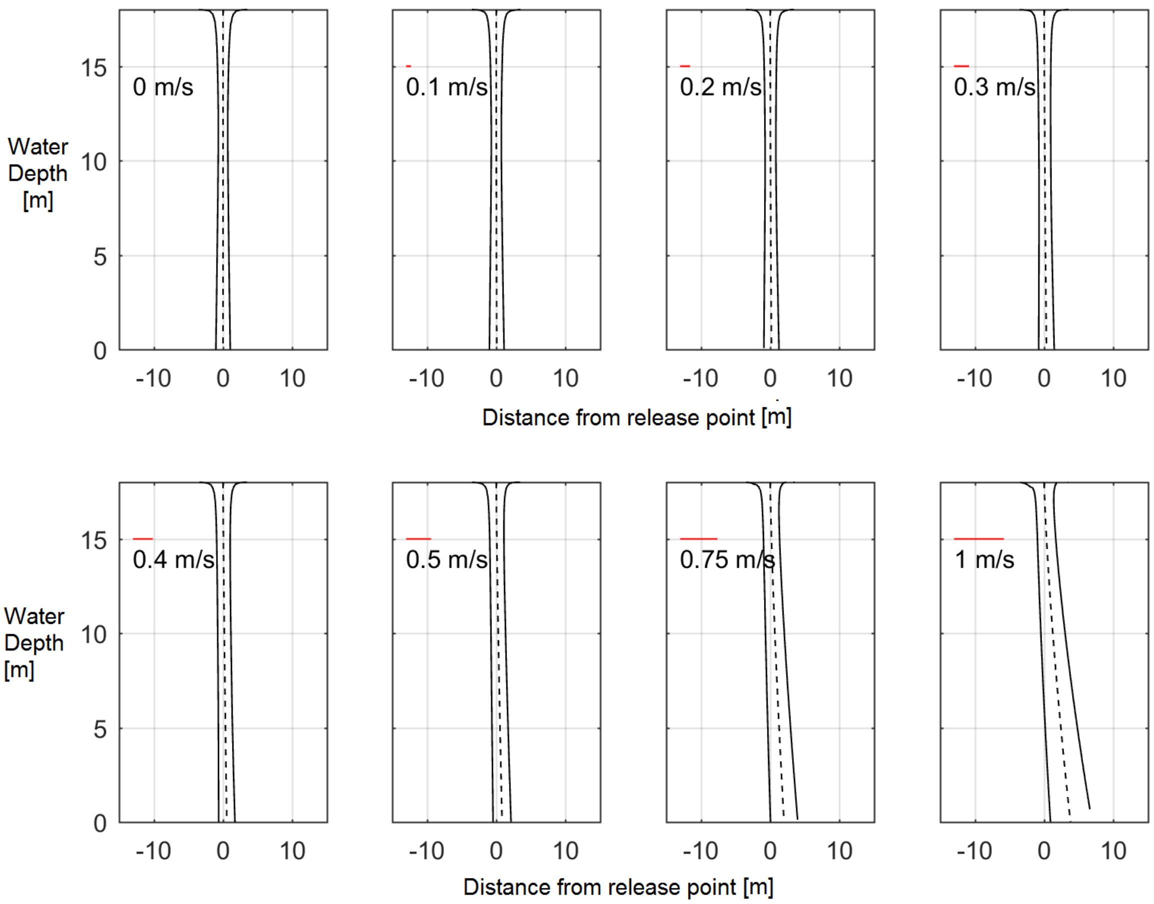

Figure 2.5 Vertical view of plume descent for different cross-current magnitude [0.0, 0.1, 0.2, 0.3, 0.4, 0.5, 0.75, 1.0 $m.s^{-1}$]. The dotted lines represent the plume centreline while continuous lines show the plume envelope. The various parameters used for the simulations are summarized in Table 2.7.

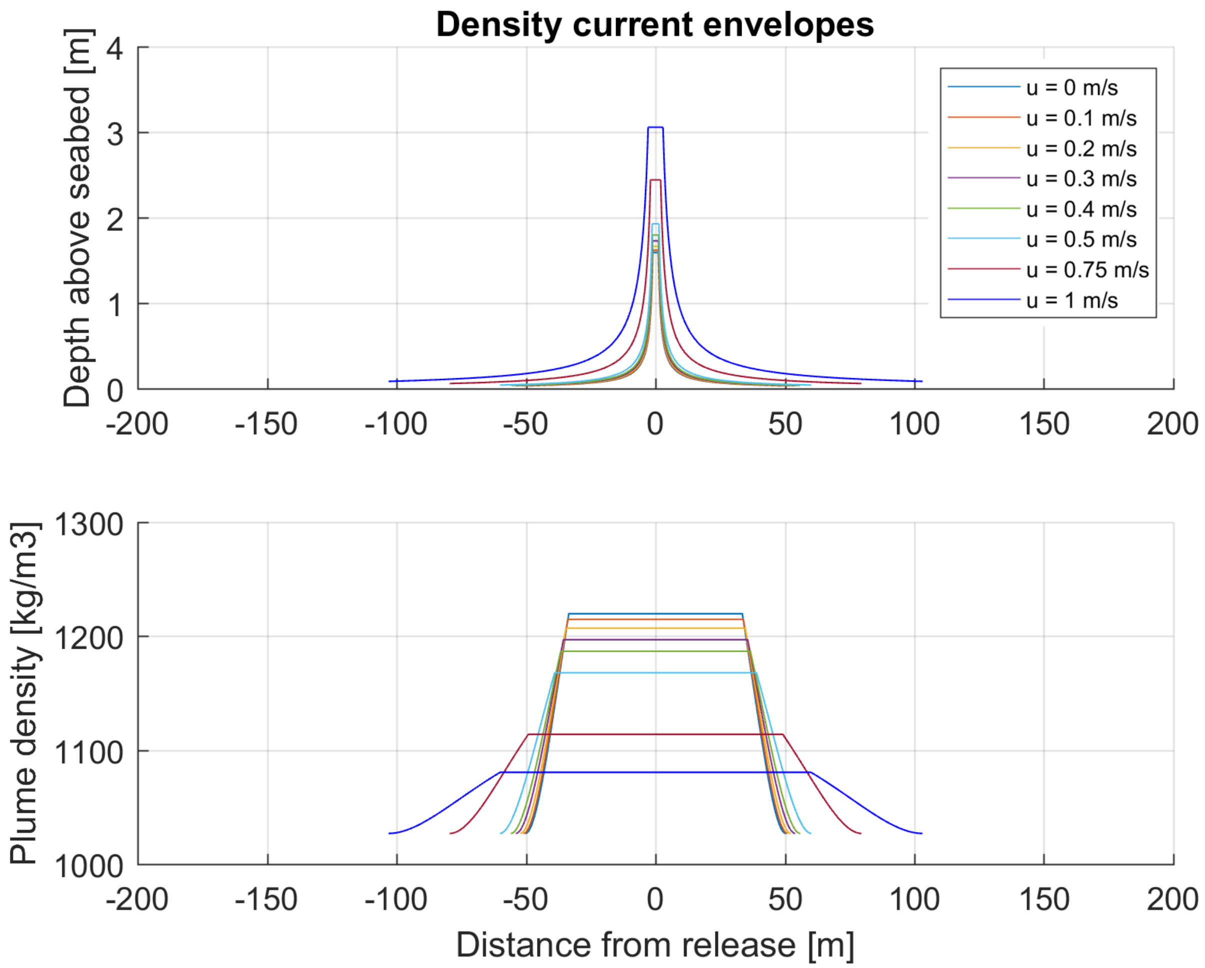

Figure 2.6 Envelopes of the predicted density current height (top) and plume density (bottom) as a function of the distance from impact (i.e. x=0 m). These indicate the density current becomes insignificant within ~100 m of the point of impact. The various parameters used for the simulations are summarized in Table 2.7.

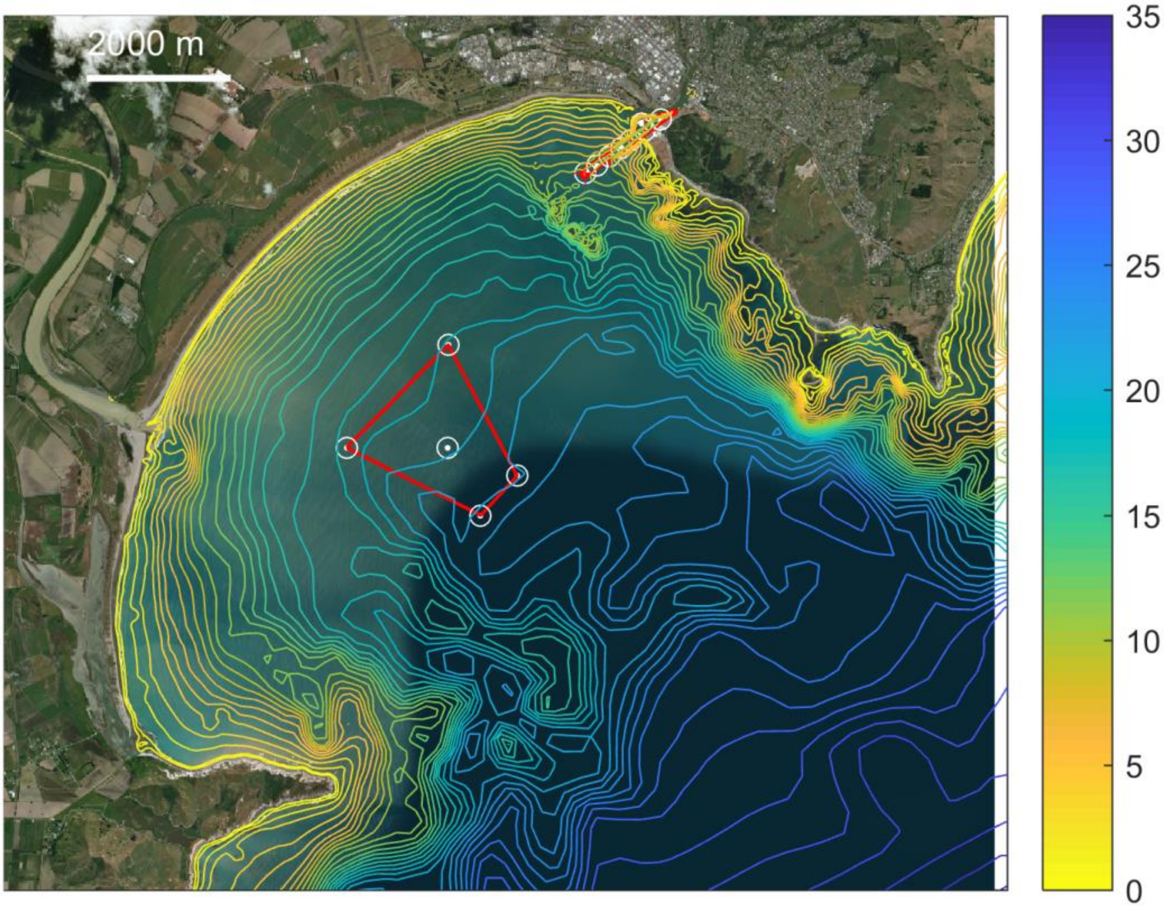

Figure 2.7 Release sites considered for the sediment disposal simulations (white circles) (see Table 2.8 for positions). The extents of the disposal ground are shown in red.

Table 2.8 Coordinates of release sites considered

Site Names	Longitude	Latitude
gsb_disp_west	177.974634	-38.714864
gsb_disp_north	177.990864	-38.702033
gsb_disp_east	178.001842	-38.718373
gsb_disp_south	177.996047	-38.723286
gsb_disp_center	177.99073	-38.714864

2.4. Post-processing

2.4.1. Concentration and depositional thickness computation

A Lagrangian model outputs a set of particles positions changing over time, thus describing their trajectories. However, often the particle concentration fields needs to be reconstructed to provide a more quantitative metric to assess actual suspended sediment concentration levels, or depositional thickness.

The "concentration" of particles at a given point (*x,y,z*) is related to the particle "density" in the region surrounding this point. Historically, the calculation of concentration at a receptor (*x,y,z*) in Lagrangian particle models has been made by the so-called *box-counting* technique. The technique consists in counting the number of particles within a "box" that is centred on the receptor and then dividing the total mass of the particles by the box volume (Bellasio, et al., 2017).

The approach has important limitations; since concentration computed in boxes containing a small numbers of particles are affected by relatively large statistical errors, simulations generally need to include a large number of particles to obtain an acceptable resolution in the computed concentration field (Vitali et al., 2006). Furthermore, a compromise needs to be made on the dimension of the boxes so that they are large enough to include a statistically significant number of particles and thus yield a continuous concentration field, but not too large so that the concentration field is not over-smoothed (e.g. Bellasio, et al., 2017). This relatively arbitrary choice can have important effects on the resulting concentration field magnitudes (De Haan, 1999). The method is very computationally expensive.

An alternative, more robust, numeric technique for computing concentrations fields from Lagrangian particles is the *kernel density estimator* (Silverman, 1986). In the kernel density approach, individual particles are assumed to represent the centre of mass of a "cloud"; the density profile of the cloud is described by the *kernel function*, while the spreading of the particle's equivalent mass is defined by the *bandwidths* associated with a given particle or receptor (Bellasio, et al., 2017; Vitali et al., 2006). These two components are then used to derive a *particle density field*, also referred to as a *probability density function*.

Here, the kernel density estimation is undertaken following the approach proposed by Botev, et al. (2010). The proposed method uses an adaptive kernel density estimation method based on the smoothing properties of linear diffusion processes. The key idea is to view the kernel from which the estimator is constructed as the transition density of a diffusion process (Botev, et al., 2010). Their methods limit the amount of guessing on the original data, notably to defining bandwidths, as well as possible excessive smoothing of the density fields (e.g. as obtained with Gaussian kernel density estimators). The kernel density estimations algorithms for both one and two dimensional spaces have been implemented in Matlab by the authors themselves[3] [4], and these processing scripts have used in the present study.

Based on a given cloud of particles (X_{part},Y_{part}), the method yields a *probability density function PDF(x,y)*, derived from the *kernel density estimator* describing the density of particles throughout the domain. The spatial integration of the *probability density function PDF(x,y)* over the entire domain equals one.

[3] https://fr.mathworks.com/matlabcentral/fileexchange/17204-kernel-density-estimation
[4] https://fr.mathworks.com/matlabcentral/fileexchange/14034-kernel-density-estimator

$$\sum_{i}^{n} PDF(x,y)\,.\,dx\,.\,dy = 1 \tag{2.7}$$

where n is the number of receptors, and (d_x,d_y) are the dimensions of the grid cells for which the *PDF* is computed.

The *PDF(x,y)* is provided over a rectangular grid with a resolution that can be adjusted by the user.

The *PDF(x,y)* values can be converted to particle density when multiplied by the total number of particles in the domain i.e. with units [particles.m^{-2}]. The particle density can in turn be converted to mass density, or mass distribution, based on the equivalent mass carried by individual particles i.e. with units [mass.m^{-2}]. Mass concentration (i.e. *SSC*) is obtained by dividing the mass density by the water depth i.e. with units [mass.m^{-3}].

A similar approach is followed for estimating the depositional thickness. The probability density function of the deposited particle is computed and converted to a sediment mass density field in [mass.m^{-2}]. Using the known density allows determining the sediment volume deposited per m^2, which effectively yields the deposition thickness i.e. [$mass^3$.m^{-2} = m].

2.4.2. Application to present study

In the present study, the results of the two different 1-year long simulations (El Niño, La Niña) were post-processed to produce probabilistic footprints of the plume *SSC* and deposition field footprints. The probabilistic approach consists of combining the entire dataset of particle trajectories predicted throughout each year under a wide range of ambient current forcing and computing the associated suspended sediment concentration (*SSC*) and sediment depositions fields. This allows identifying the key dispersion pathways from each release site and assessing general plume *SSC* and deposition expected magnitudes. Here, results are normalized in order to provide a general picture of the *SSC* and sediment deposition footprints resulting from one disposal load.

Two reference vessels were simulated, the Pukunui operated by Eastland Port, and the Albatros. Both vessels have been recently used for the maintenance dredging and disposal. Pukunui's main characteristics are summarized in Table 2.5, while the Albatros's main characteristics are provided in Table 2.6

The KDEs and resulting plume *SSC* and deposition fields for the probabilistic cases (i.e. combining all outputs) were computed over a grid of 512 by 512 cells, centred on each release site, with a spatial resolution of (d_x,d_y) of ~20 m, within three different layers of the water column, namely surface, mid-depth and bottom. Each layer is 3 m thick.

To further characterise the expected variability in plume dispersion in response to the ambient forcing, time-varying *SSC* and deposition fields throughout the year were also computed, although on a slightly smaller and coarser grid (d_x~30m) for computational reasons. This dataset allows determining statistics of the spatial distribution of the plume *SSC* and deposition magnitudes such as percentile levels (e.g. extremes) or exceedance times (i.e. percentage of time a given *SSC* level is exceeded).

3. RESULTS

3.1. Hydrodynamics

The distribution of the total currents at the centre of the disposal ground (see Figure 2.7), at three levels in the water column are shown in Figure 3.1 and Figure 3.2 for the El Niño and La Niña annual periods, respectively.

Annual current regimes during the two periods are very similar; both exhibit a distinct stratification of the water column with dominant east-directed currents in the surface layer switching to predominant northwest-directed currents deeper in the water column at mid-depth and bottom levels. Such stratification can be attributed to the interaction between the seawater and freshwater sources originating from the various river inputs, notably from the Waipaoa and Turanganui Rivers. Note these illustrate the importance of using 3D hydrodynamic fields to simulate sediment dispersion for this application.

Most evident difference between current roses during the two annual episodes are found on the surface levels, with a more marked occurrence of north-directed currents during El Niño relative to La Niña.

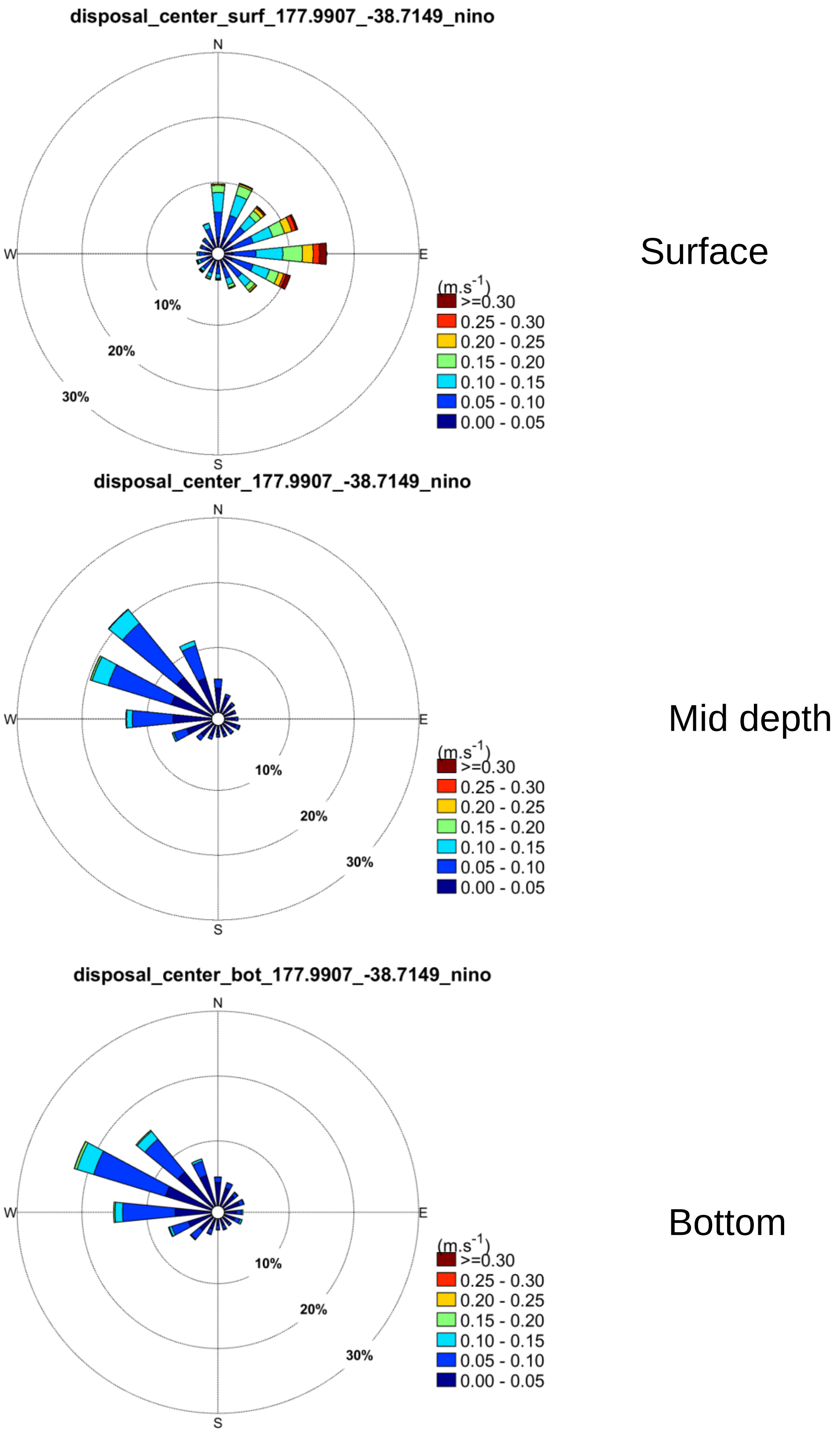

Figure 3.1 Annual current roses of surface, mid-depth, and bottom currents at the centre of the disposal site for the El Niño period (June 2002- June 2003) (see Figure 2.7 for position).

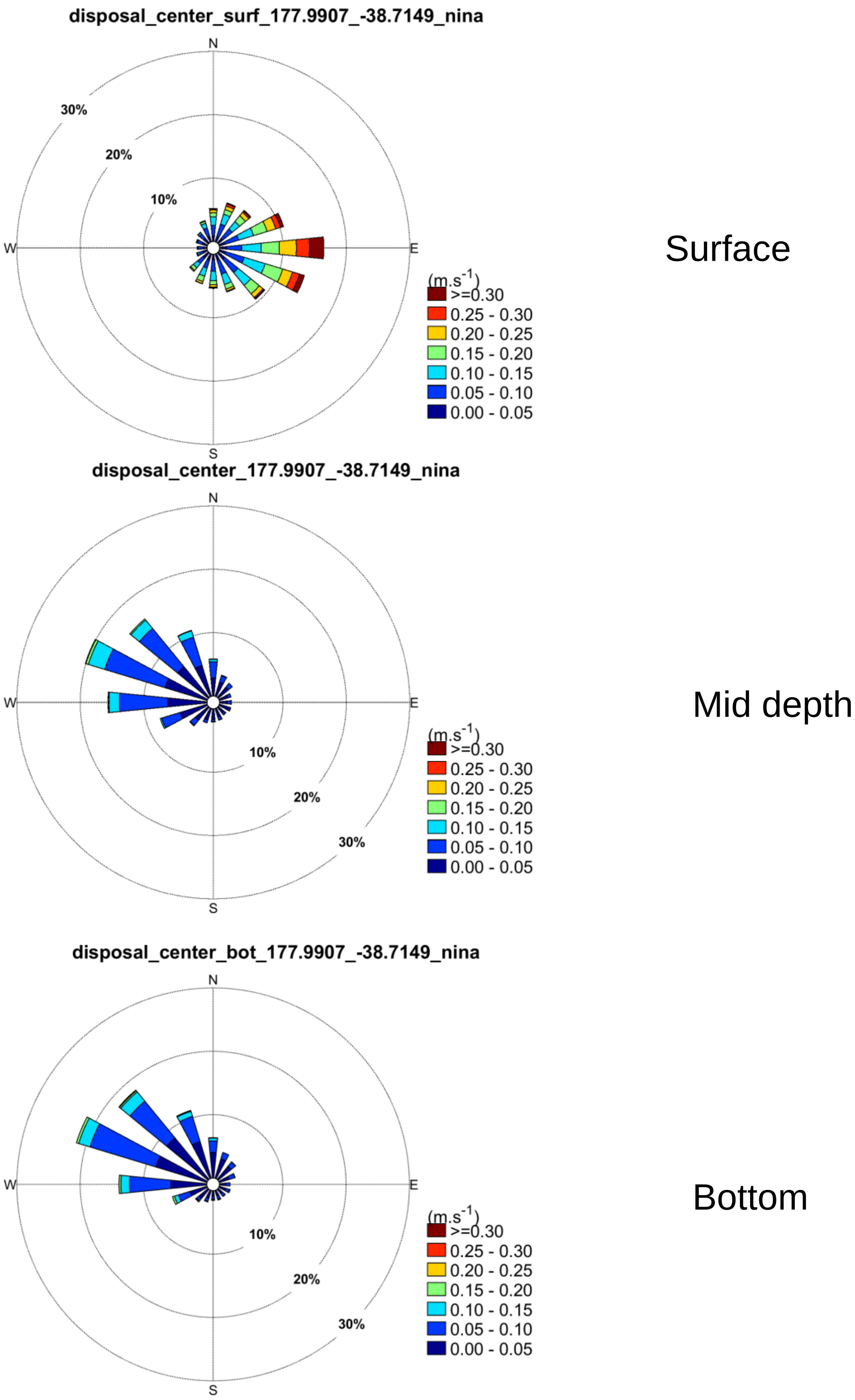

Figure 3.2 Annual current roses of surface, mid-depth, and bottom currents at the centre of the disposal site for the La Niña period (June 1998- June 1999) (see Figure 2.7 for position).

3.2. Probabilistic suspended sediment plumes (*SSC*) plumes and deposition – Pukunui vessel

The section presents the probabilistic results derived from the entire dataset of particle trajectories predicted throughout each annual scenario, assuming the use of the Pukunui vessel (V=480 m^3). The approach allows capturing a wide range of ambient current forcing on an annual timescale and thus provides a robust picture of the *SSC* plume and deposition footprints.

The probabilistic *SSC* plume fields, assuming a settling velocity of 1 $mm.s^{-1}$ for the cohesive class, are shown in Figure 3.3 and Figure 3.4 for the La Niña (June 1998-June 1999) and El Niño (June 2002-June 2003) respectively.

The general *SSC* plume pattern, which combines various source terms (see section 2.3.3) consists of a relatively limited surface *SSC* plume, progressively widening at the mid-depth and bottom levels. The highest *SSC* magnitude are predicted in the bottom layers and are due to the source term representing the density current (cylinder with 150 m radius and 2 m high), which is assumed to include 25% of the total disposed sediment (see Table 2.4). Largest *SSC* magnitudes (>100 $mg.L^{-1}$) are generally contained within 250 m of the disposal location and quickly become one to two orders of magnitudes smaller beyond that.

The relative widening of the plume at it settles is expected. Suspended particles are subject to current advection and diffusion; the longer they remain suspended, the larger distances they can travel. For example, a compact cloud of particle released at the surface will have significant time to disperse by the time they reach the seabed, thus widening its overall footprint, but also reducing its *SSC* levels through dilution.

The surface component of the *SSC* plumes are generally elongated toward the east quadrant while mid-depth and bottom plume components show footprints elongated in a general northwest direction. These patterns are expectedly consistent with the current regimes outlined in Section 3.1. Interestingly, *SSC* plume can be relatively shifted slightly towards the north in the El Niño results, or even exhibit a distinct north-directed “branch” (e.g. disposal ground centre). These features may be signature of the slight variation in current regime identified in Section 3.1.

The results assuming a smaller settling velocity of 0.1 $mm.s^{-1}$ are shown in Figure 3.5 and Figure 3.6. A smaller settling velocity results in particles remaining suspended in the water column for longer, and thus able to disperse over larger distances. This is combined with relatively larger potential for suspended sediment concentration dilution (i.e. same amount of material is dispersed over a larger area). The bottom *SSC* plume footprints for the smaller settling velocity of 0.1 $mm.s^{-1}$ expectedly appear larger than for the results using 1 $mm.s^{-1}$. *SSC* levels of order 1-10 $mg.L^{-1}$ can extend beyond the 500 m radius while strictly contained within 250 m previously for the 1 $mm.s^{-1}$ simulations. Irrespective, *SSC* generally still fall below 1 $mg.L^{-1}$ within 1000 m of the release point.

Interestingly, the surface and mid-depth plumes appear smaller than the 1 $mm.s^{-1}$ footprints which may seem counter intuitive. Here, though the effective dispersion may be larger (i.e., particles travelling further), the effective *SSC* fall below the 1 $mg.L^{-1}$ threshold quicker than for the 1 $mm.s^{-1}$ due to more efficient dilution, which results in an apparent plume footprint reduction.

The deposition fields associated with the *SSC* plumes described above are shown in Figure 3.7 to Figure 3.10. The deposition footprints are predominantly circular, which is consistent with the density current source term (i.e. bottom cylinder) including most of the disposed sediment (see Table 2.4), with thin components elongated in the northwest direction resulting from the settling of the dispersed *SSC* plumes.

Note that these deposition fields describe the net depositions associated with the settling of sediment of the passive plume only (~32% of total load, see Table 2.4). The remaining fraction of sediment is expected to deposit quasi instantaneously, when the dynamic plume impacts the seabed, over a limited area (i.e. of order the diameter of the plume when it hits the seabed).

The above results focused on the disposal of sediment loads composed primarily of silt material (80% silt, 20% sand) since finer sediment will remain much longer in suspension in the water column and is potentially the most problematic with respect to the spatial excursion of the produced sediment plumes.

For reference, the *SSC* and deposition fields predicted for a disposal of predominantly “sandy” and “silty” material are compared in Figure 3.11 to Figure 3.18. The key differences between the disposal of a “sandy” versus “silty” sediment load is expectedly the total footprints of the *SSC* plumes and deposition fields; they are larger for the “silty” load than for the “sandy” load due to the difference in settling times. That being, the relatively more compact sediment dispersion footprint as well as the larger density used in that case (1350 $kg.m^{-3}$ for a “silty” load versus 650 $kg.m^{-3}$ for a “sandy” load) also results in locally larger *SSC* magnitudes and deposition thicknesses. Note that for the *SSC* plume, the larger levels will only be sustained for a short period of time, given the fast settling.

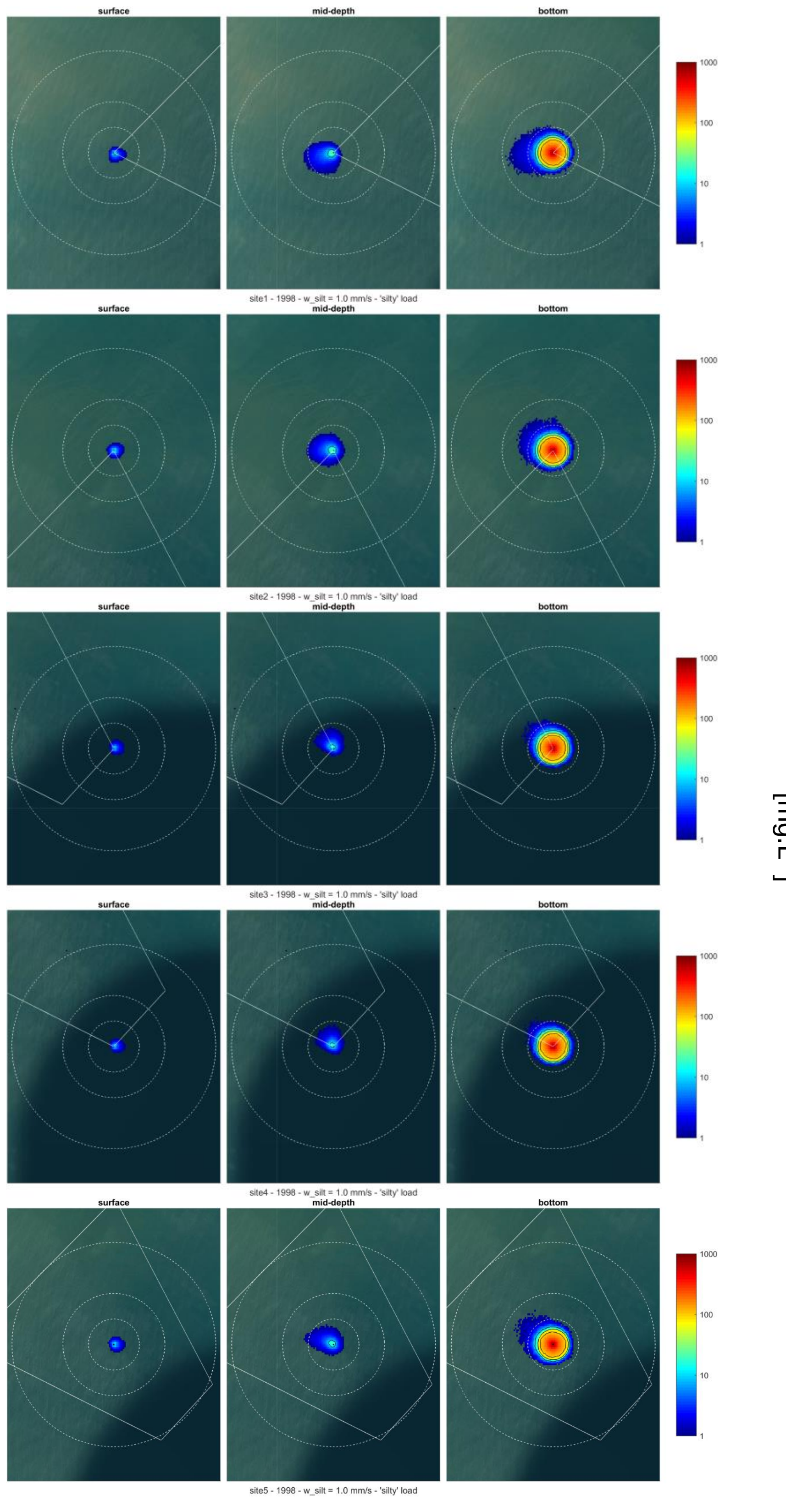

Figure 3.3 Probabilistic *SSC* fields resulting from the disposal of one hopper load of the Pukunui vessel (V=480 m^3), derived from the annual La Niña period (June 1998-June 1999). The results assumed a settling velocity of 1 $mm.s^{-1}$ for the cohesive sediment class. Dashed grey circles have radiuses of 250, 500 and 1000 m. The 10, 50 and 100 $mg.L^{-1}$ contours are shown in black.

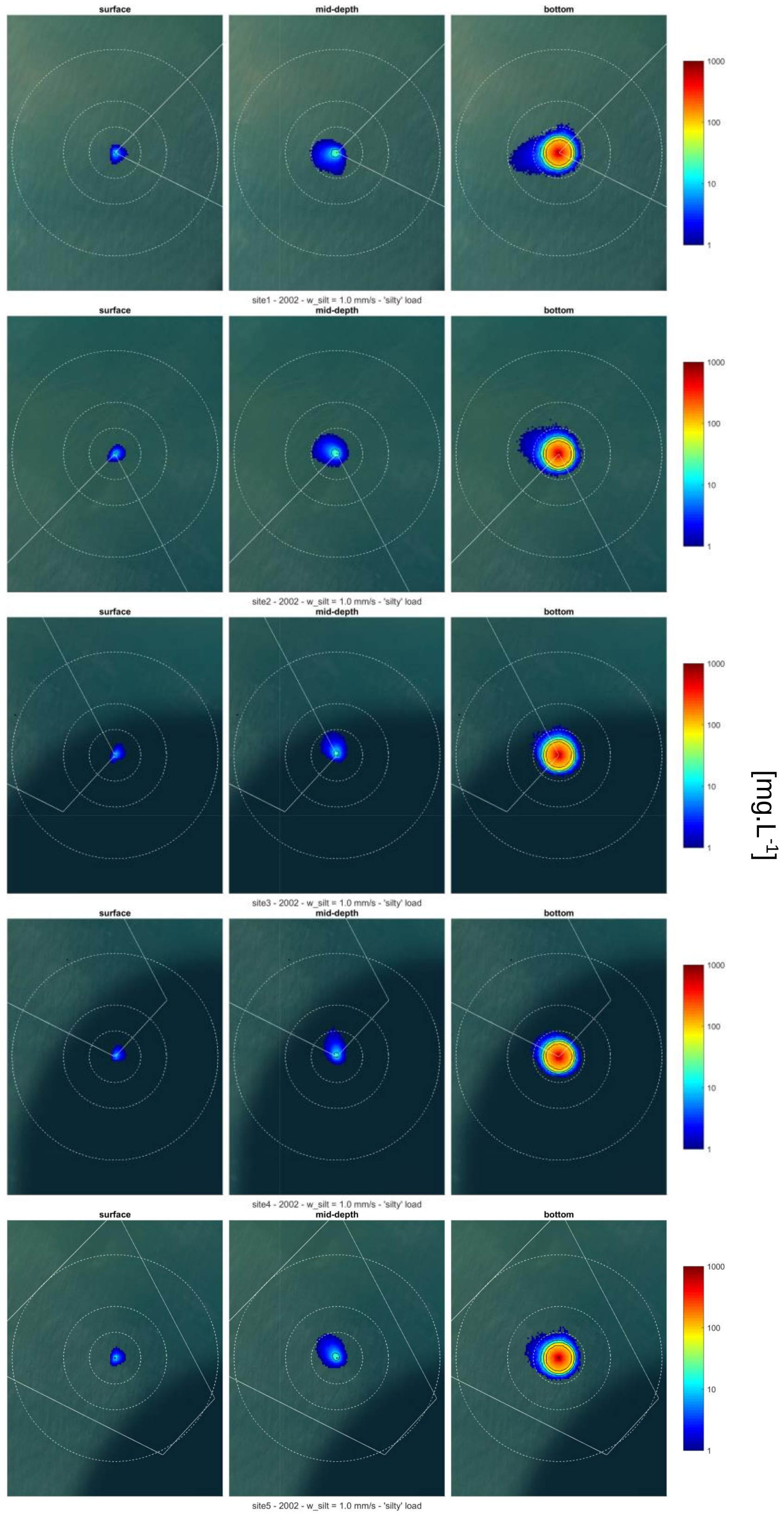

Figure 3.4 Probabilistic *SSC* fields resulting from the disposal of one hopper load of the Pukunui vessel (V=480 m^3), derived from the annual El Niño period (June 2002-June 2003). The results assumed a settling velocity of 1 $mm.s^{-1}$ for the cohesive sediment class. Dashed grey circles have radiuses of 250, 500 and 1000 m. The 10, 50 and 100 $mg.L^{-1}$ contours are shown in black.

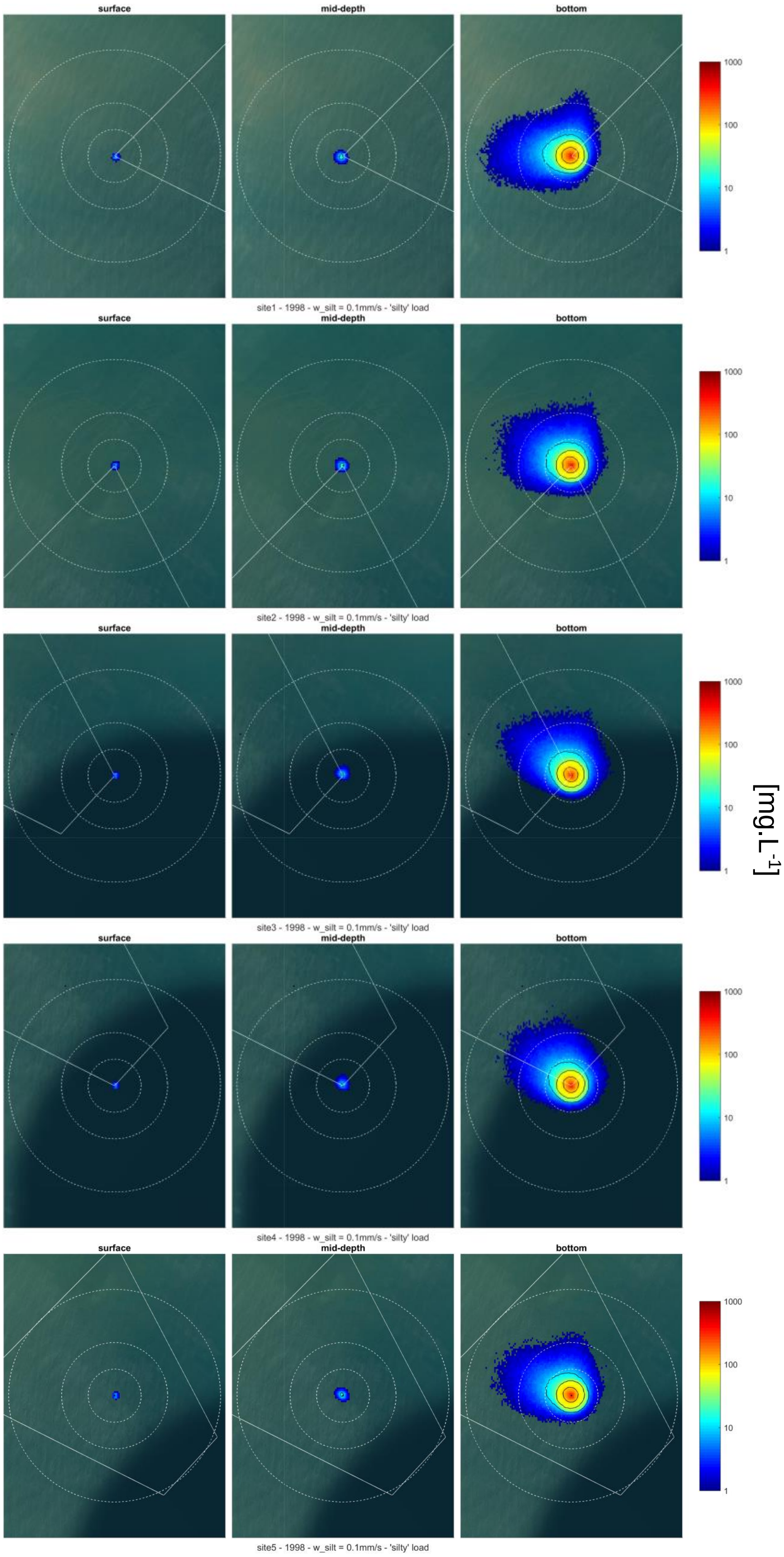

Figure 3.5 Probabilistic *SSC* fields resulting from the disposal of one hopper load of the Pukunui vessel (V=480 m^3), derived from the annual La Niña period (June 1998-June 1999). The results assumed a settling velocity of 0.1 $mm.s^{-1}$ for the cohesive sediment class. Dashed grey circles have radiuses of 250, 500 and 1000 m. The 10, 50 and 100 $mg.L^{-1}$ contours are shown in black.

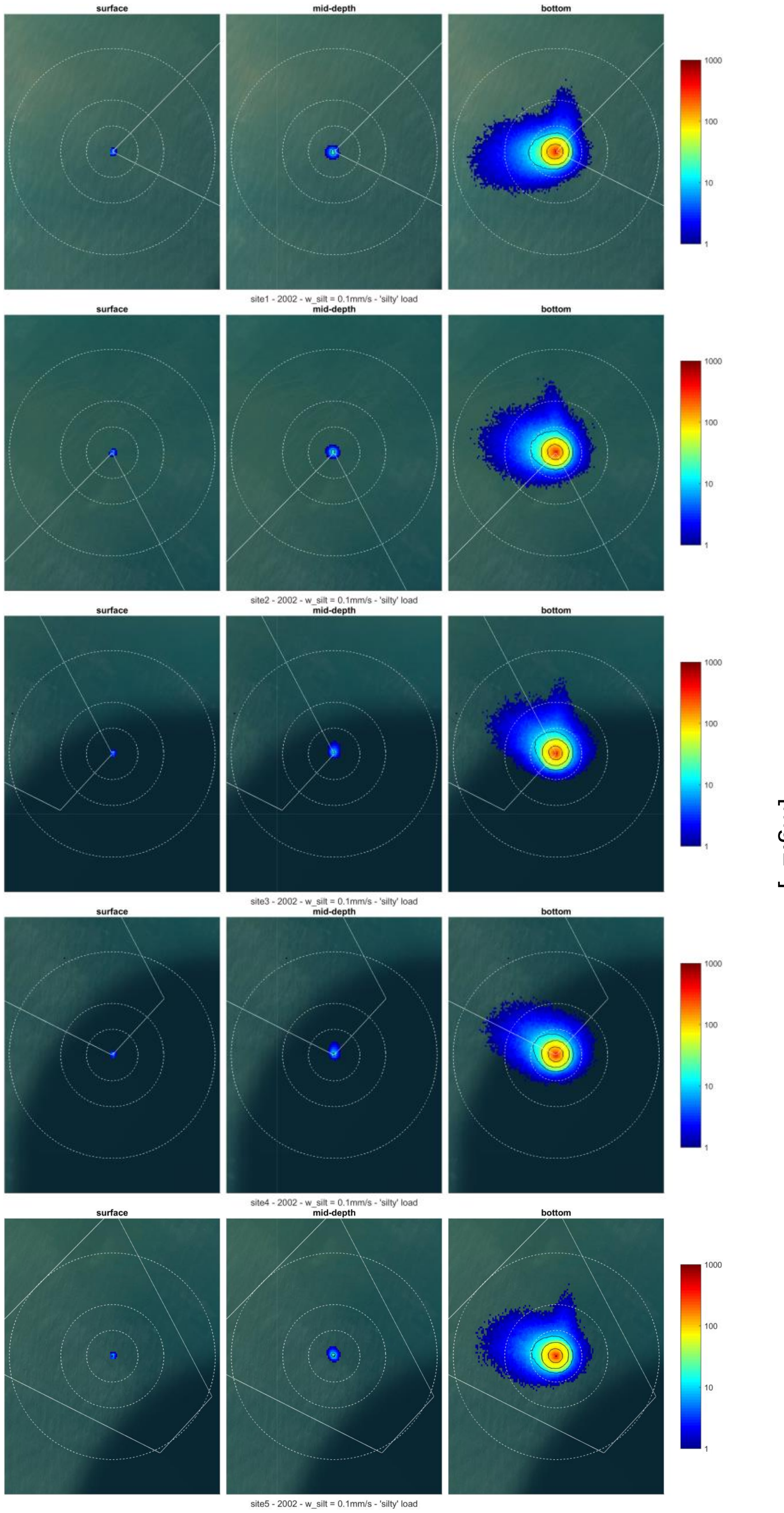

Figure 3.6 Probabilistic *SSC* fields resulting from the disposal of one hopper load of the Pukunui vessel (V=480 m^3), derived from the annual El Niño period (June 2002-June 2003). The results assumed a settling velocity of 0.1 mm.s^{-1} for the cohesive sediment class. Dashed grey circles have radiuses of 250, 500 and 1000 m. The 10, 50 and 100 mg.L^{-1} contours are shown in black.

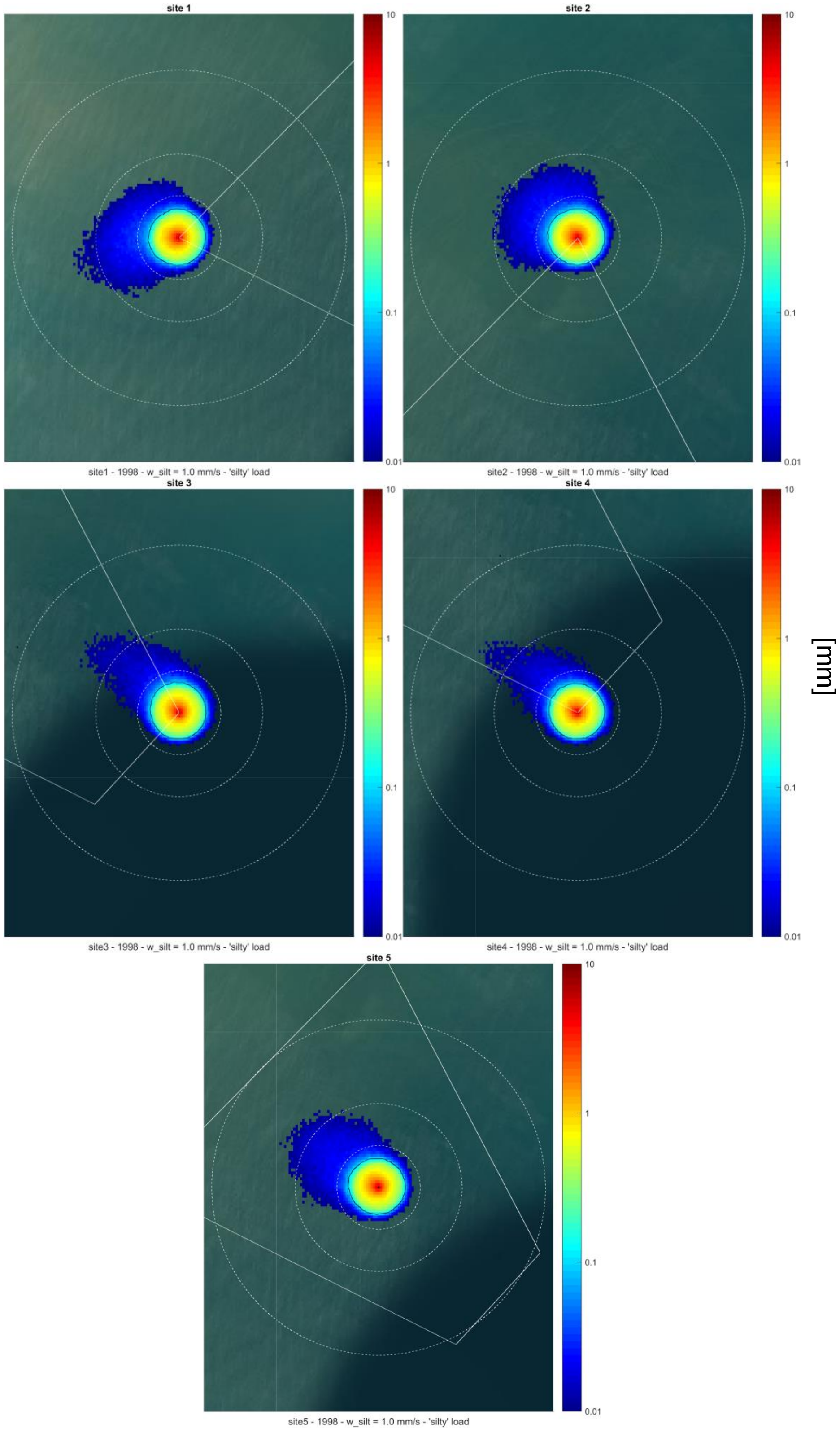

Figure 3.7 Probabilistic sediment deposition fields resulting from the disposal of one hopper load of the Pukunui vessel (V=480 m^3), derived from the annual La Niña period (June 1998-June 1999). The results assumed a settling velocity of 1.0 $mm.s^{-1}$ for the cohesive sediment class. Dashed grey circles have radiuses of 250, 500 and 1000 m. The 0.1 mm contour is shown in black.

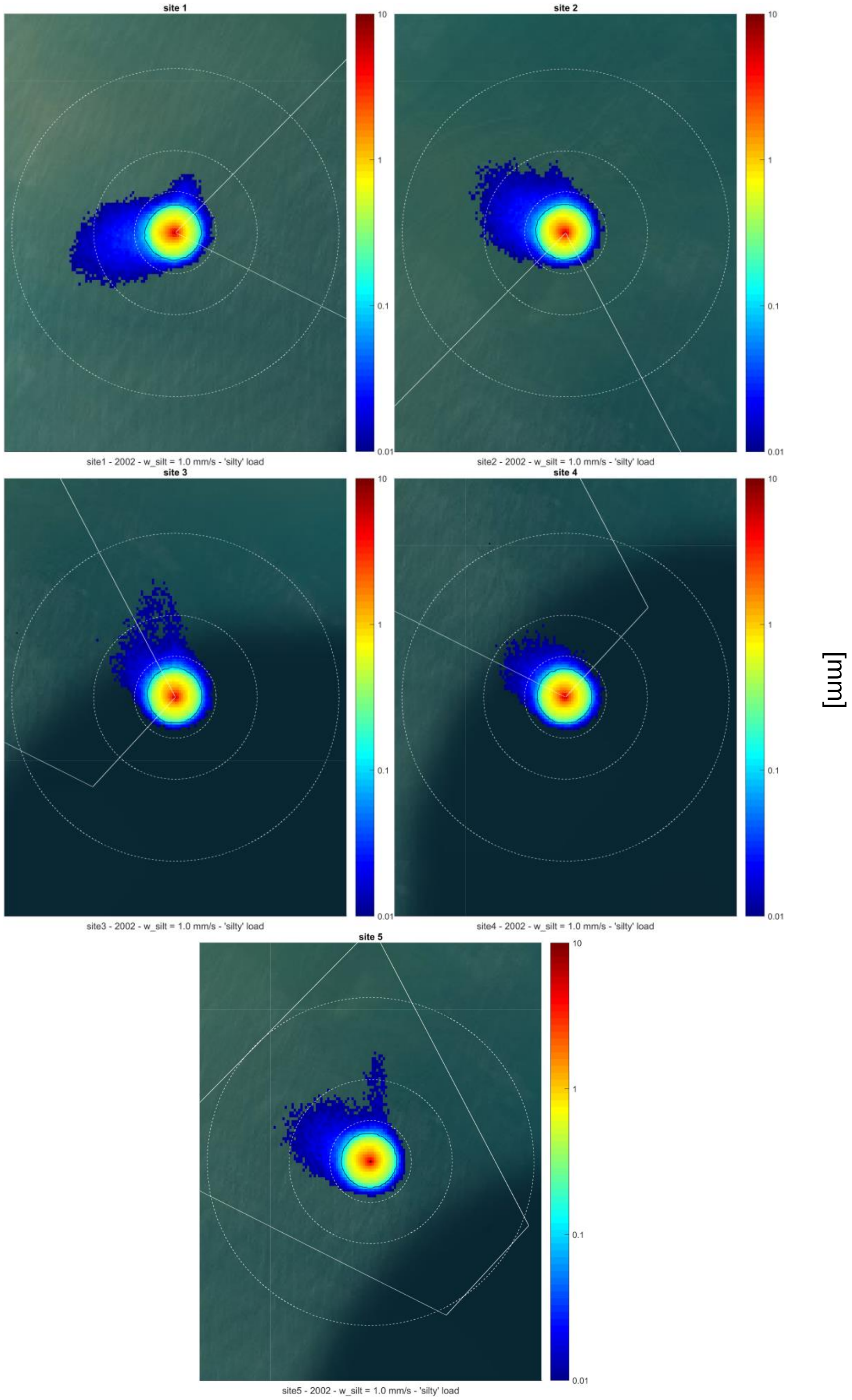

Figure 3.8 Probabilistic sediment deposition fields resulting from the disposal of one hopper load of the Pukunui vessel (V=480 m^3), derived from the annual El Niño period (June 2002-June 2003). The results assumed a settling velocity of 1.0 $mm.s^{-1}$ for the cohesive sediment class. Dashed grey circles have radiuses of 250, 500 and 1000 m. The 0.1 mm contour is shown in black.

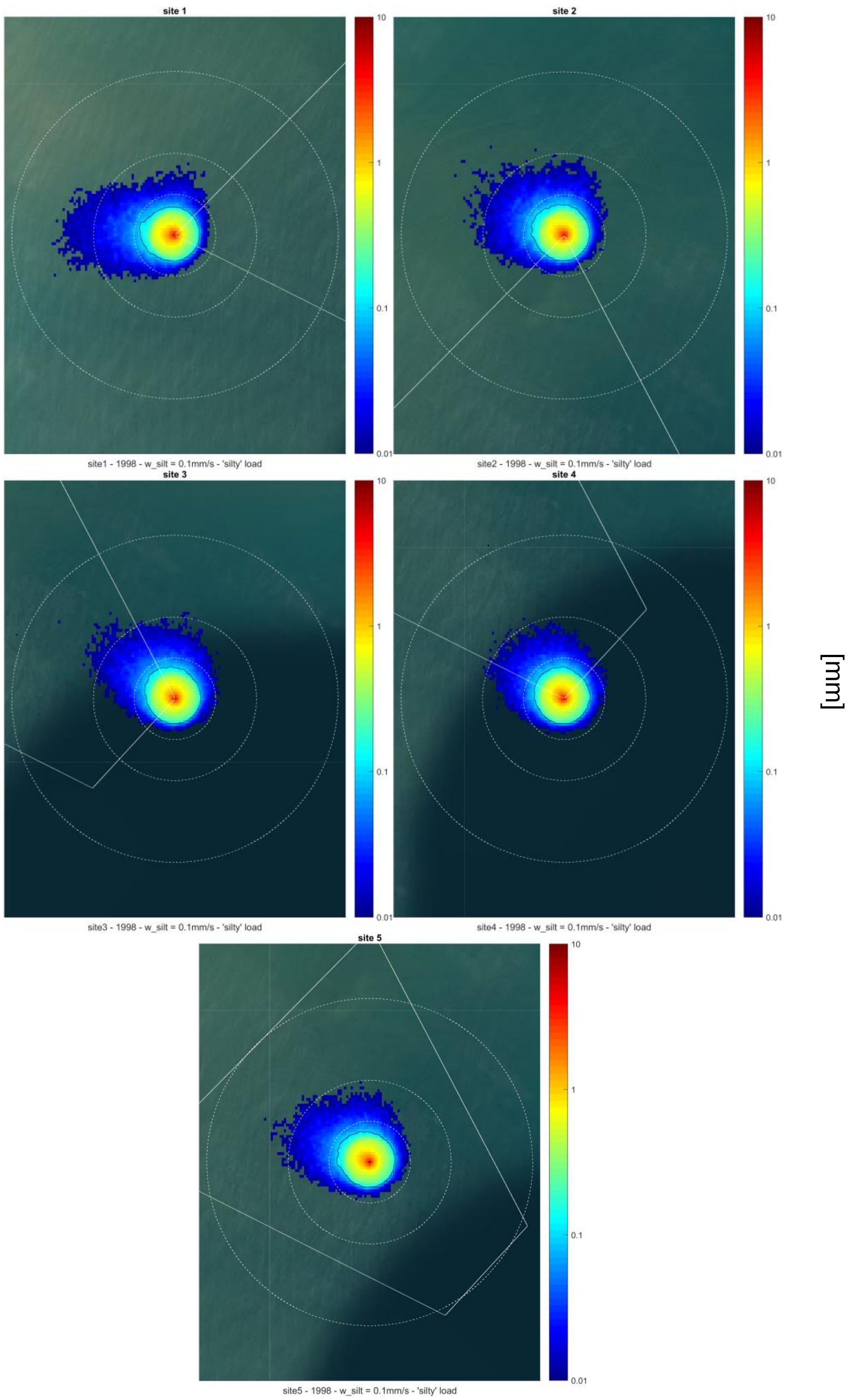

Figure 3.9 Probabilistic sediment deposition fields resulting from the disposal of one hopper load of the Pukunui vessel (V=480 m^3), derived from the annual La Niña period (June 1998-June 1999). The results assumed a settling velocity of 0.1 $mm.s^{-1}$ for the cohesive sediment class. Dashed grey circles have radiuses of 250, 500 and 1000 m. The 0.1 mm contour is shown in black.

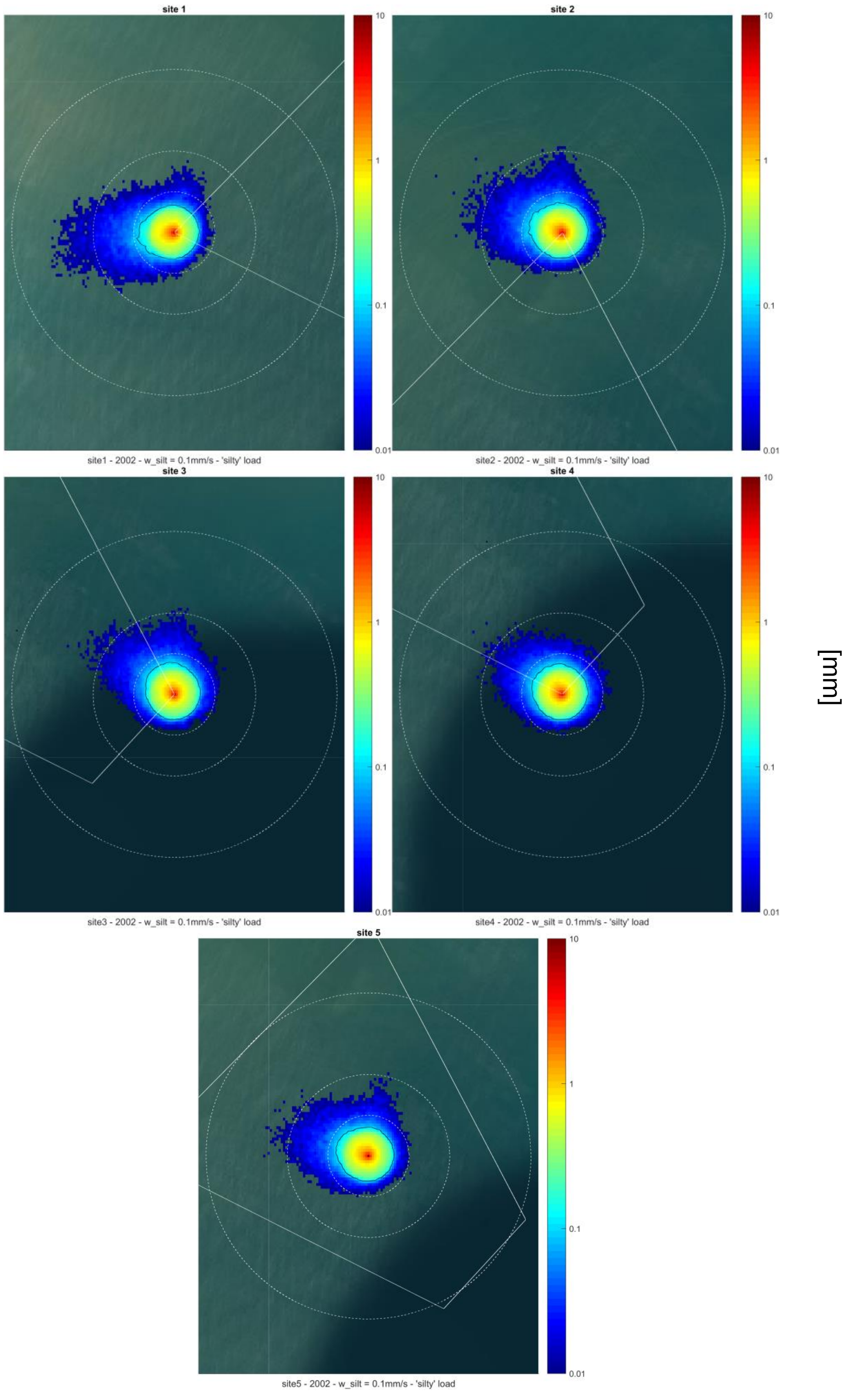

Figure 3.10 Probabilistic sediment deposition fields resulting from the disposal of one hopper load of the Pukunui vessel (V=480 m^3), derived from the annual El Niño period (June 2002-June 2003). The results assumed a settling velocity of 0.1 mm.s^{-1} for the cohesive sediment class. Dashed grey circles have radiuses of 250, 500 and 1000 m. The 0.1 mm contour is shown in black.

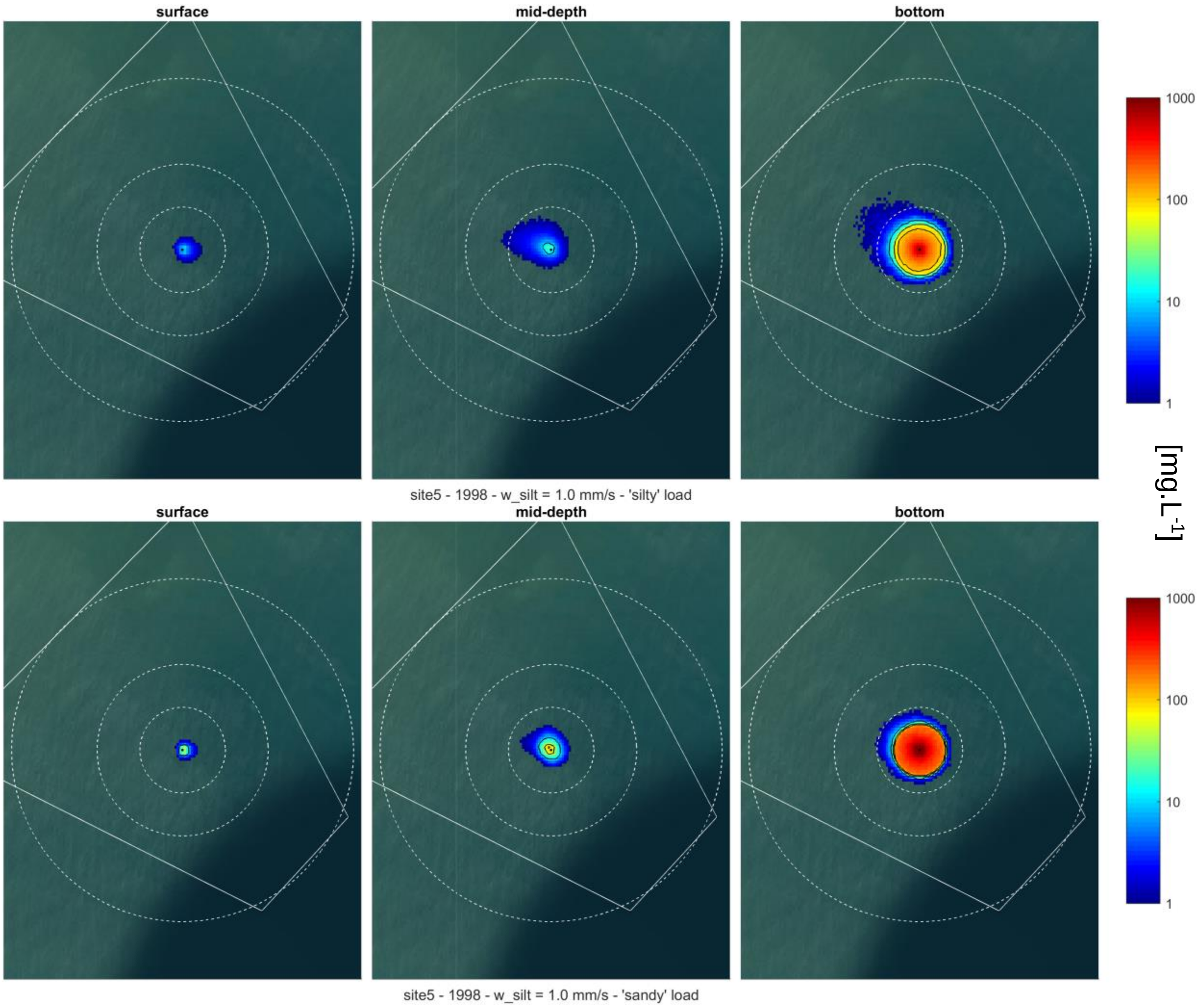

Figure 3.11 Probabilistic *SSC* fields resulting from the disposal of one hopper load of the Pukunui vessel (V=480 m^3), derived from the annual La Niña period (June 1998-June 1999). The results compare the plumes associated with the release of a sediment load composed of 80% silt and 20 % sand (top), and 20% silt 80% sand (bottom). The results assumed a settling a settling velocity of 1.0 $mm.s^{-1}$ for the cohesive sediment class. Dashed grey circles have radiuses of 250, 500 and 1000 m. The 10, 50 and 100 $mg.L^{-1}$ contours are shown in black.

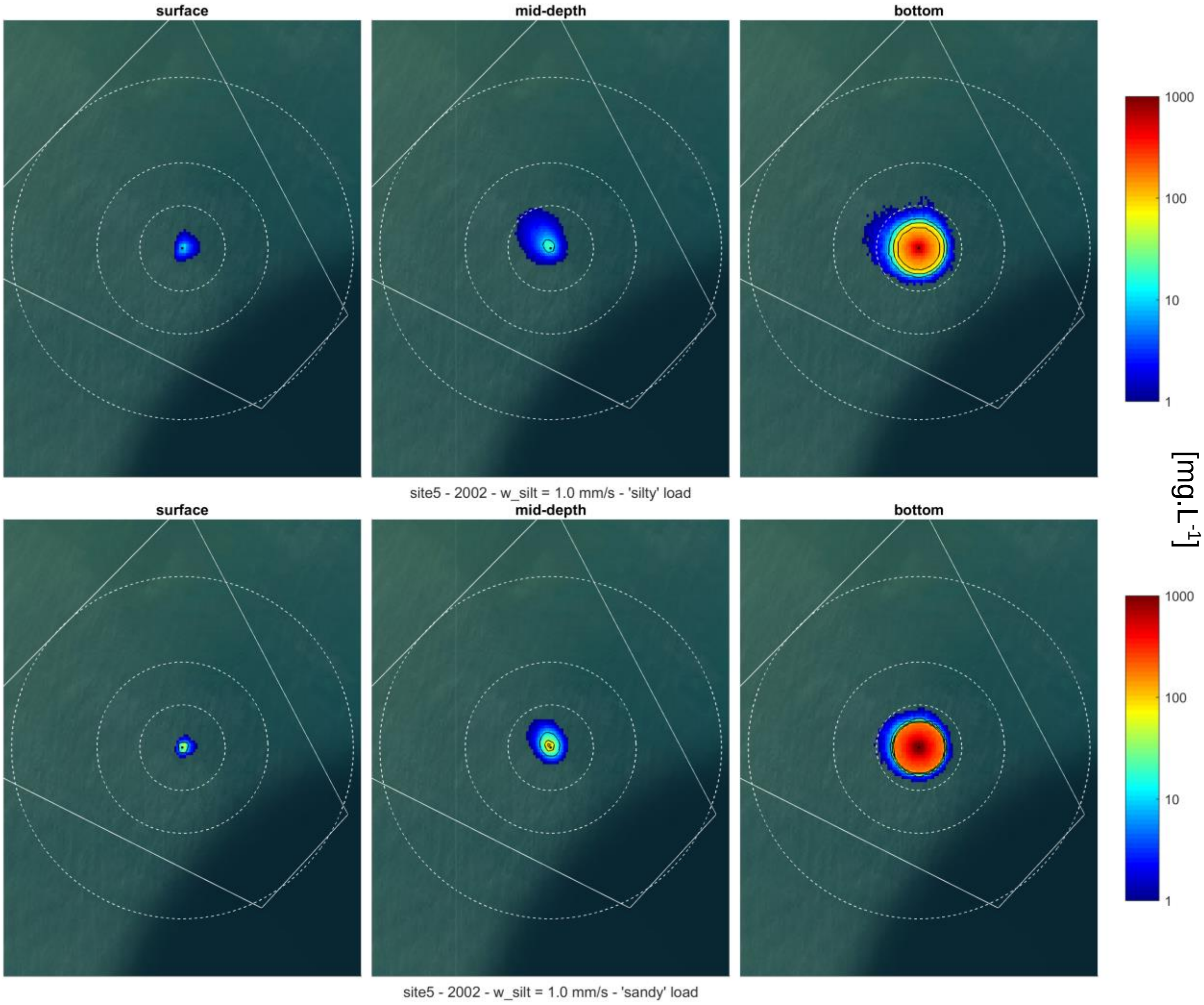

Figure 3.12 Probabilistic *SSC* fields resulting from the disposal of one hopper load of the Pukunui vessel (V=480 m^3), derived from the annual El Niño period (June 2002-June 2003). The results compare the plumes associated with the release of a sediment load composed of 80% silt and 20 % sand (top), and 20% silt 80% sand (bottom). The results assumed a settling a settling velocity of 1.0 $mm.s^{-1}$ for the cohesive sediment class. Dashed grey circles have radiuses of 250, 500 and 1000 m. The 10, 50 and 100 $mg.L^{-1}$ contours are shown in black.

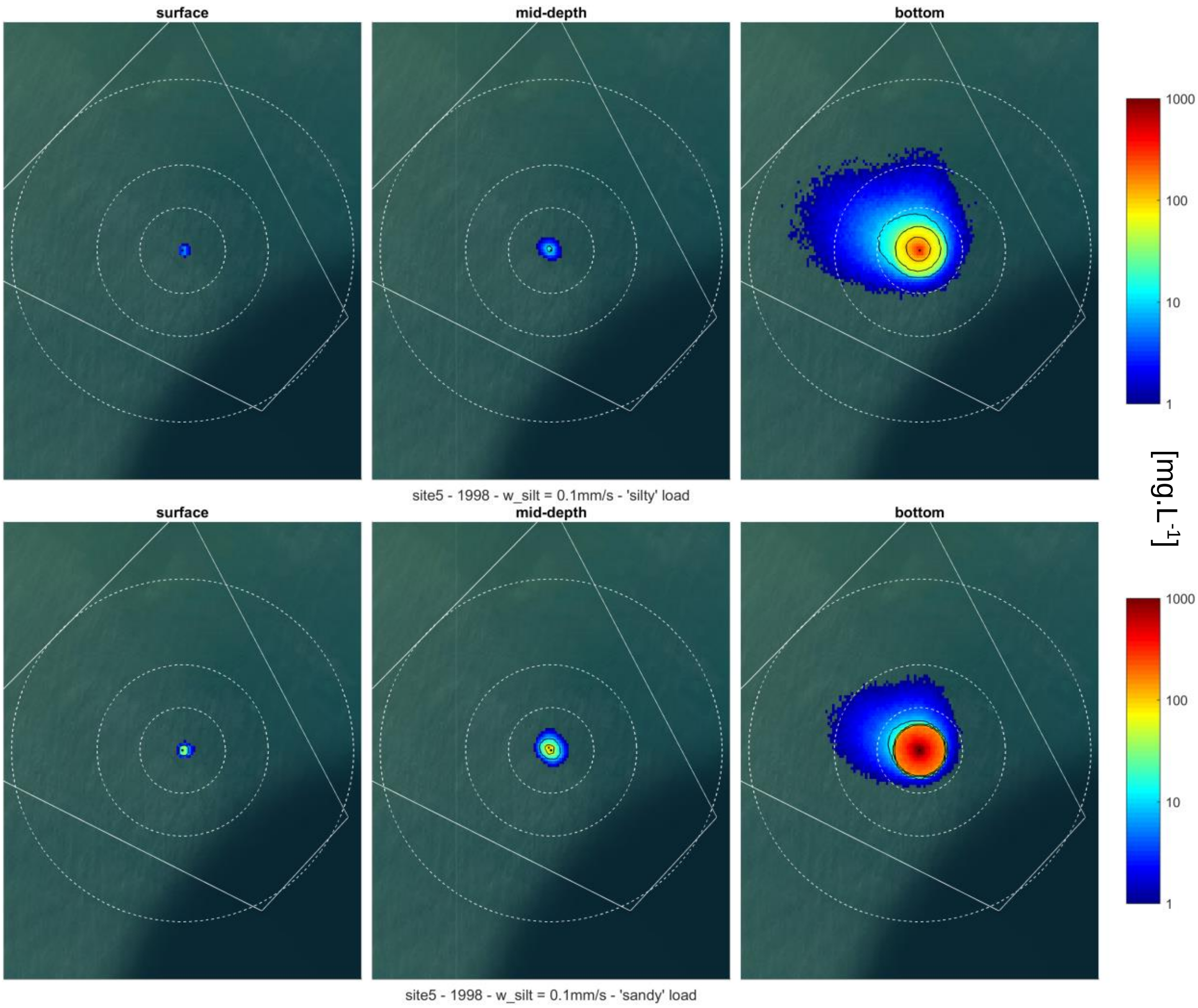

Figure 3.13 Probabilistic *SSC* fields resulting from the disposal of one hopper load of the Pukunui vessel (V=480 m^3), derived from the annual La Niña period (June 1998-June 1999). The results compare the plumes associated with the release of a sediment load composed of 80% silt and 20 % sand (top), and 20% silt 80% sand (bottom). The results assumed a settling a settling velocity of 0.1 $mm.s^{-1}$ for the cohesive sediment class. Dashed grey circles have radiuses of 250, 500 and 1000 m. The 10, 50 and 100 $mg.L^{-1}$ contours are shown in black.

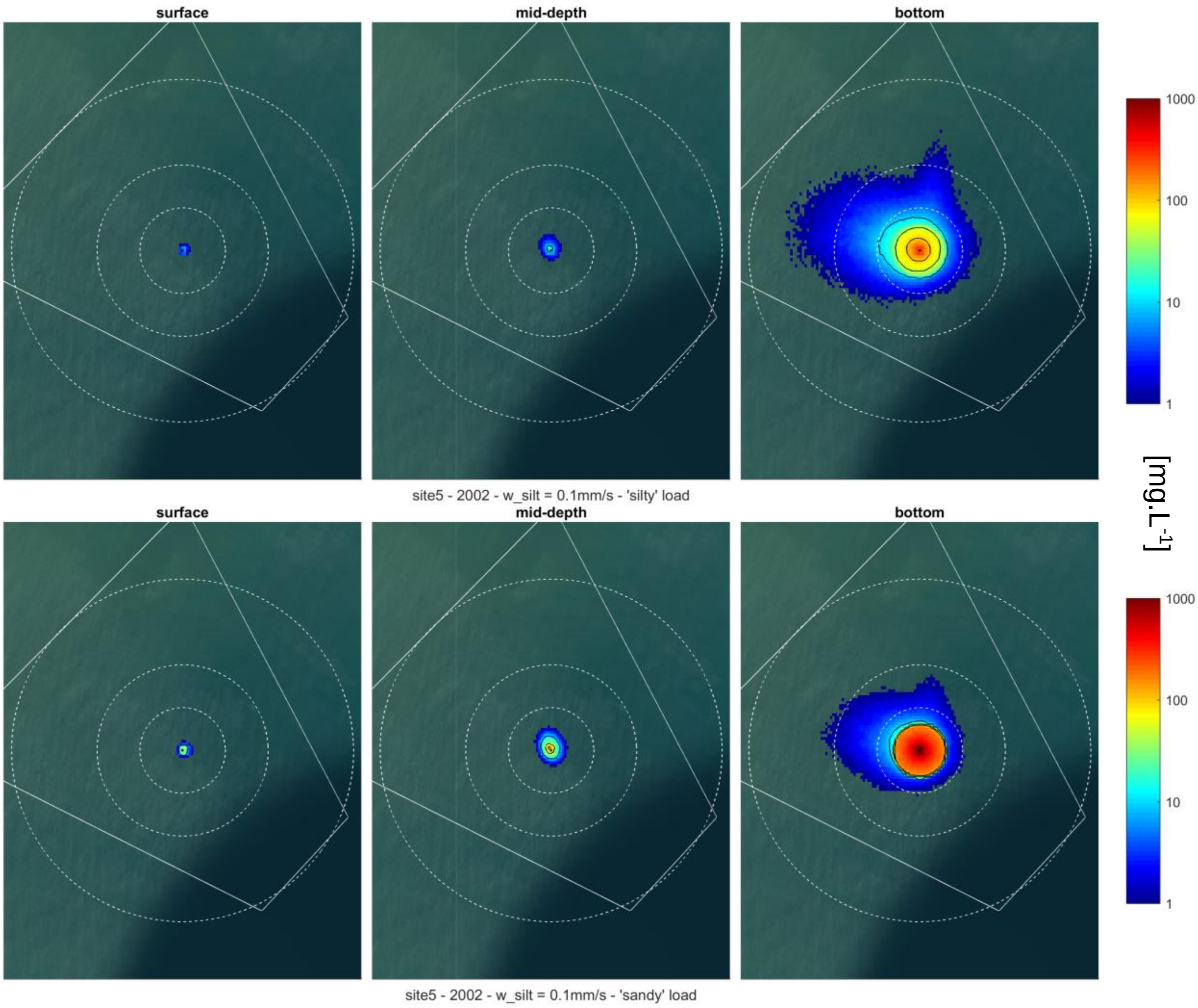

Figure 3.14 Probabilistic *SSC* fields resulting from the disposal of one hopper load of the Pukunui vessel (V=480 m^3), derived from the annual El Niño period (June 2002-June 2003). The results compare the plumes associated with the release of a sediment load composed of 80% silt and 20 % sand (top), and 20% silt 80% sand (bottom). The results assumed a settling a settling velocity of 0.1 mm.s^{-1} for the cohesive sediment class. Dashed grey circles have radiuses of 250, 500 and 1000 m. The 10, 50 and 100 mg.L^{-1} contours are shown in black.

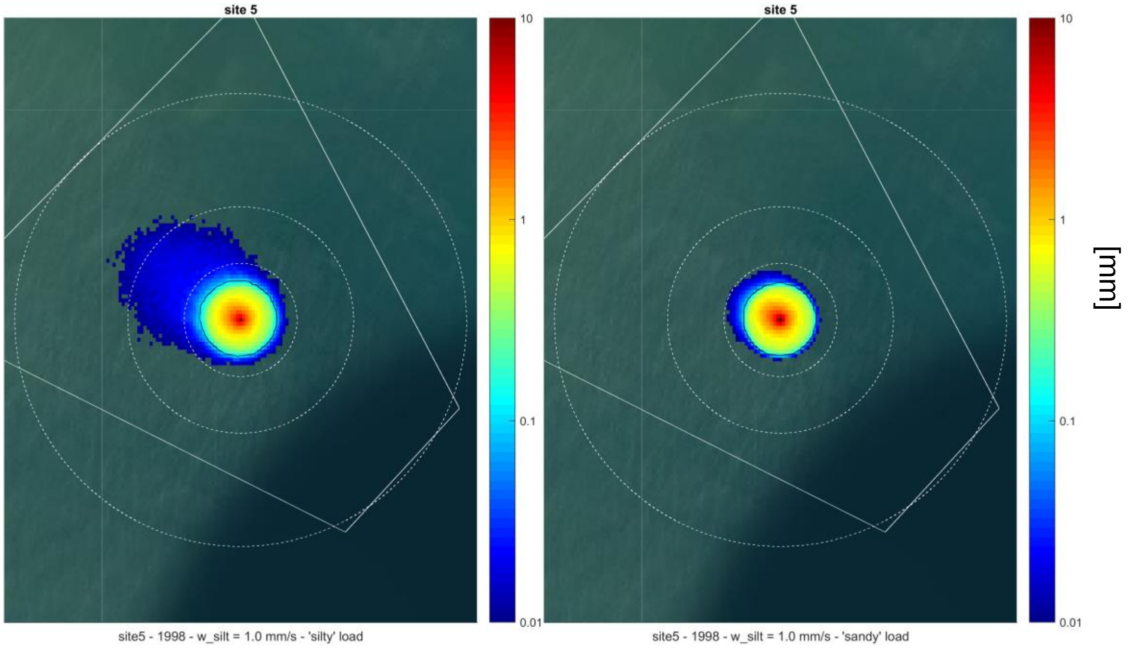

Figure 3.15 Probabilistic sediment deposition fields resulting from the disposal of one hopper load of the Pukunui vessel (V=480 m^3), derived from the annual La Niña period (June 1998-June 1999). The results compare the plumes associated with the release of a sediment load composed of 80% silt and 20 % sand (left), and 20% silt 80% sand (right). The results assumed a settling a settling velocity of 1.0 mm.s^{-1} for the cohesive sediment class. Dashed grey circles have radiuses of 250, 500 and 1000 m. The 10, 50 and 100 mg.L^{-1} contours are shown in black.

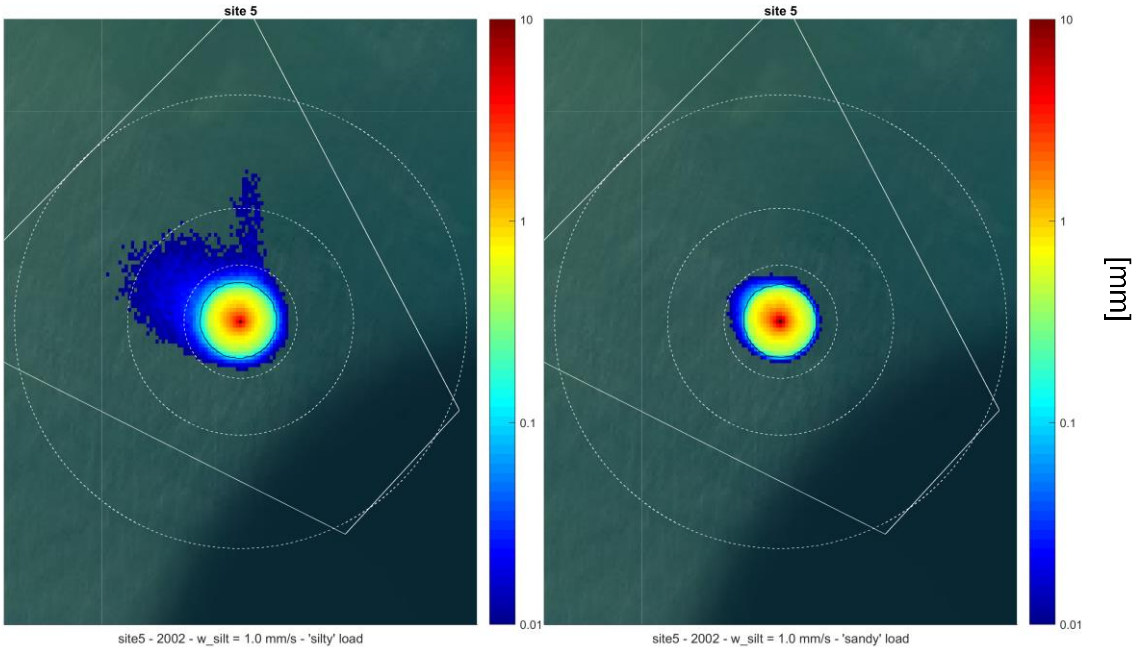

Figure 3.16 Probabilistic sediment deposition fields resulting from the disposal of one hopper load of the Pukunui vessel (V=480 m^3), derived from the annual El Niño period (June 2002-June 2003). The results compare the plumes associated with the release of a sediment load composed of 80% silt and 20 % sand (left), and 20% silt 80% sand (right). The results assumed a settling a settling velocity of 1.0 mm.s^{-1} for the cohesive sediment class. Dashed grey circles have radiuses of 250, 500 and 1000 m. The 10, 50 and 100 mg.L^{-1} contours are shown in black.

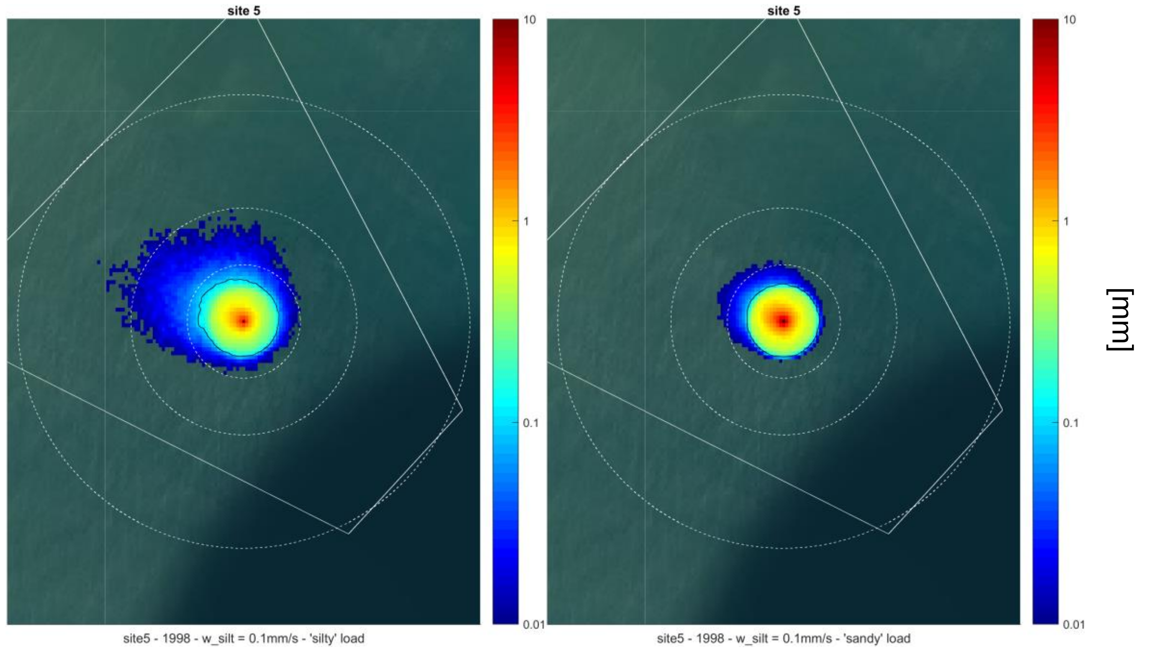

Figure 3.17 Probabilistic sediment deposition fields resulting from the disposal of one hopper load of the Pukunui vessel (V=480 m^3), derived from the annual La Niña period (June 1998-June 1999). The results compare the plumes associated with the release of a sediment load composed of 80% silt and 20 % sand (left), and 20% silt 80% sand (right). The results assumed a settling a settling velocity of 0.1 mm.s^{-1} for the cohesive sediment class. Dashed grey circles have radiuses of 250, 500 and 1000 m. The 10, 50 and 100 mg.L^{-1} contours are shown in black.

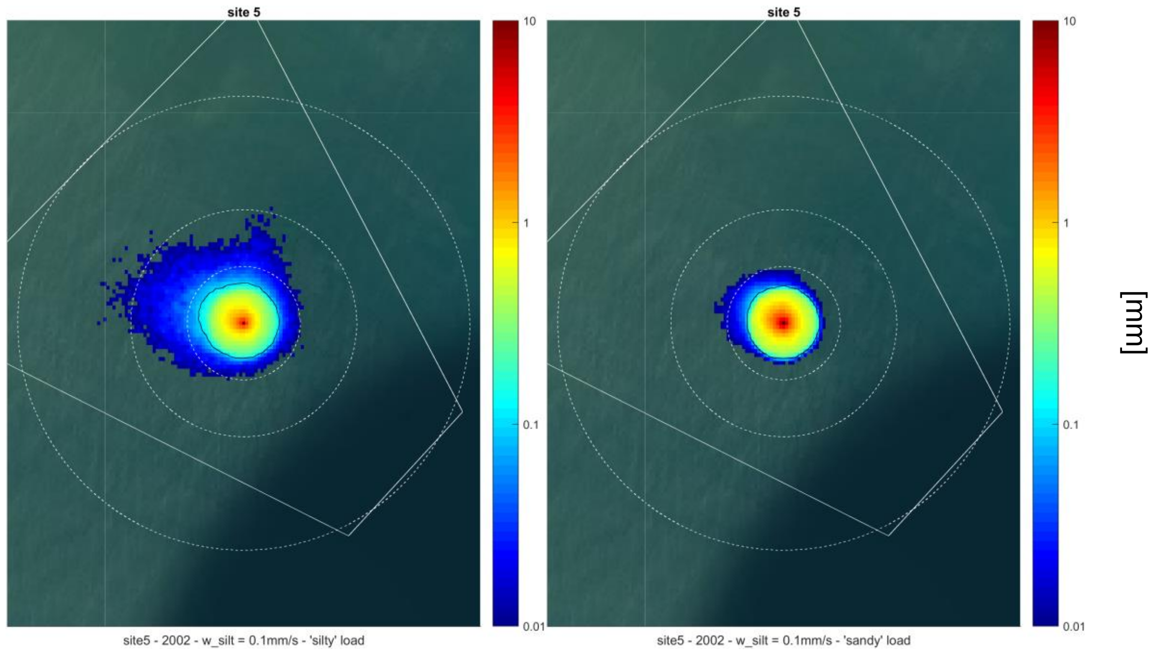

Figure 3.18 Probabilistic sediment deposition fields resulting from the disposal of one hopper load of the Pukunui vessel (V=480 m^3), derived from the annual El Niño period (June 2002-June 2003). The results compare the plumes associated with the release of a sediment load composed of 80% silt and 20 % sand (left), and 20% silt 80% sand (right). The results assumed a settling a settling velocity of 0.1 mm.s^{-1} for the cohesive sediment class. Dashed grey circles have radiuses of 250, 500 and 1000 m. The 10, 50 and 100 mg.L^{-1} contours are shown in black.

3.3. Suspended sediment (*SSC*) plumes and deposition statistics – Pukunui vessel

This section supplements the probabilistic results by assessing the plume pattern variability over time in response to the instantaneous forcing. This is done by computing *SSC* and deposition fields at each model time step (i.e. rather than combining all trajectory outputs into one cloud). The approach allows defining statistical properties of the *SSC* plume and deposition fields such as mean and median or extremes (e.g. 90th percentile), as well as information on exceedance times (i.e. percentage of time a given *SSC* threshold is exceeded).

Note these results assume the disposal of a hopper load composed predominantly of silt material (i.e. 80% silt, 20 %); finer sediment will remain much longer in suspension in the water column and are therefore the most problematic with respect to the spatial excursion of the produced sediment plumes.

3.3.1. Mean, median and 90th percentile *SSC* plumes and deposition

Since the computation of the time-varying *SSC* and deposition spatial fields can become very expensive computationally, the two 1-month periods of January and July were selected in each annual simulations (El Niño /La Niña) to capture typical winter and summer forcing conditions. Results are presented for sediment discharged at the centre of the disposal ground.

The mean, median and 90th percentile *SSC* plumes for a summer period, assuming a settling velocity of 1 mm.s^{-1} for the cohesive sediment, are shown in Figure 3.19 and Figure 3.20, while results using a smaller settling velocity of 0.1 mm.s^{-1} are provided in Figure 3.21 and Figure 3.22. Resulting deposition footprints are provided in Figure 3.23 to Figure 3.26.

Not surprisingly, the mean and median footprint patterns are similar to the probabilistic results outlined in Section 3.2. Here, the 90th footprints are useful to assess largest expected plume dispersion (extents exceeded only 10% of the time). For the results using a settling velocity of 1 mm.s^{-1}, the highest *SSC* (bottom layer) of order ~100-1000 mg.L^{-1} are generally contained within 250m of the release point, dropping to less than 10 mg.L^{-1} or less at 300-350 m from release. The use of a smaller settling velocity of 0.1 mm.s^{-1} results in a relative widening of the general *SSC* footprints; bottom *SSC* levels immediately in the immediate vicinity of the release are relatively smaller than those predicted using 1 mm.s^{-1} , however the footprint of the 10 mg.L^{-1} contour can extend up to 600 m from release.

Equivalent results for the winter period are provided in Figure 3.27 to Figure 3.34. Some modulations of the plume shapes are visible, as with previous results, but there are no significant differences in terms of the largest footprints excursions.

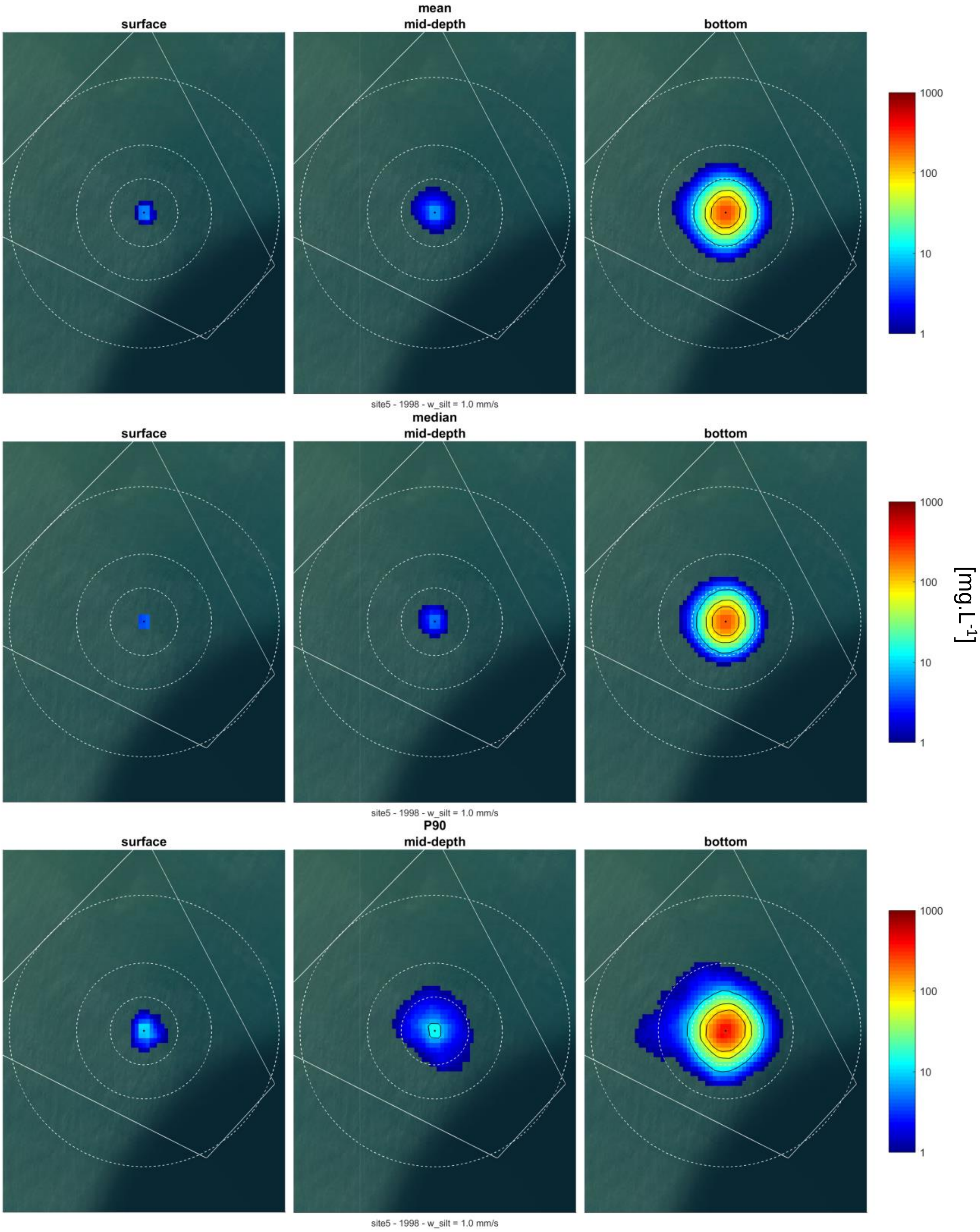

Figure 3.19 Mean, median, and 90th percentile *SSC* fields for disposal at the centre of the disposal ground using the Pukunui vessel (V=480 m^3) computed for January 1999 (during the La Niña episode). The results assumed a settling velocity of 1.0 mm.s^{-1} for the cohesive sediment class. Dashed grey circles have radiuses of 250, 500 and 1000 m. Dashed grey circles have radiuses of 250, 500 and 1000 m. The 10, 50 and 100 mg.L^{-1} contours are shown in black.

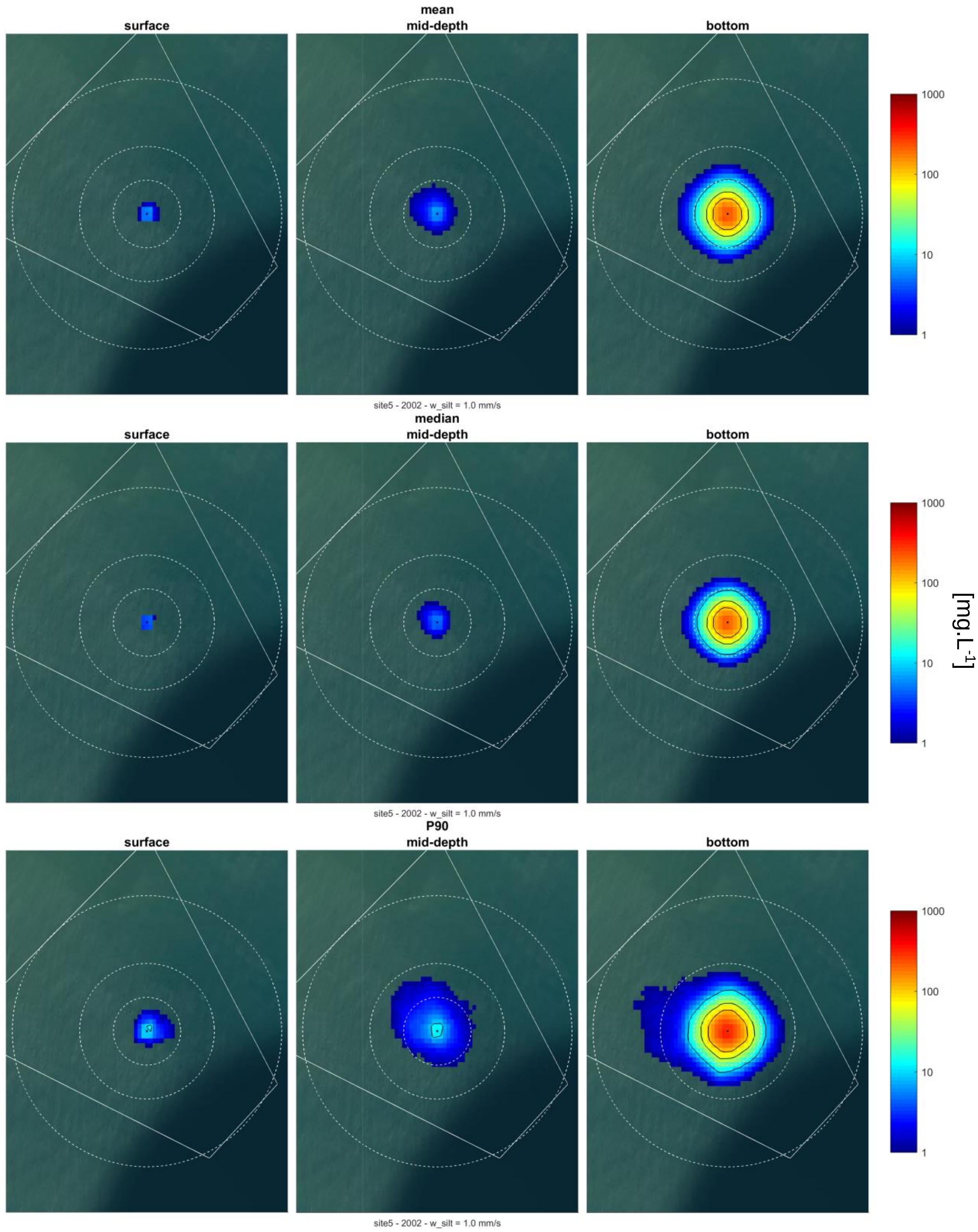

Figure 3.20 Mean, median, and 90th percentile *SSC* fields for disposal at the centre of the disposal ground using the Pukunui vessel (V=480 m^3) computed for January 2003 (during the El Niño episode). The results assumed a settling velocity of 1.0 mm.s^{-1} for the cohesive sediment class. Dashed grey circles have radiuses of 250, 500 and 1000 m. Dashed grey circles have radiuses of 250, 500 and 1000 m. The 10, 50 and 100 mg.L^{-1} contours are shown in black.

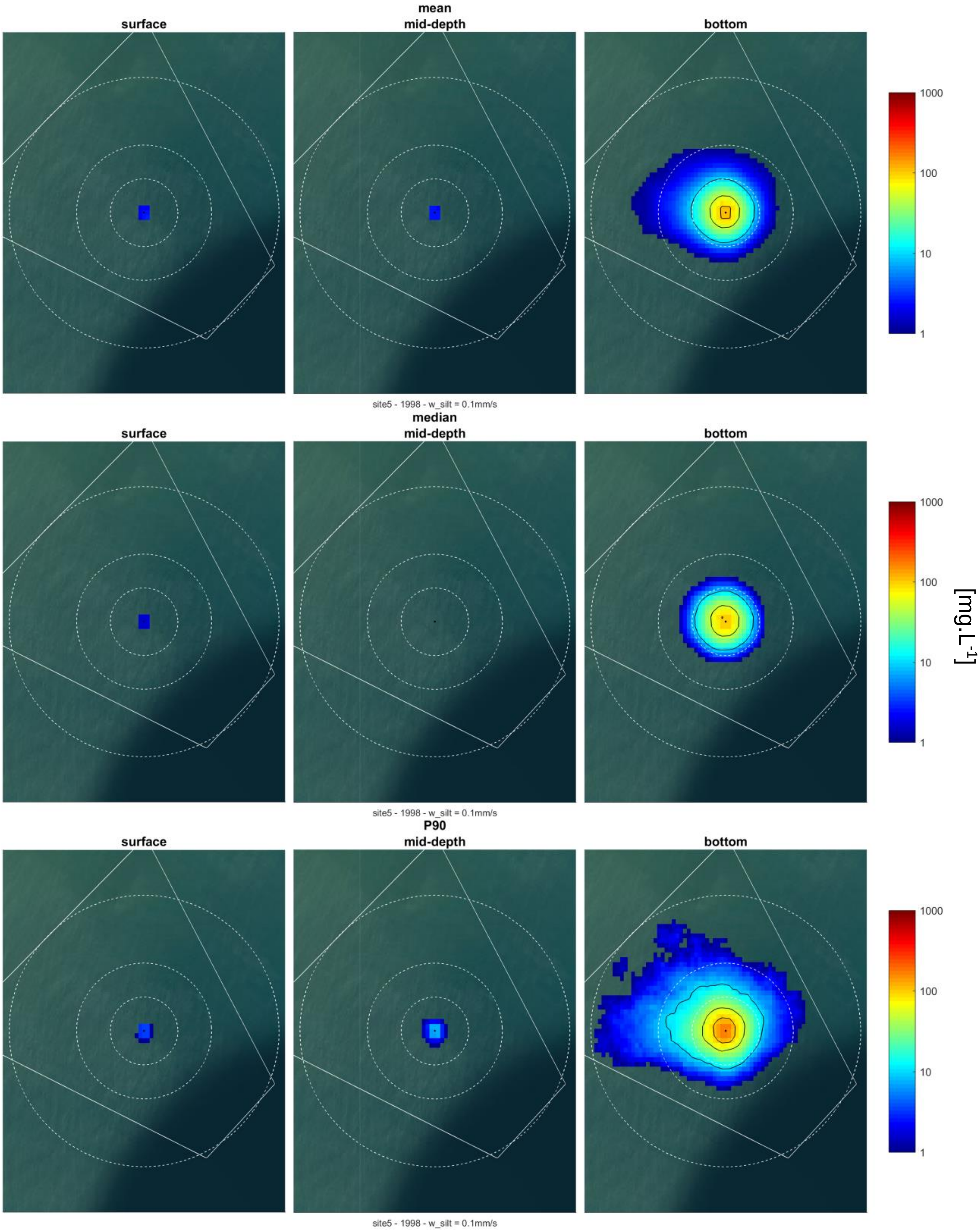

Figure 3.21 Mean, median, and 90th percentile *SSC* fields for disposal at the centre of the disposal ground using the Pukunui vessel (V=480 m^3) computed for January 1999 (during the La Niña episode). The results assumed a settling velocity of 0.1 $mm.s^{-1}$ for the cohesive sediment class. Dashed grey circles have radiuses of 250, 500 and 1000 m. Dashed grey circles have radiuses of 250, 500 and 1000 m. The 10, 50 and 100 $mg.L^{-1}$ contours are shown in black.

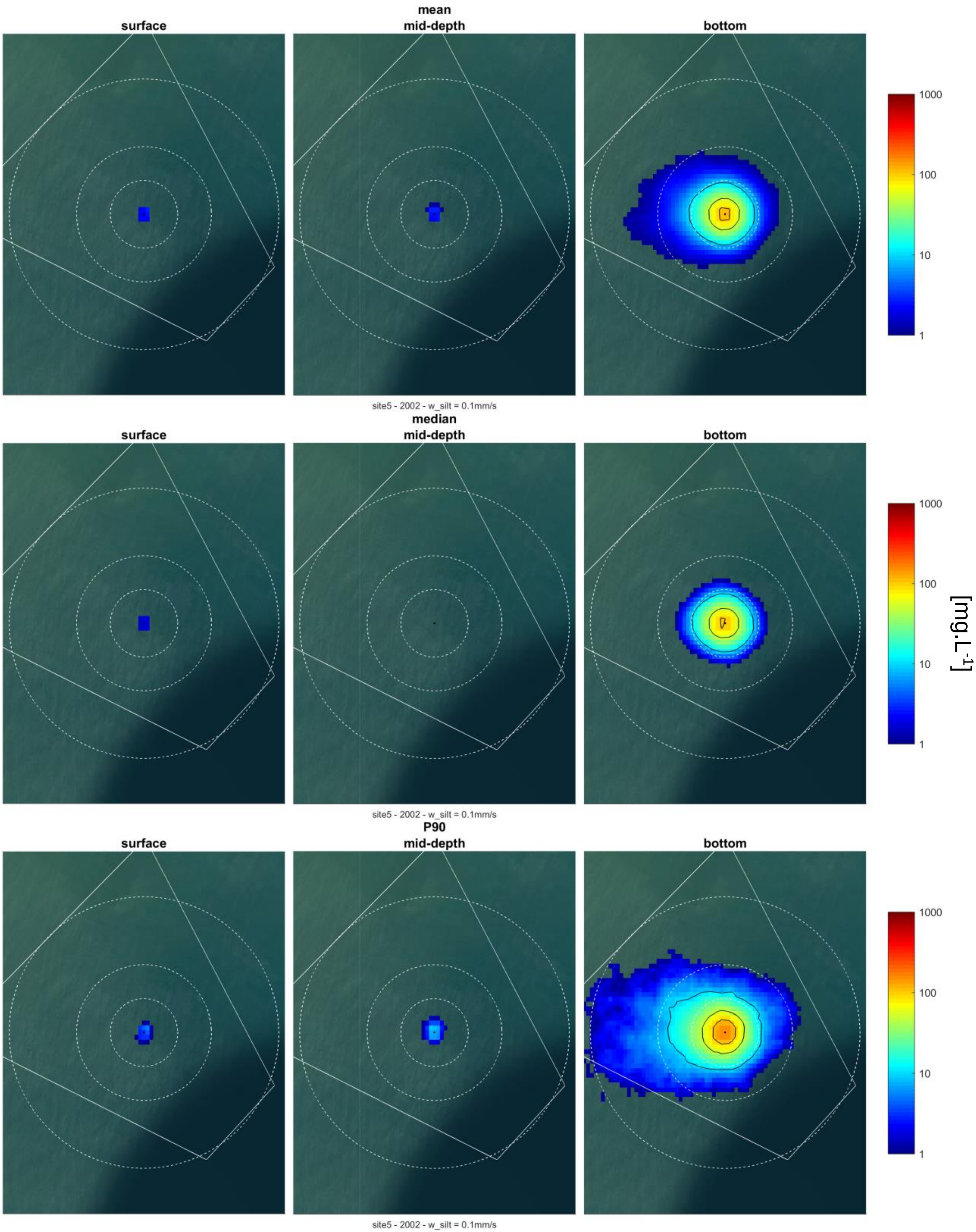

Figure 3.22 Mean, median, and 90th percentile *SSC* fields for disposal at the centre of the disposal ground using the Pukunui vessel (V=480 m^3) computed for January 2003 (during the El Niño episode). The results assumed a settling velocity of 0.1 mm.s^{-1} for the cohesive sediment class. Dashed grey circles have radiuses of 250, 500 and 1000 m. Dashed grey circles have radiuses of 250, 500 and 1000 m. The 10, 50 and 100 mg.L^{-1} contours are shown in black.

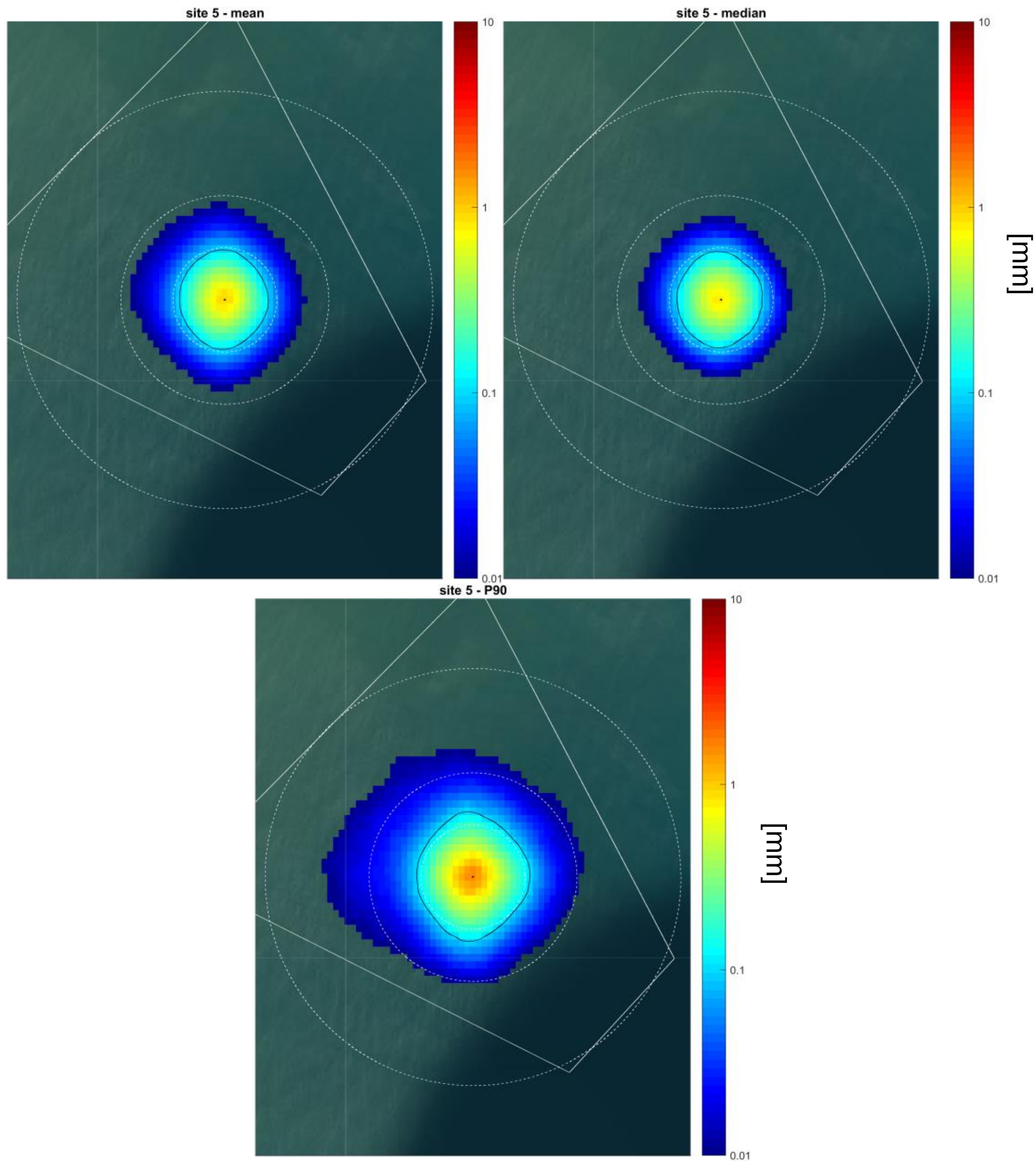

Figure 3.23 Mean, median, and 90th percentile deposition fields for disposal at the centre of the disposal ground using the Pukunui vessel (V=480 m^3) computed for January 1999 (during the La Niña episode). The results assumed a settling velocity of 1.0 mm.s^{-1} for the cohesive sediment class. Dashed grey circles have radiuses of 250, 500 and 1000 m. Dashed grey circles have radiuses of 250, 500 and 1000 m. The 0.1 mm contour is shown in black.

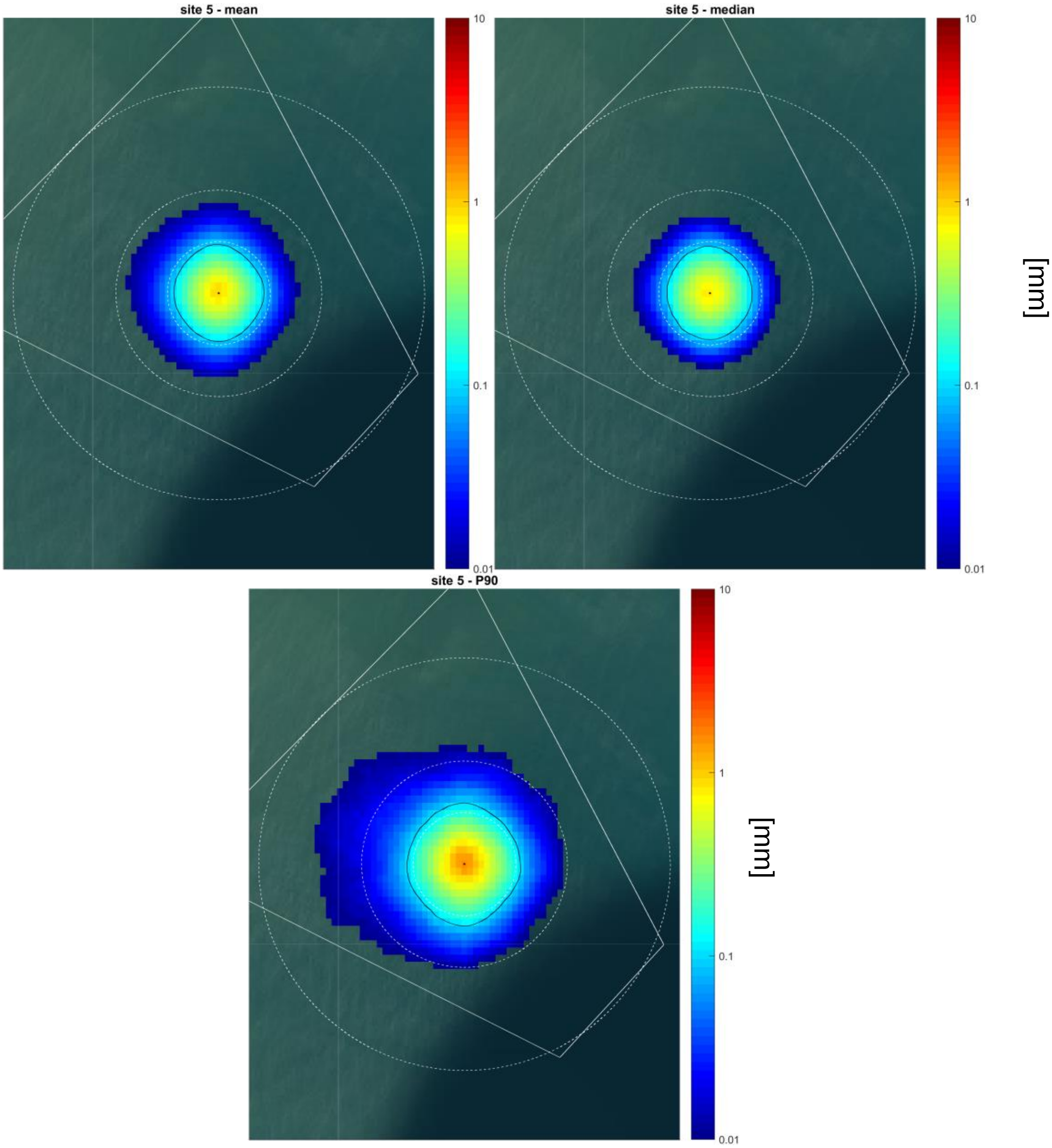

Figure 3.24 Mean, median, and 90th percentile deposition fields for disposal at the centre of the disposal ground using the Pukunui vessel (V=480 m^3) computed for January 2003 (during the El Niño episode). The results assumed a settling velocity of 1.0 $mm.s^{-1}$ for the cohesive sediment class. Dashed grey circles have radiuses of 250, 500 and 1000 m. Dashed grey circles have radiuses of 250, 500 and 1000 m. The 0.1 mm contour is shown in black.

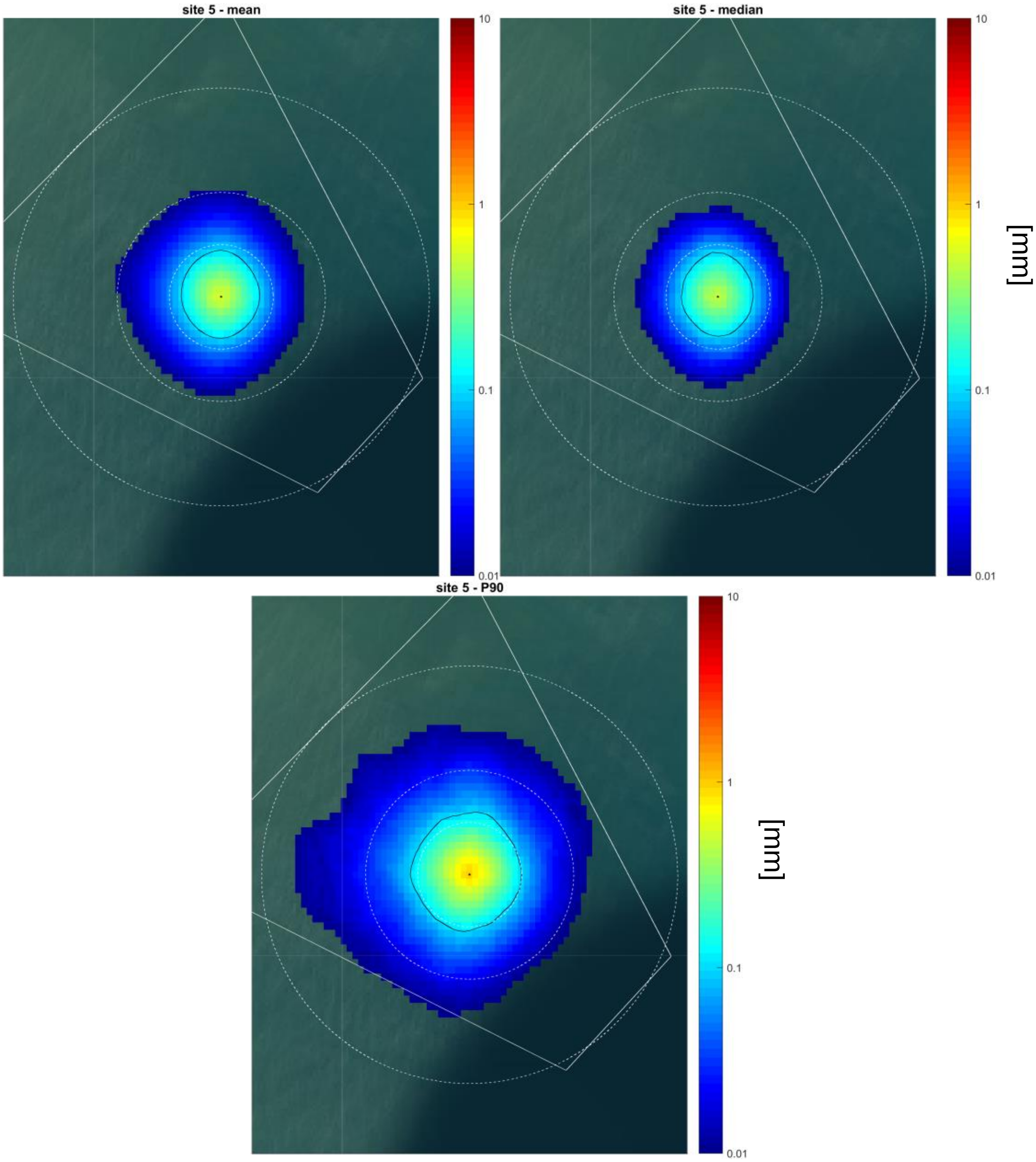

Figure 3.25 Mean, median, and 90th percentile deposition fields for disposal at the centre of the disposal ground using the Pukunui vessel (V=480 m^3) computed for January 1999 (during the La Niña episode). The results assumed a settling velocity of 0.1 mm.s^{-1} for the cohesive sediment class. Dashed grey circles have radiuses of 250, 500 and 1000 m. Dashed grey circles have radiuses of 250, 500 and 1000 m. The 0.1 mm contour is shown in black.

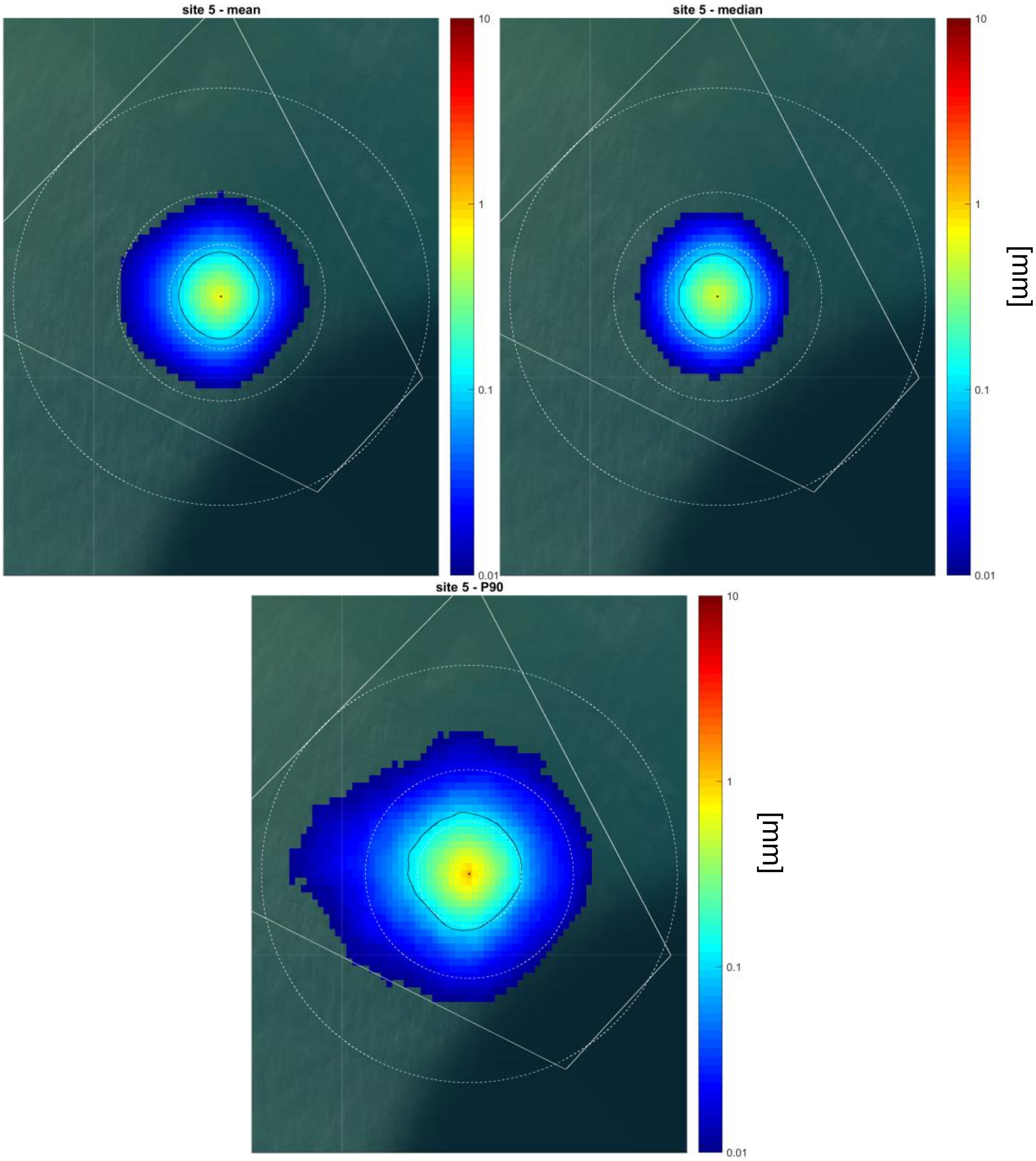

Figure 3.26 Mean, median, and 90th percentile deposition fields for disposal at the centre of the disposal ground using the Pukunui vessel (V=480 m^3) computed for January 2003 (during the El Niño episode). The results assumed a settling velocity of 0.1 $mm.s^{-1}$ for the cohesive sediment class. Dashed grey circles have radiuses of 250, 500 and 1000 m. Dashed grey circles have radiuses of 250, 500 and 1000 m. The 0.1 mm contour is shown in black.

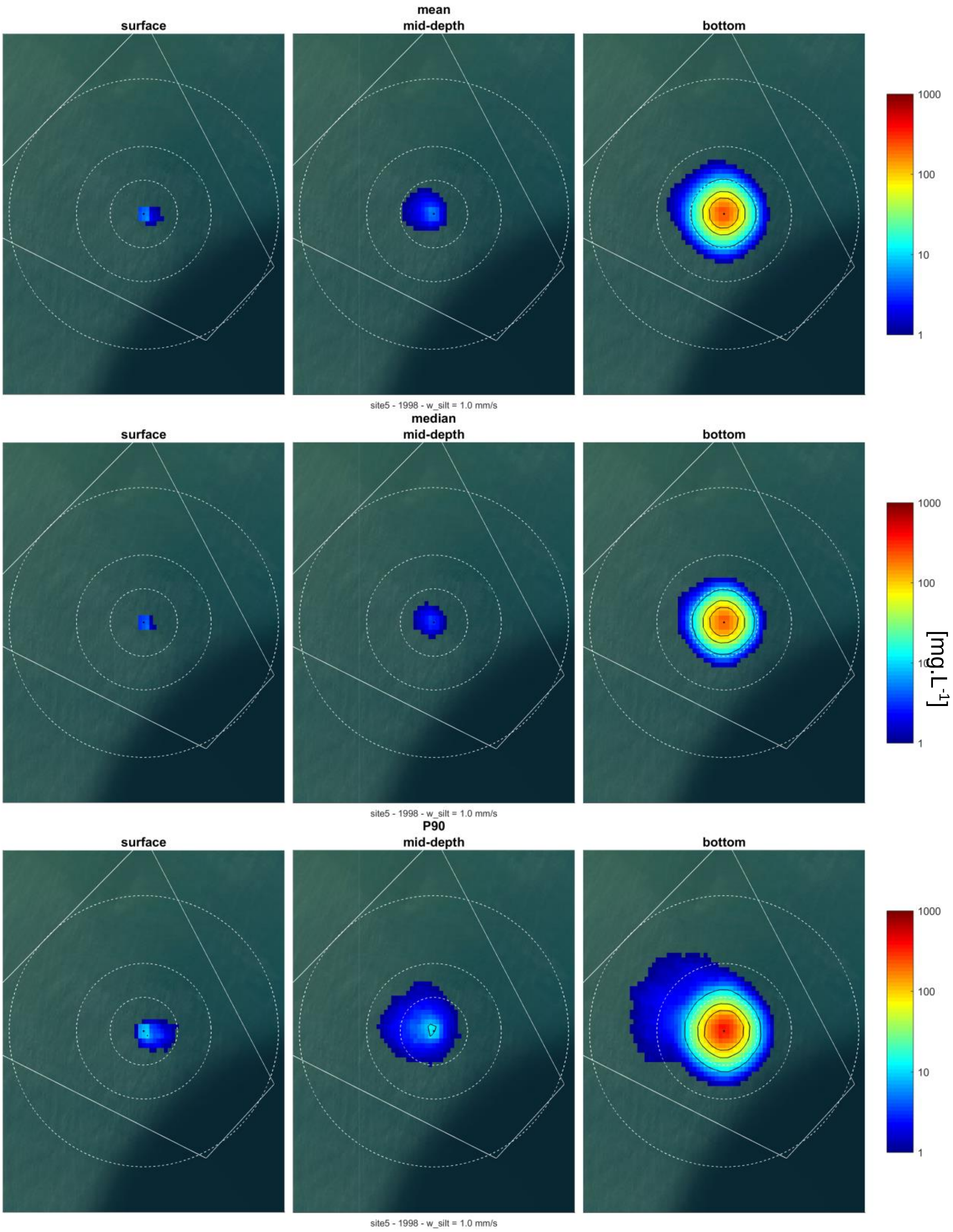

Figure 3.27 Mean, median, and 90th percentile *SSC* fields for disposal at the centre of the disposal ground using the Pukunui vessel (V=480 m^3) computed for July 1998 (during the La Niña episode). The results assumed a settling velocity of 1.0 mm.s^{-1} for the cohesive sediment class. Dashed grey circles have radiuses of 250, 500 and 1000 m. Dashed grey circles have radiuses of 250, 500 and 1000 m. The 10, 50 and 100 mg.L-1 mm contour are shown in black.

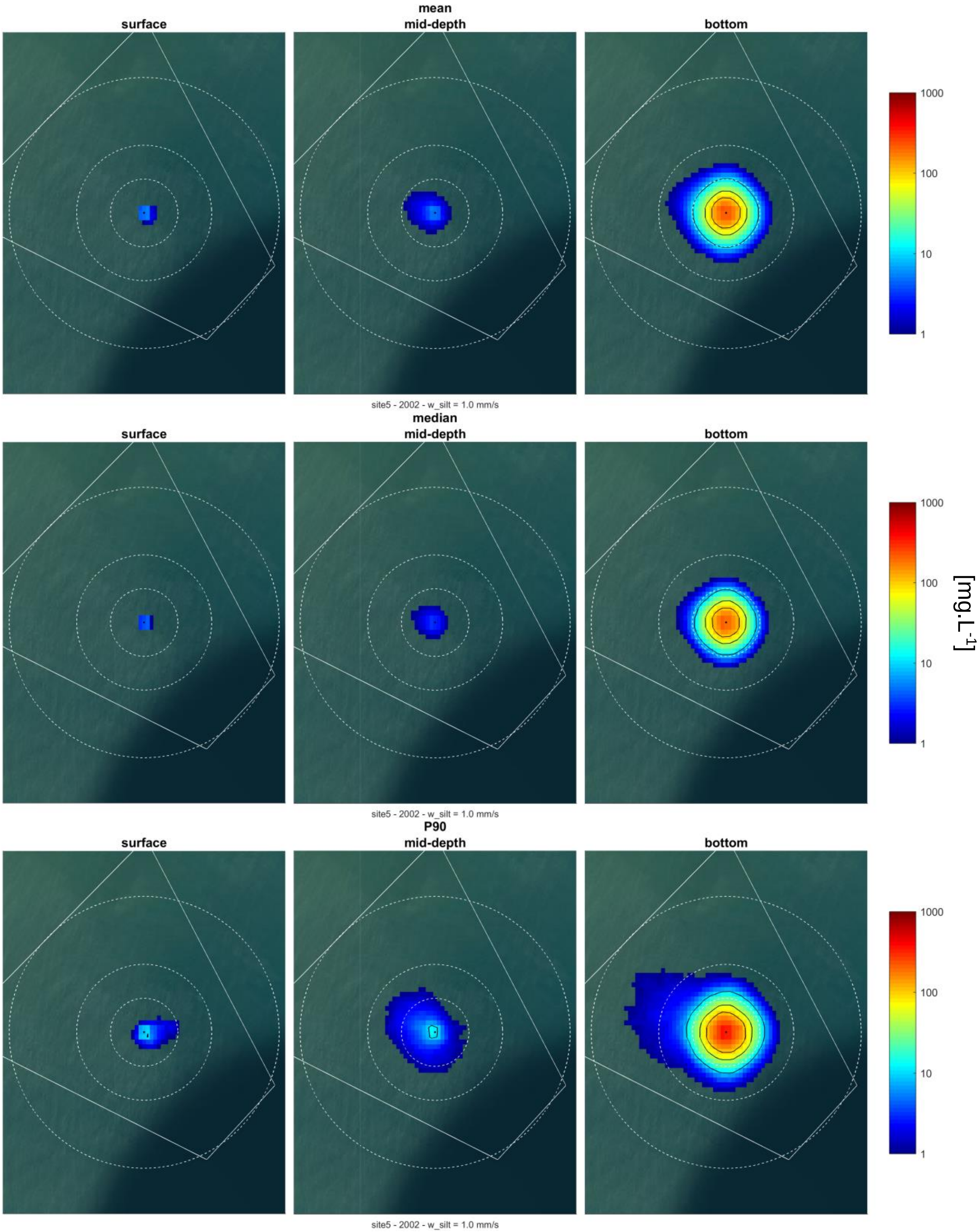

Figure 3.28 Mean, median, and 90th percentile *SSC* fields for disposal at the centre of the disposal ground using the Pukunui vessel (V=480 m^3) computed for July 2002 (during the El Niño episode). The results assumed a settling velocity of 1.0 mm.s^{-1} for the cohesive sediment class. Dashed grey circles have radiuses of 250, 500 and 1000 m. Dashed grey circles have radiuses of 250, 500 and 1000 m. The 10, 50 and 100 mg.L-1 mm contour are shown in black.

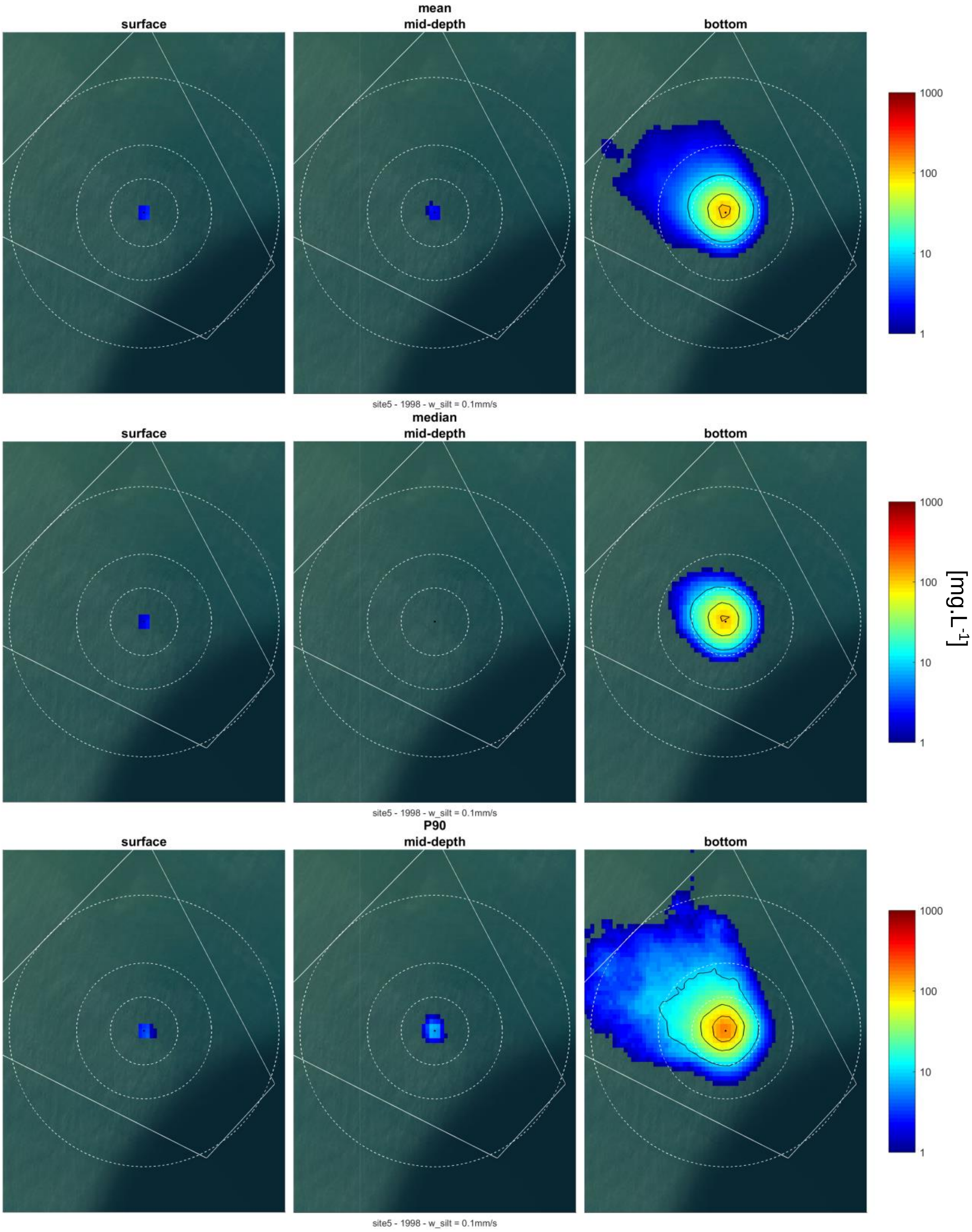

Figure 3.29 Mean, median, and 90th percentile *SSC* fields for disposal at the centre of the disposal ground using the Pukunui vessel (V=480 m^3) computed for July 1998 (during the La Niña episode). The results assumed a settling velocity of 0.1 $mm.s^{-1}$ for the cohesive sediment class. Dashed grey circles have radiuses of 250, 500 and 1000 m. Dashed grey circles have radiuses of 250, 500 and 1000 m. The 10, 50 and 100 mg.L-1 mm contour are shown in black.

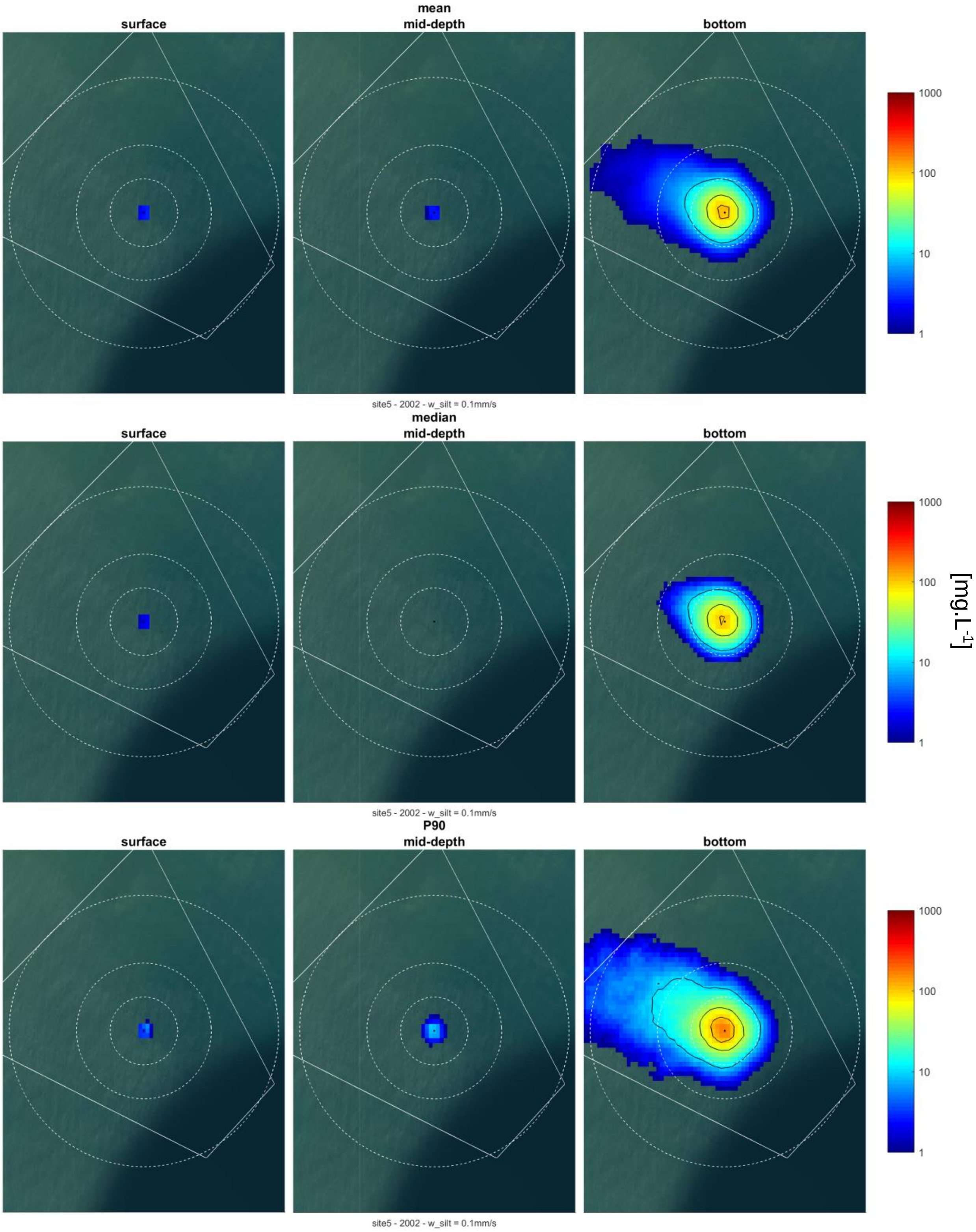

Figure 3.30 Mean, median, and 90th percentile *SSC* fields for disposal at the centre of the disposal ground using the Pukunui vessel (V=480 m^3) computed for July 2002 (during the El Niño episode). The results assumed a settling velocity of 0.1 $mm.s^{-1}$ for the cohesive sediment class. Dashed grey circles have radiuses of 250, 500 and 1000 m. Dashed grey circles have radiuses of 250, 500 and 1000 m. The 10, 50 and 100 mg.L-1 mm contour are shown in black.

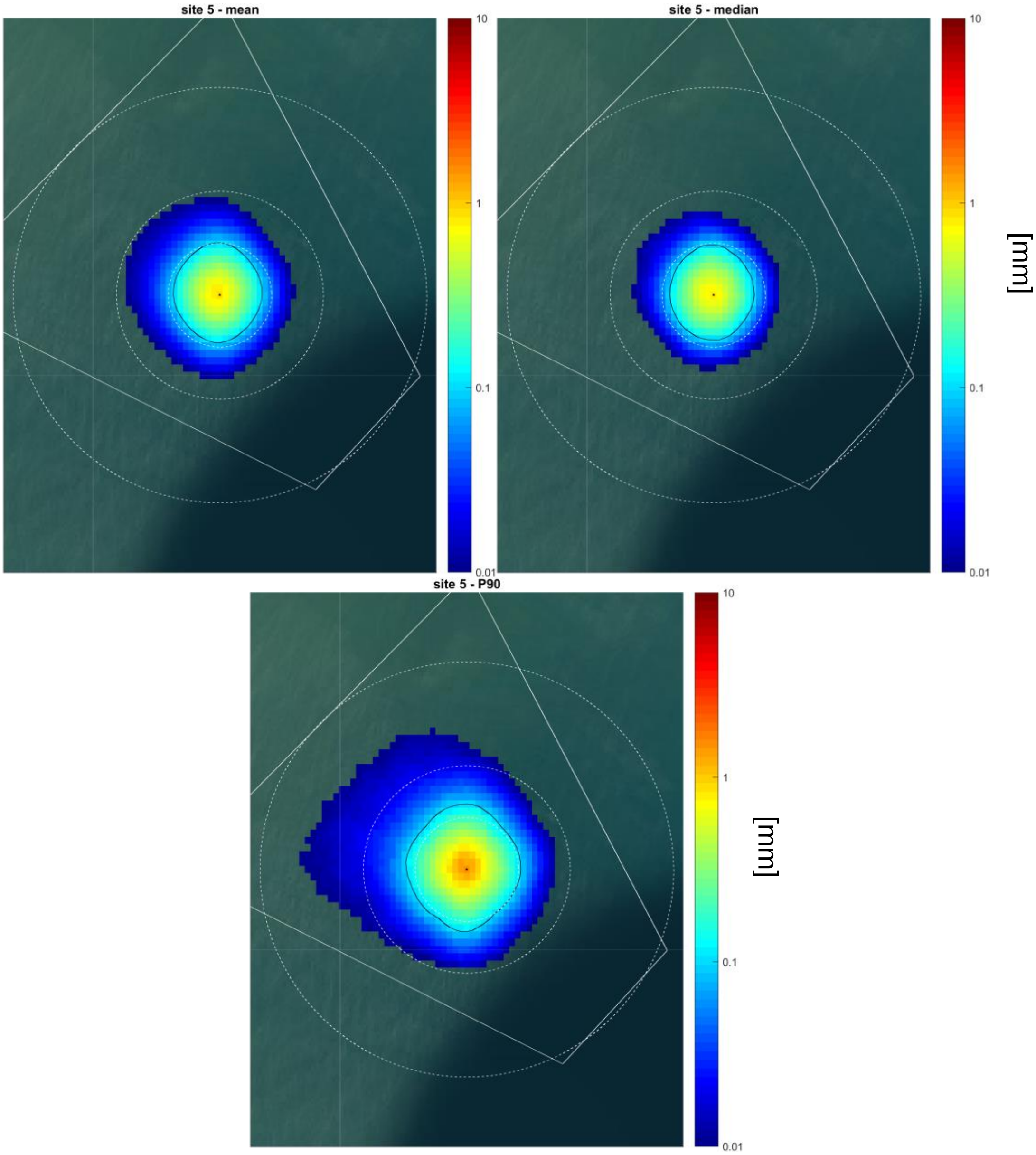

Figure 3.31 Mean, median, and 90th percentile deposition fields for disposal at the centre of the disposal ground using the Pukunui vessel (V=480 m^3) computed for July 1998 (during the La Niña episode). The results assumed a settling velocity of 1.0 mm.s^{-1} for the cohesive sediment class. Dashed grey circles have radiuses of 250, 500 and 1000 m. Dashed grey circles have radiuses of 250, 500 and 1000 m. The 0.1 mm contour is shown in black.

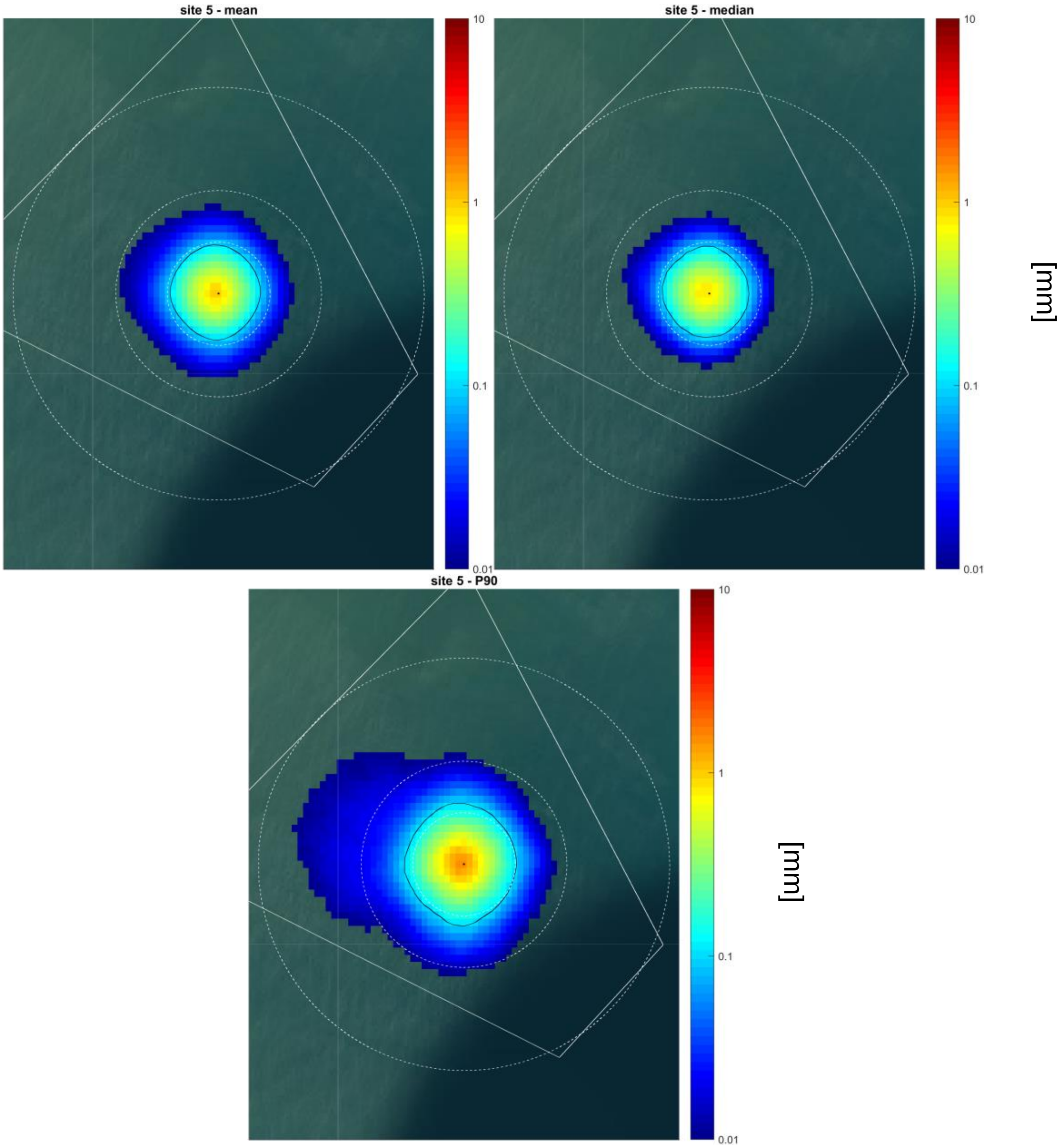

Figure 3.32 Mean, median, and 90th percentile deposition fields for disposal at the centre of the disposal ground using the Pukunui vessel (V=480 m^3) computed for July 2002 (during the El Niño episode). The results assumed a settling velocity of 1.0 mm.s^{-1} for the cohesive sediment class. Dashed grey circles have radiuses of 250, 500 and 1000 m. Dashed grey circles have radiuses of 250, 500 and 1000 m. The 0.1 mm contour is shown in black.

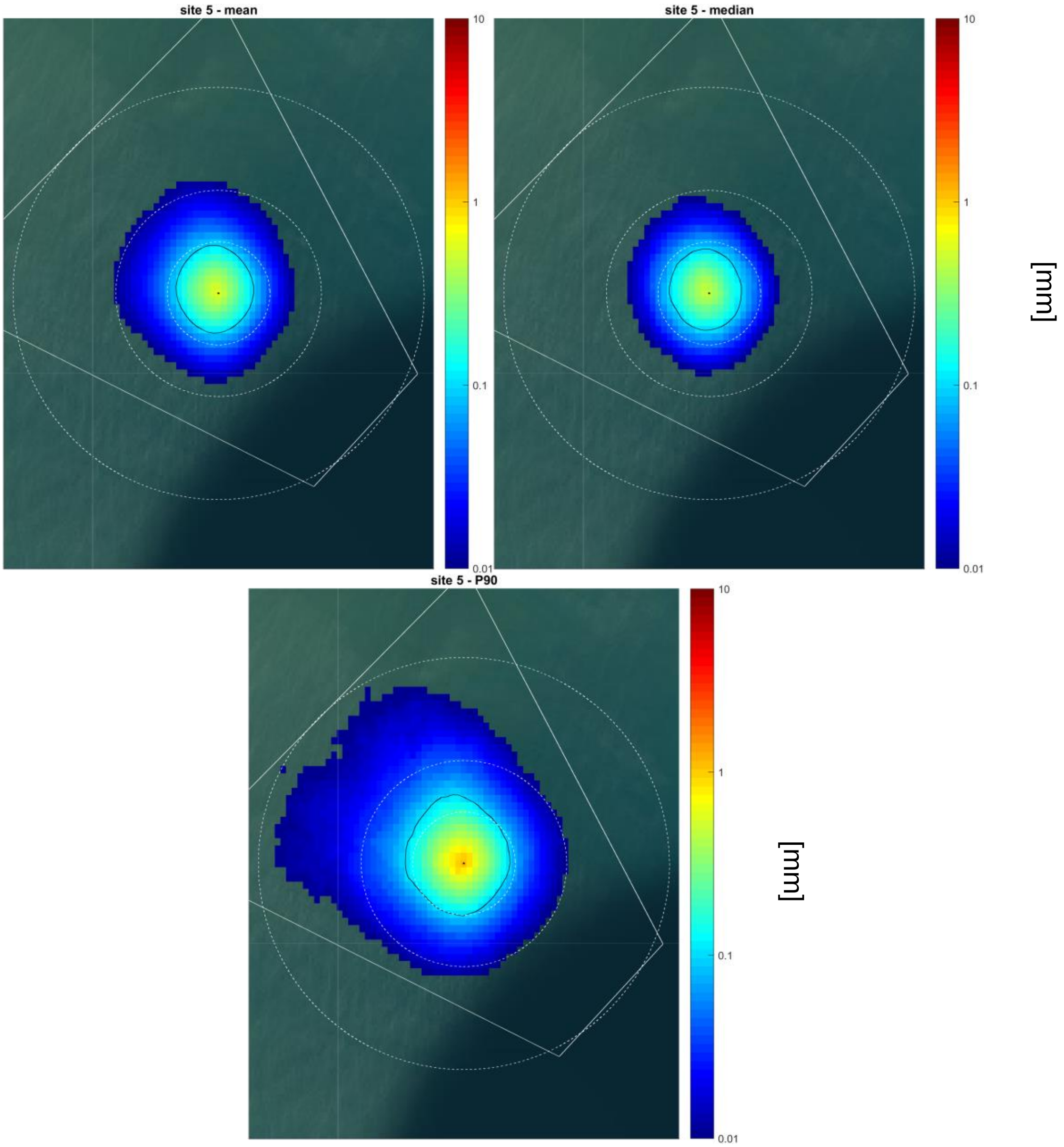

Figure 3.33 Mean, median, and 90th percentile deposition fields for disposal at the centre of the disposal ground using the Pukunui vessel (V=480 m^3) computed for July 1998 (during the La Niña episode). The results assumed a settling velocity of 0.1 $mm.s^{-1}$ for the cohesive sediment class. Dashed grey circles have radiuses of 250, 500 and 1000 m. Dashed grey circles have radiuses of 250, 500 and 1000 m. The 0.1 mm contour is shown in black.

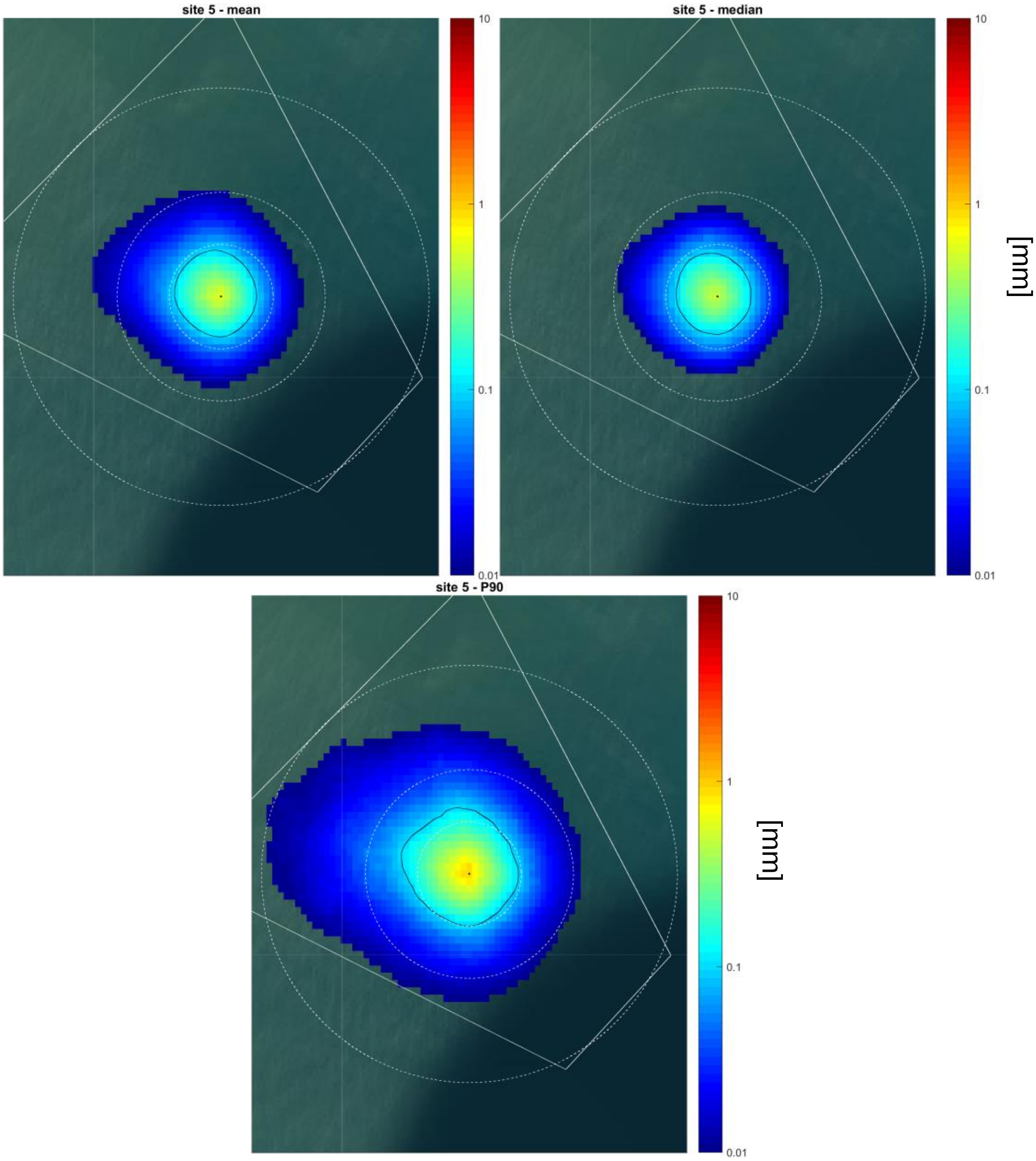

Figure 3.34 Mean, median, and 90th percentile deposition fields for disposal at the centre of the disposal ground using the Pukunui vessel (V=480 m^3) computed for July 2002 (during the El Niño episode). The results assumed a settling velocity of 0.1 mm.s^{-1} for the cohesive sediment class. Dashed grey circles have radiuses of 250, 500 and 1000 m. Dashed grey circles have radiuses of 250, 500 and 1000 m. The 0.1 mm contour is shown in black.

3.3.2. Exceedance time

Exceedance times represent the percentages of time a given *SSC* threshold is exceeded. This is often a useful metric in the context of ecological impact assessment. The exceedance times presented are computed relative to three *SSC* threshold of 10, 50, and 100 $mg.L^{-1}$, and assume a disposal cycle of 4 hours for the Pukunui, sustained continuously throughout the 1-month simulations periods. We note that in reality it is most likely that disposal will be discontinued overnight, and disposal is not expected to be repeated at a single location repeatedly; therefore presented results can be considered conservative.

Results for the <u>summer</u> period (January), assuming a settling velocity of 1 $mm.s^{-1}$ for the cohesive sediment, are shown in Figure 3.35 and Figure 3.36 for the La Niña and El Niño context respectively. The predicted exceedance time maps indicate that all three thresholds will be consistently exceeded (~30% of the time) in the bottom layer of the water column within a radius of 200-250 m, which is attributed to the density current source term. Exceedance time percentage remain very limited in the surface and mid water levels, even for the smallest *SSC* threshold considered (10% of the time or less, contained within ~50-100 m of release site).

The use of a smaller settling velocity (Figure 3.37 and Figure 3.38) results in an increase of the *visible* footprint of exceedance times in the bottom layer for the smallest *SSC* threshold considered (10 $mg.L^{-1}$), with exceedance times of order 3-5% extend up to 500 m from the disposal ground centre. This is though accompanied by a reduction of effective exceedance time within a radius of ~200m from the release relative to the results using 1$mm.s^{-1}$. This feature can be attributed to the fact that although lighter sediment, settling slower, will have the potential to travel further from the source, this will be accompanied by a relative increase of the *SSC* dilution (i.e. smaller absolute *SSC* magnitudes). This also causes the relative reduction of exceedance times in the surface and mid depth levels for the 0.1 $mm.s^{-1}$ results (e.g. Figure 3.35 versus Figure 3.37); the increased dilution of the *SSC* plume results in smaller exceedance time with respect to the fixed *SSC* thresholds.

The equivalent results for the winter monthly period (July) are shown in Figure 3.39 to Figure 3.42. These results reproduce the general modulations of the *SSC* plume patterns, for example with respect to elongation direction (e.g. see Section 3.3.1), but overall extents and magnitude remain comparable to these predicted for the summer period.

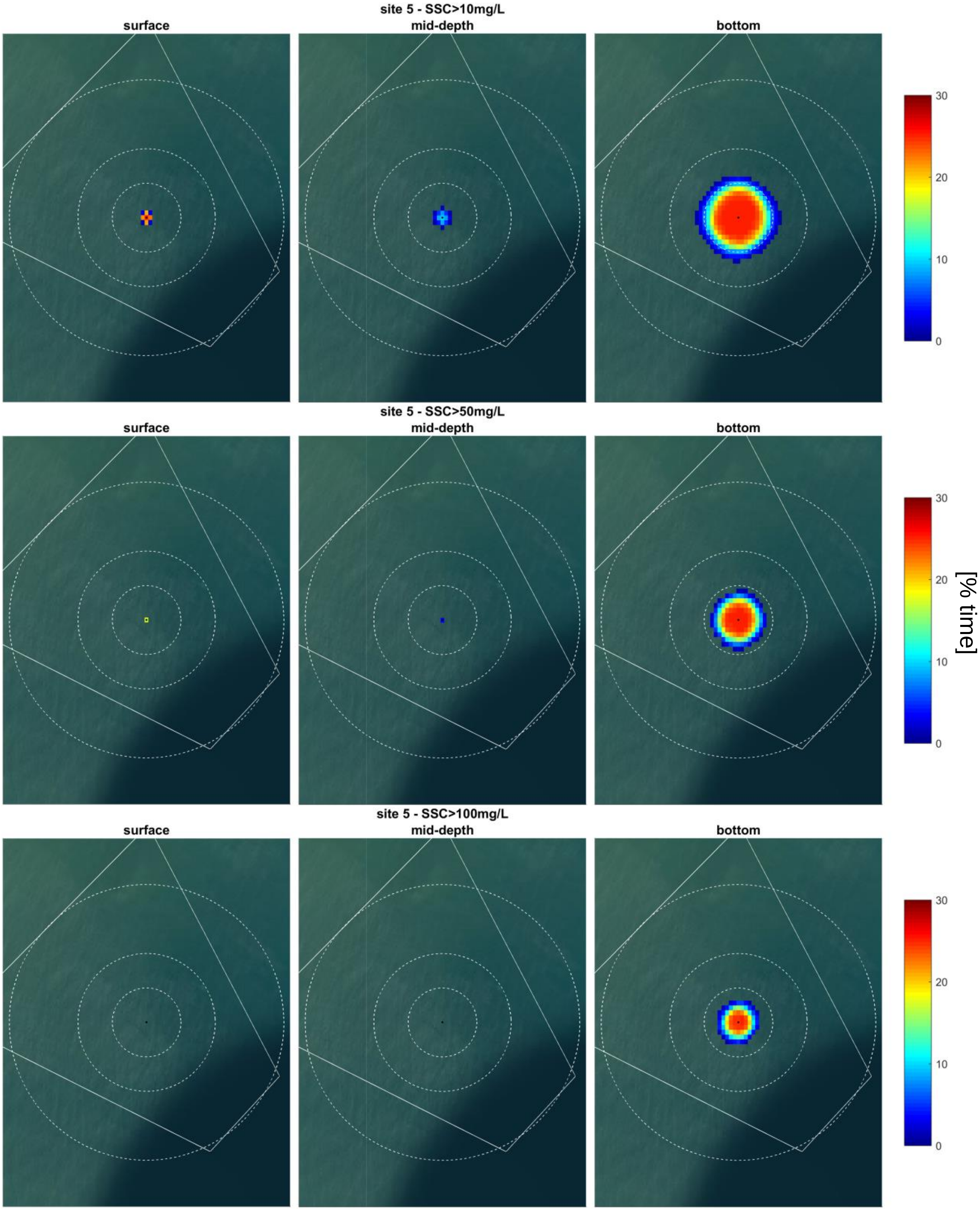

Figure 3.35 *SSC* exceedance for disposal at the centre of the disposal ground using the Pukunui vessel (V=480 m^3) computed for January 1999 (during the La Niña episode), for three *SSC* thresholds, 10, 50 and 100 mg.L^{-1}. The results assumed a settling velocity of 1.0 mm.s^{-1} for the cohesive sediment class. Dashed grey circles have radiuses of 250, 500 and 1000 m. Dashed grey circles have radiuses of 250, 500 and 1000 m.

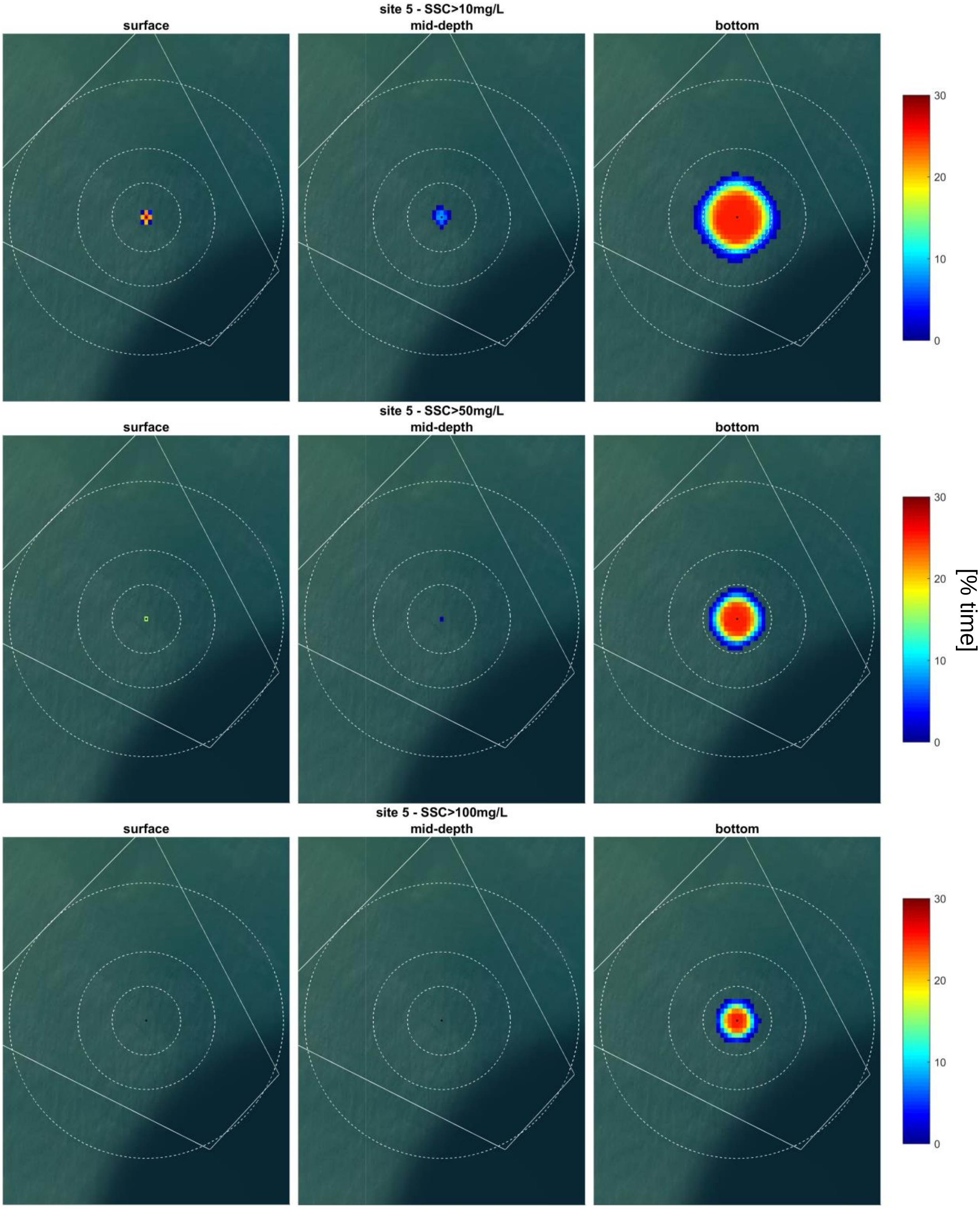

Figure 3.36 *SSC* exceedance for disposal at the centre of the disposal ground using the Pukunui vessel (V=480 m^3) computed for January 2003 (during the El Niño episode) , for three *SSC* thresholds, 10, 50 and 100 $mg.L^{-1}$. The results assumed a settling velocity of 1.0 $mm.s^{-1}$ for the cohesive sediment class. Dashed grey circles have radiuses of 250, 500 and 1000 m. Dashed grey circles have radiuses of 250, 500 and 1000 m.

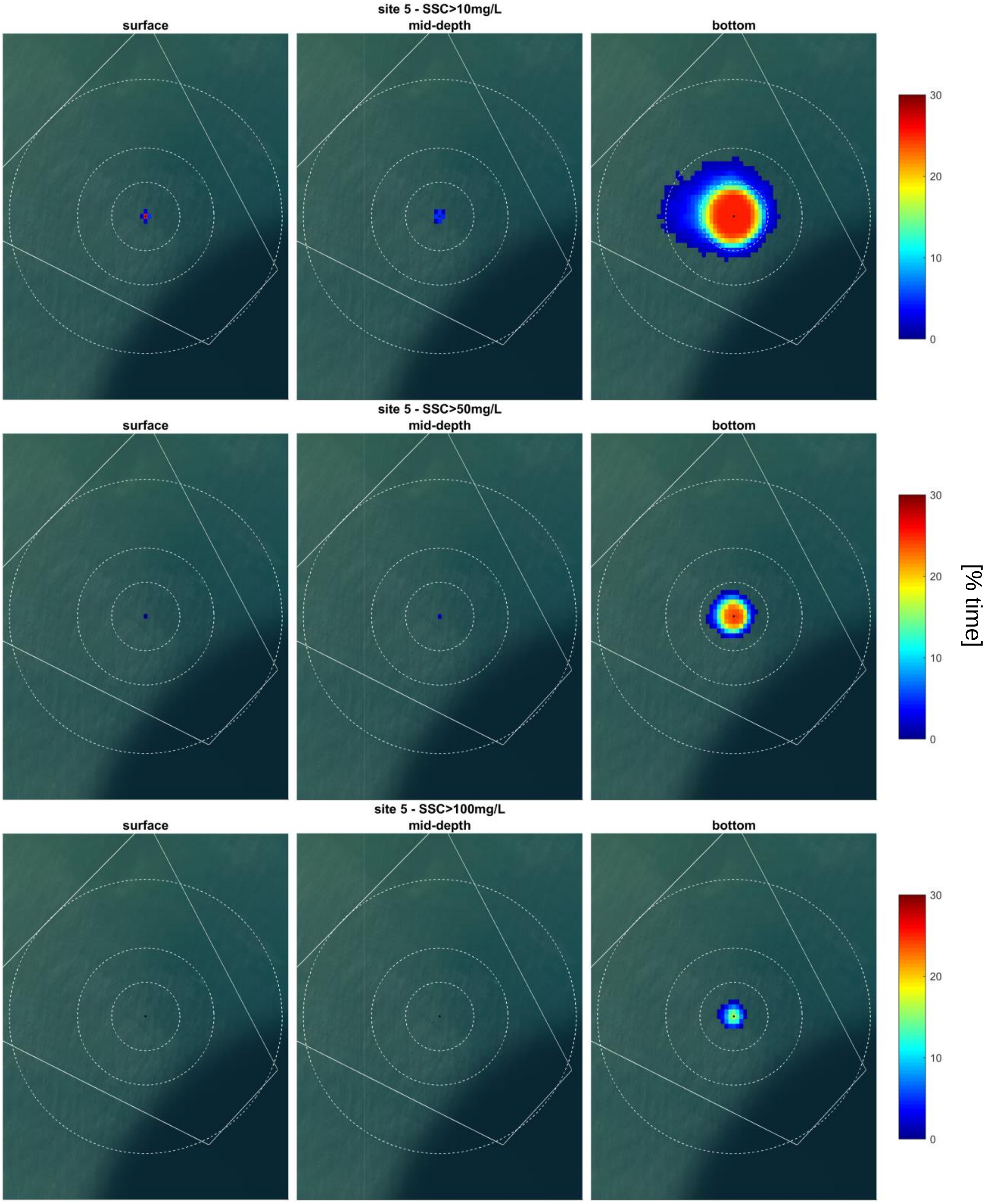

Figure 3.37 *SSC* exceedance for disposal at the centre of the disposal ground using the Pukunui vessel (V=480 m^3) computed for January 1999 (during the La Niña episode) , for three *SSC* thresholds, 10, 50 and 100 mg.L^{-1}. The results assumed a settling velocity of 0.1 mm.s^{-1} for the cohesive sediment class. Dashed grey circles have radiuses of 250, 500 and 1000 m. Dashed grey circles have radiuses of 250, 500 and 1000 m.

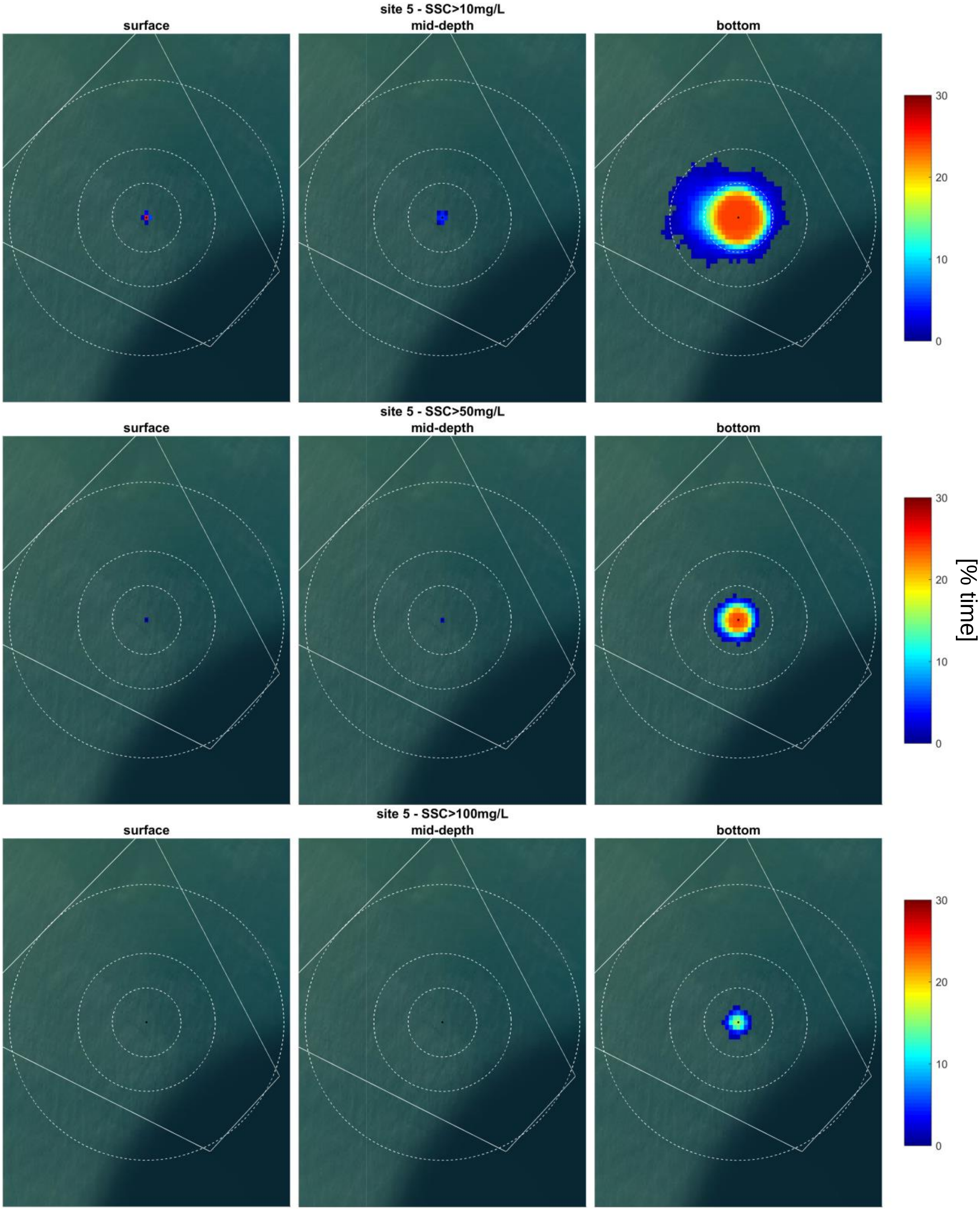

Figure 3.38 *SSC* exceedance for disposal at the centre of the disposal ground using the Pukunui vessel (V=480 m^3) computed for January 2003 (during the El Niño episode) , for three *SSC* thresholds, 10, 50 and 100 $mg.L^{-1}$. The results assumed a settling velocity of 0.1 $mm.s^{-1}$ for the cohesive sediment class. Dashed grey circles have radiuses of 250, 500 and 1000 m. Dashed grey circles have radiuses of 250, 500 and 1000 m.

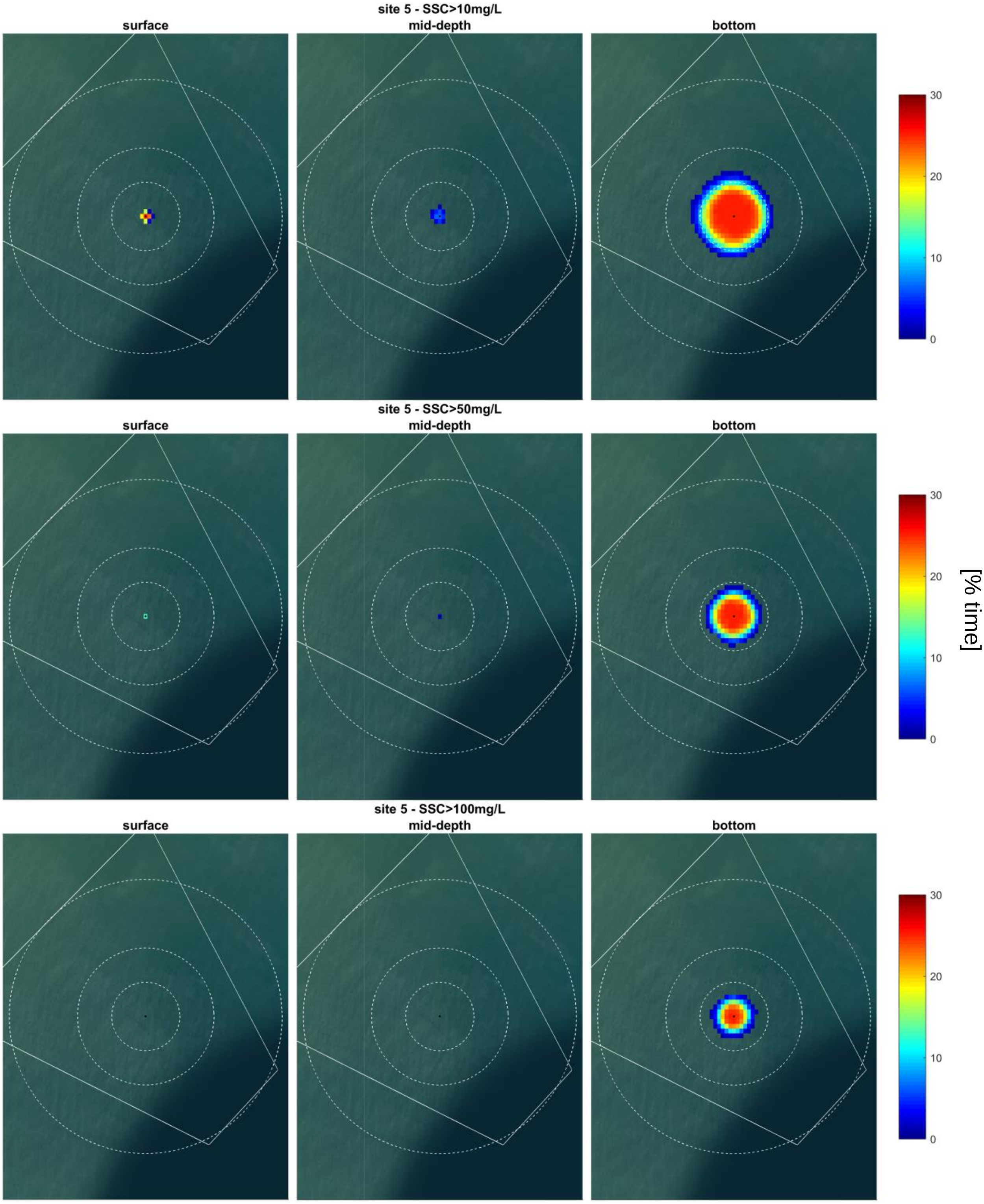

Figure 3.39 *SSC* exceedance for disposal at the centre of the disposal ground using the Pukunui vessel (V=480 m^3) computed for July 1998 (during the La Niña episode), for three *SSC* thresholds, 10, 50 and 100 mg.L^{-1}. The results assumed a settling velocity of 1.0 mm.s^{-1} for the cohesive sediment class. Dashed grey circles have radiuses of 250, 500 and 1000 m. Dashed grey circles have radiuses of 250, 500 and 1000 m.

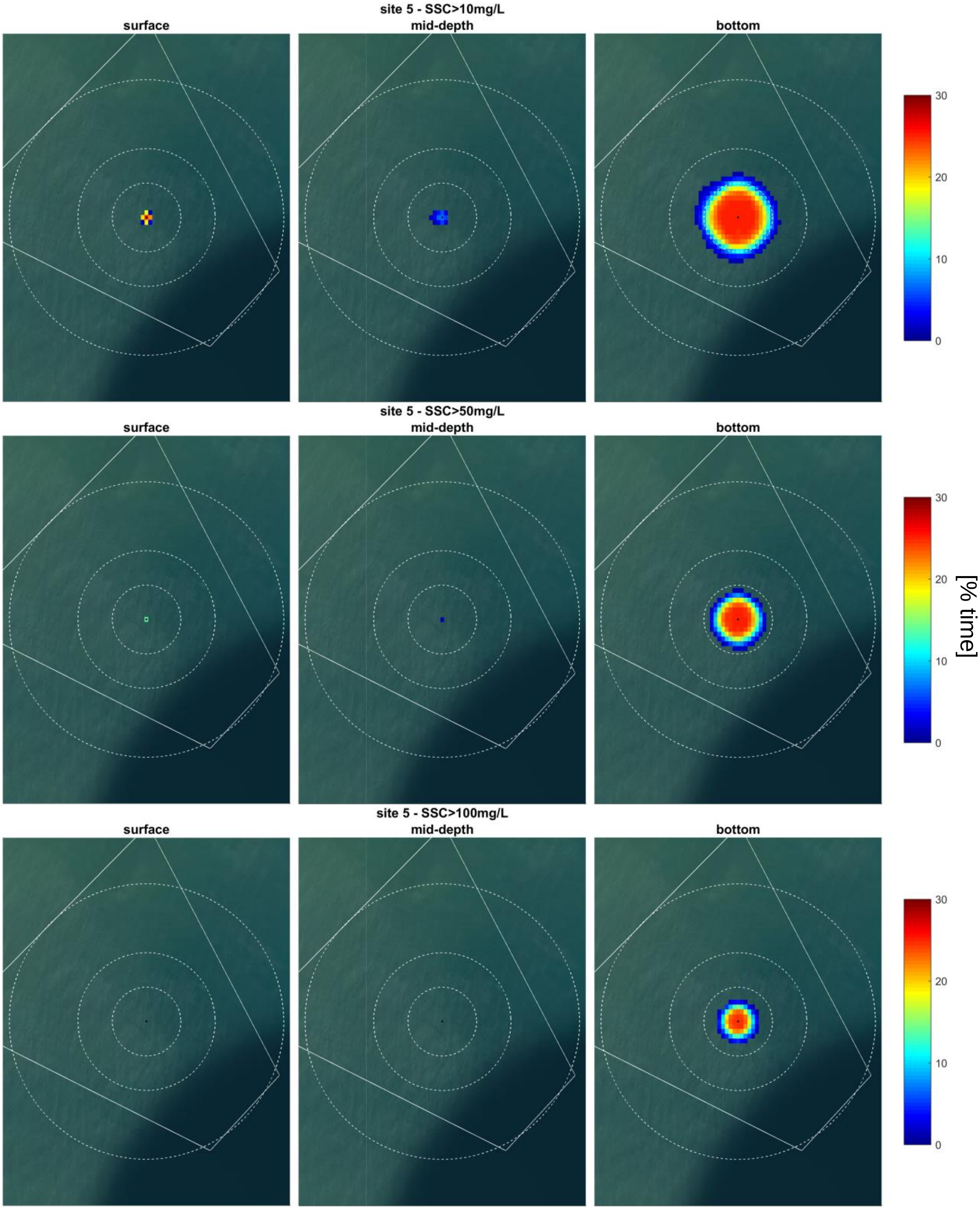

Figure 3.40 *SSC* exceedance for disposal at the centre of the disposal ground using the Pukunui vessel (V=480 m^3) computed for July 2002 (during the El Niño episode), for three *SSC* thresholds, 10, 50 and 100 $mg.L^{-1}$. The results assumed a settling velocity of 1.0 $mm.s^{-1}$ for the cohesive sediment class. Dashed grey circles have radiuses of 250, 500 and 1000 m. Dashed grey circles have radiuses of 250, 500 and 1000 m.

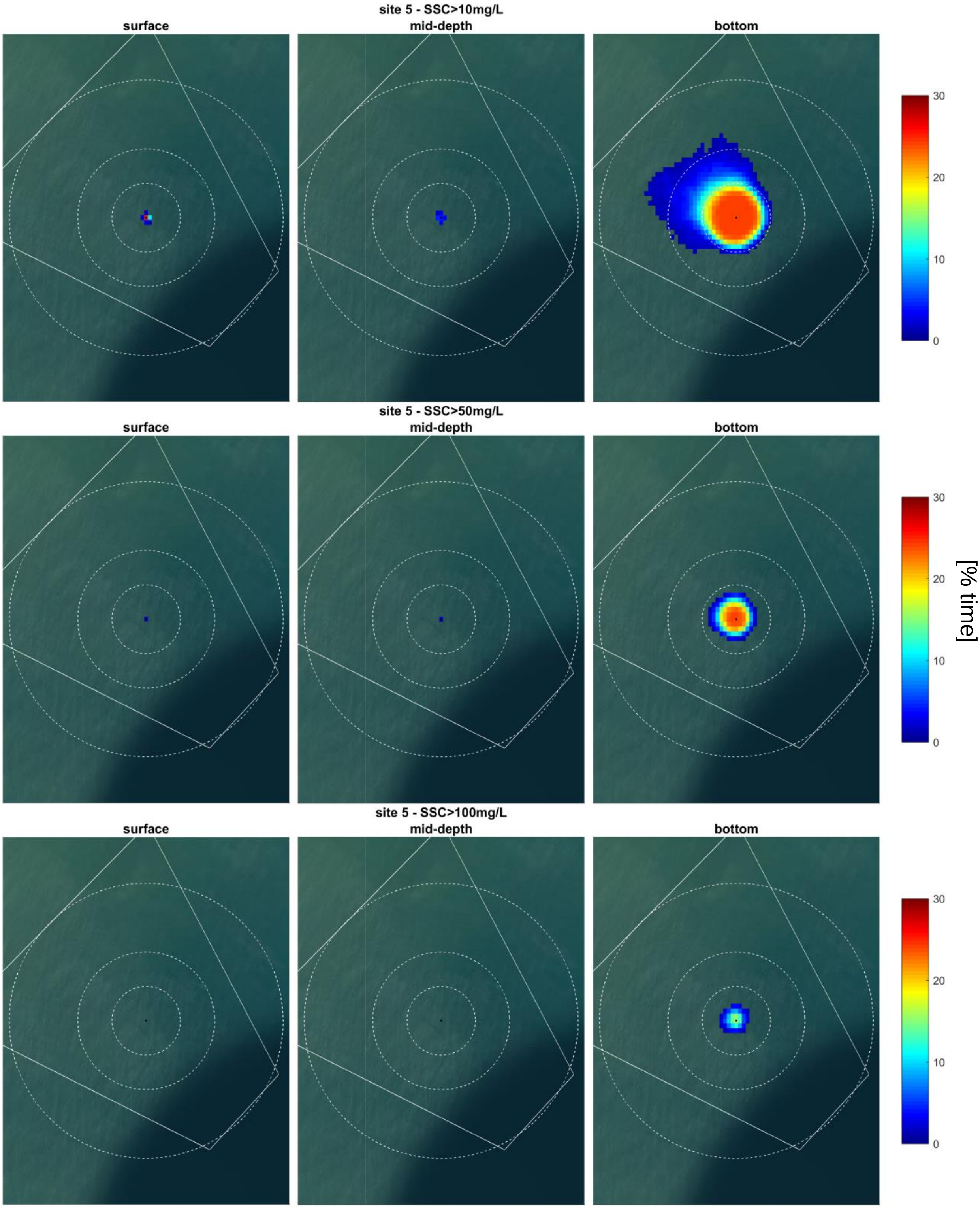

Figure 3.41 *SSC* exceedance for disposal at the centre of the disposal ground using the Pukunui vessel (V=480 m^3) computed for July 1998 (during the La Niña episode) , for three *SSC* thresholds, 10, 50 and 100 mg.L^{-1}. The results assumed a settling velocity of 0.1 mm.s^{-1} for the cohesive sediment class. Dashed grey circles have radiuses of 250, 500 and 1000 m. Dashed grey circles have radiuses of 250, 500 and 1000 m.

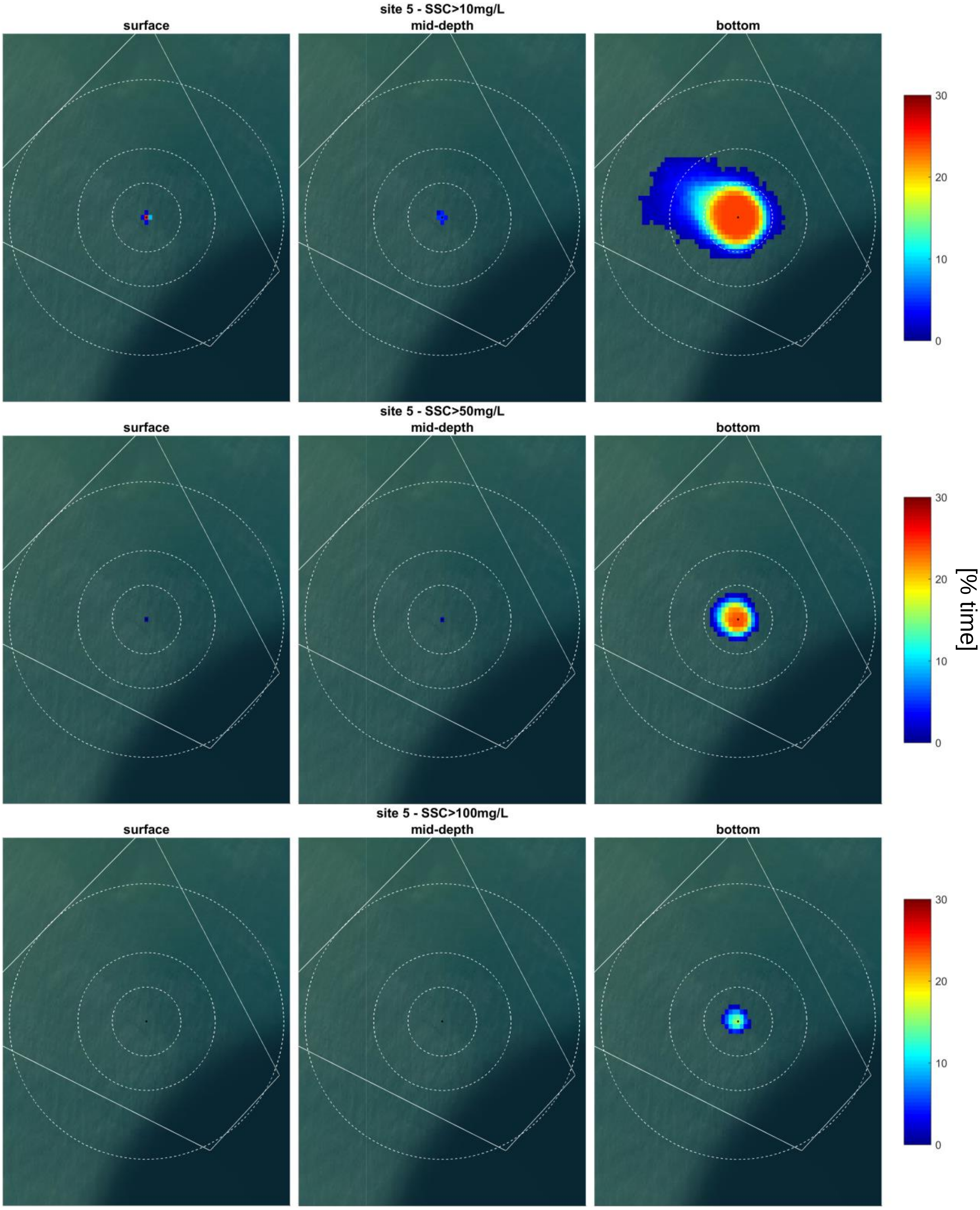

Figure 3.42 *SSC* exceedance for disposal at the centre of the disposal ground using the Pukunui vessel (V=480 m^3) computed for July 2002 (during the El Niño episode) , for three *SSC* thresholds, 10, 50 and 100 $mg.L^{-1}$. The results assumed a settling velocity of 0.1 $mm.s^{-1}$ for the cohesive sediment class. Dashed grey circles have radiuses of 250, 500 and 1000 m. Dashed grey circles have radiuses of 250, 500 and 1000 m.

3.4. Probabilistic suspended sediment plumes (*SSC*) plumes and deposition – Albatros vessel

The section presents probabilistic *SSC* and deposition footprints for the larger TSHD dredger Albatros (V=1860 m^3) that may be used for maintenance dredging.

The probabilistic *SSC* plume fields, assuming a settling velocity of 1 $mm.s^{-1}$ for the cohesive class, are shown in Figure 3.43 and Figure 3.44 for the La Niña (June 1998-June 1999) and El Niño (June 2002-June 2003) respectively. The results assuming a smaller settling velocity of 0.1 $mm.s^{-1}$ are shown in Figure 3.45 and Figure 3.46. A smaller settling velocity results in particles remaining suspended in the water column for longer, and thus able to disperse over larger distances. This is combined with relatively larger potential for suspended sediment concentration dilution (i.e. same amount of material is dispersed over a larger area). The deposition fields associated with the *SSC* plumes described above are shown in Figure 3.47 to Figure 3.50.

Key dispersion patterns outlined in section 3.2 for the Pukunui vessel are conserved; however, the larger amount of sediment disposed results in a relative increase of the *SSC* and deposition magnitudes.

For reference, as for the Pukunui vessel (section 3.2), the *SSC* and deposition fields predicted for a disposal of predominantly “sandy” and “silty” material are compared Figure 3.51 to Figure 3.58.

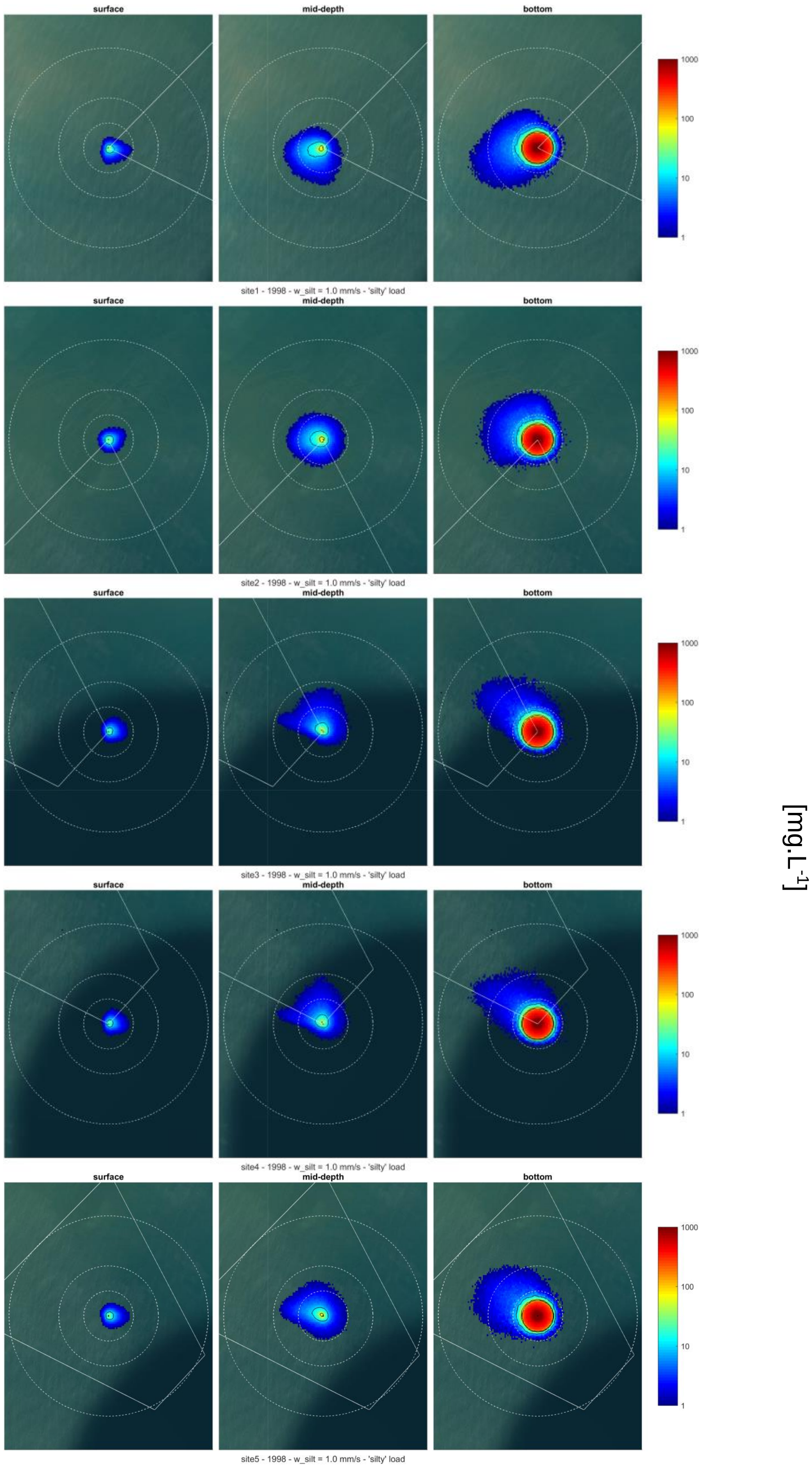

Figure 3.43 Probabilistic *SSC* fields resulting from the disposal of one hopper load of the Albatros vessel (V=1860 m^3), derived from the annual La Niña period (June 1998-June 1999). The results assumed a settling velocity of 1 mm.s^{-1} for the cohesive sediment class. Dashed grey circles have radiuses of 250, 500 and 1000 m. The 10, 50 and 100 mg.L^{-1} contours are shown in black.

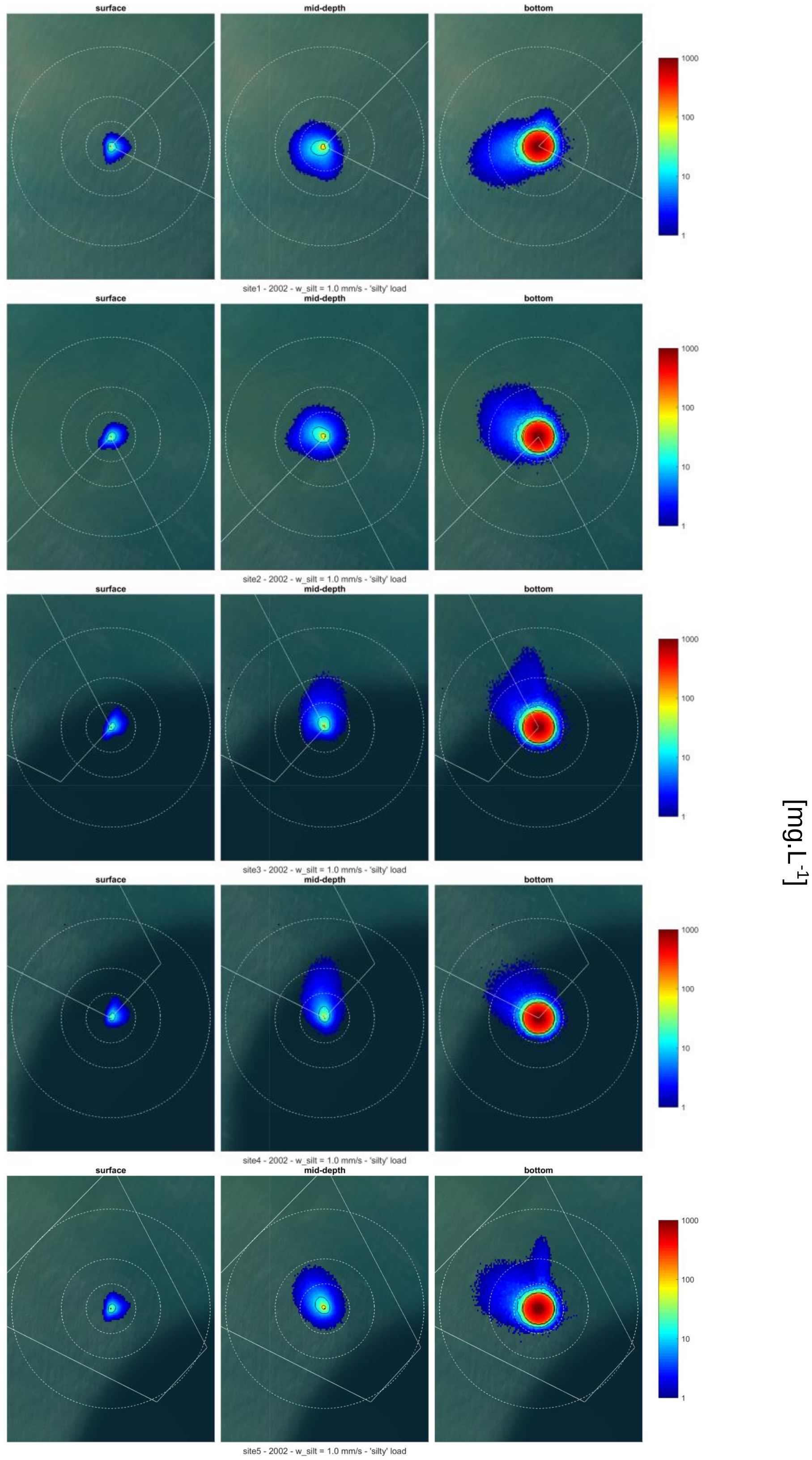

Figure 3.44 Probabilistic *SSC* fields resulting from the disposal of one hopper load of the Albatros vessel (V=1860 m^3), derived from the annual El Niño period (June 2002-June 2003). The results assumed a settling velocity of 1 $mm.s^{-1}$ for the cohesive sediment class. Dashed grey circles have radiuses of 250, 500 and 1000 m. The 10, 50 and 100 $mg.L^{-1}$ contours are shown in black.

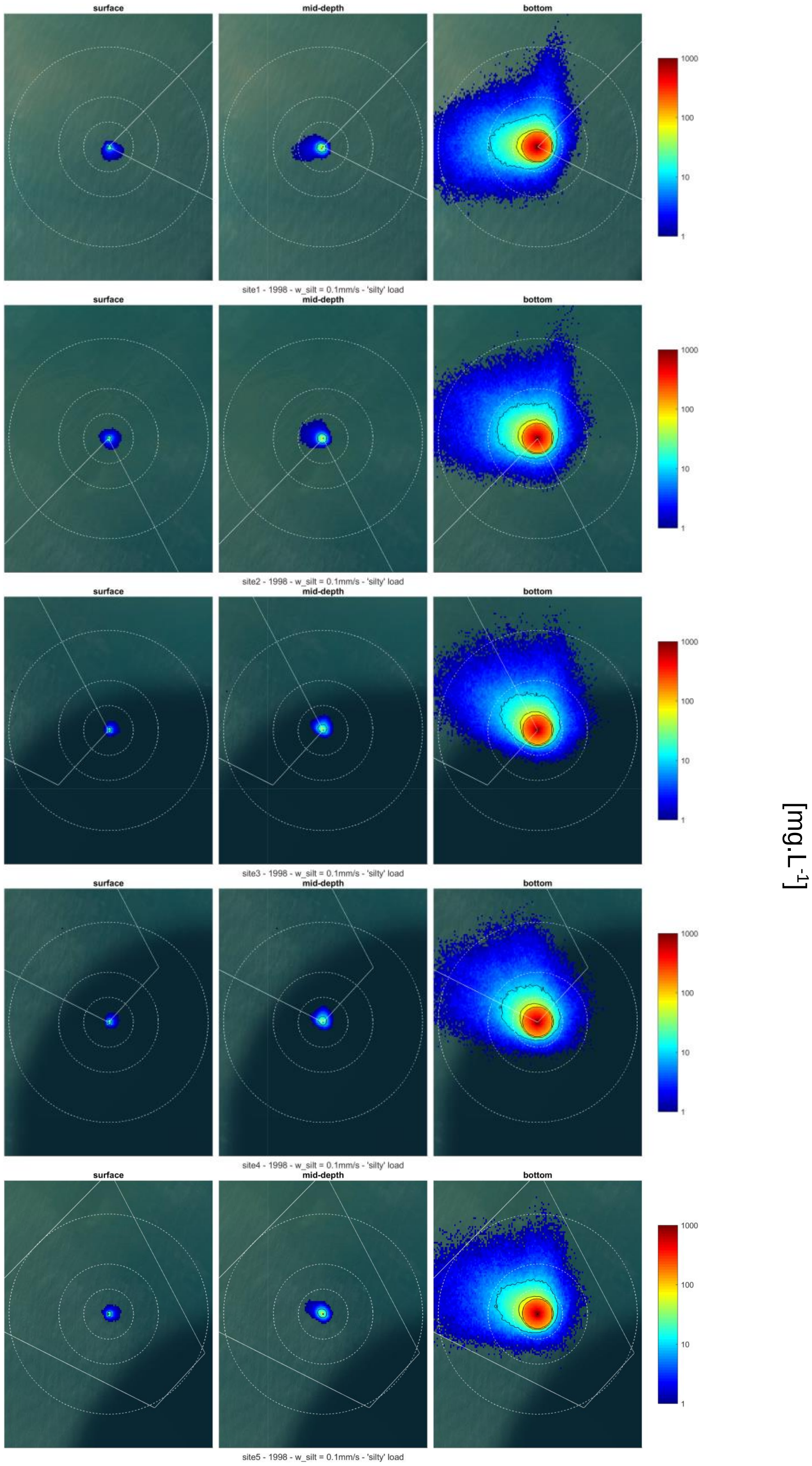

Figure 3.45 Probabilistic *SSC* fields resulting from the disposal of one hopper load of the Albatros vessel (V=1860 m^3), derived from the annual La Niña period (June 1998-June 1999). The results assumed a settling velocity of 0.1 $mm.s^{-1}$ for the cohesive sediment class. Dashed grey circles have radiuses of 250, 500 and 1000 m. The 10, 50 and 100 $mg.L^{-1}$ contours are shown in black.

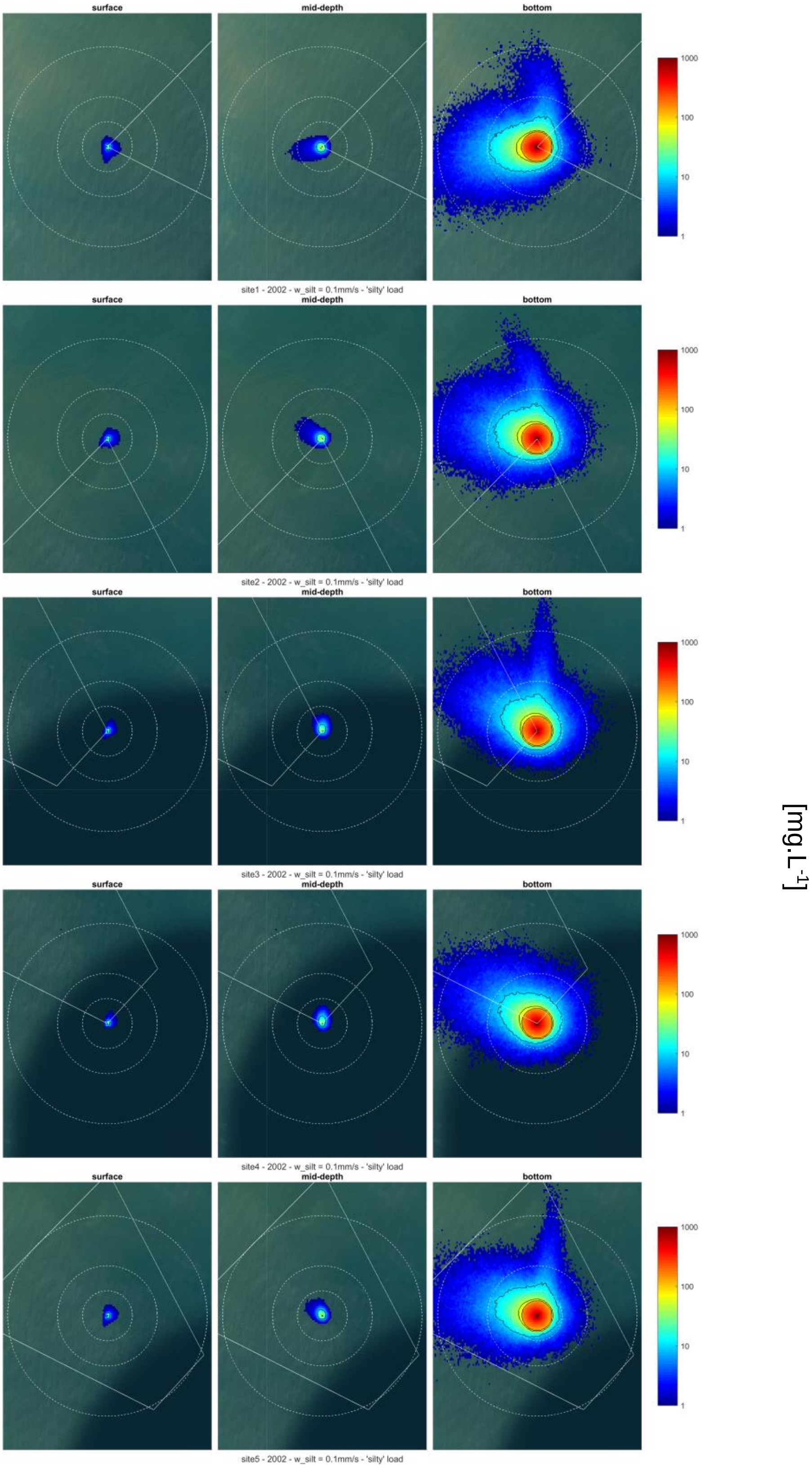

Figure 3.46 Probabilistic *SSC* fields resulting from the disposal of one hopper load of the Albatros vessel (V=1860 m^3), derived from the annual El Niño period (June 2002-June 2003). The results assumed a settling velocity of 0.1 mm.s^{-1} for the cohesive sediment class. Dashed grey circles have radiuses of 250, 500 and 1000 m. The 10, 50 and 100 mg.L^{-1} contours are shown in black.

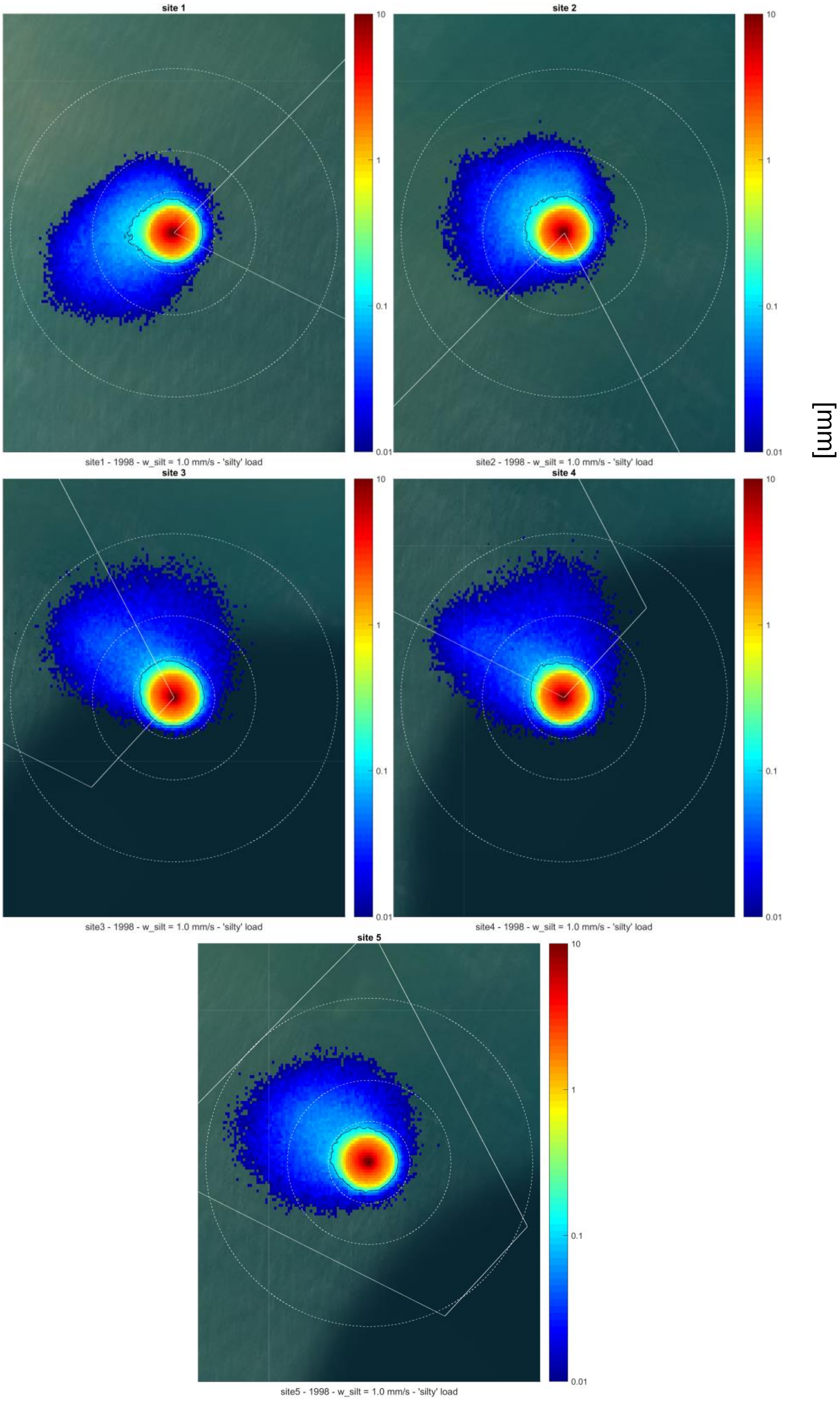

Figure 3.47 Probabilistic sediment deposition fields resulting from the disposal of one hopper load of the Albatros vessel (V=1860 m^3), derived from the annual La Niña period (June 1998-June 1999). The results assumed a settling velocity of 1.0 $mm.s^{-1}$ for the cohesive sediment class. Dashed grey circles have radiuses of 250, 500 and 1000 m. The 0.1 mm contour is shown in black.

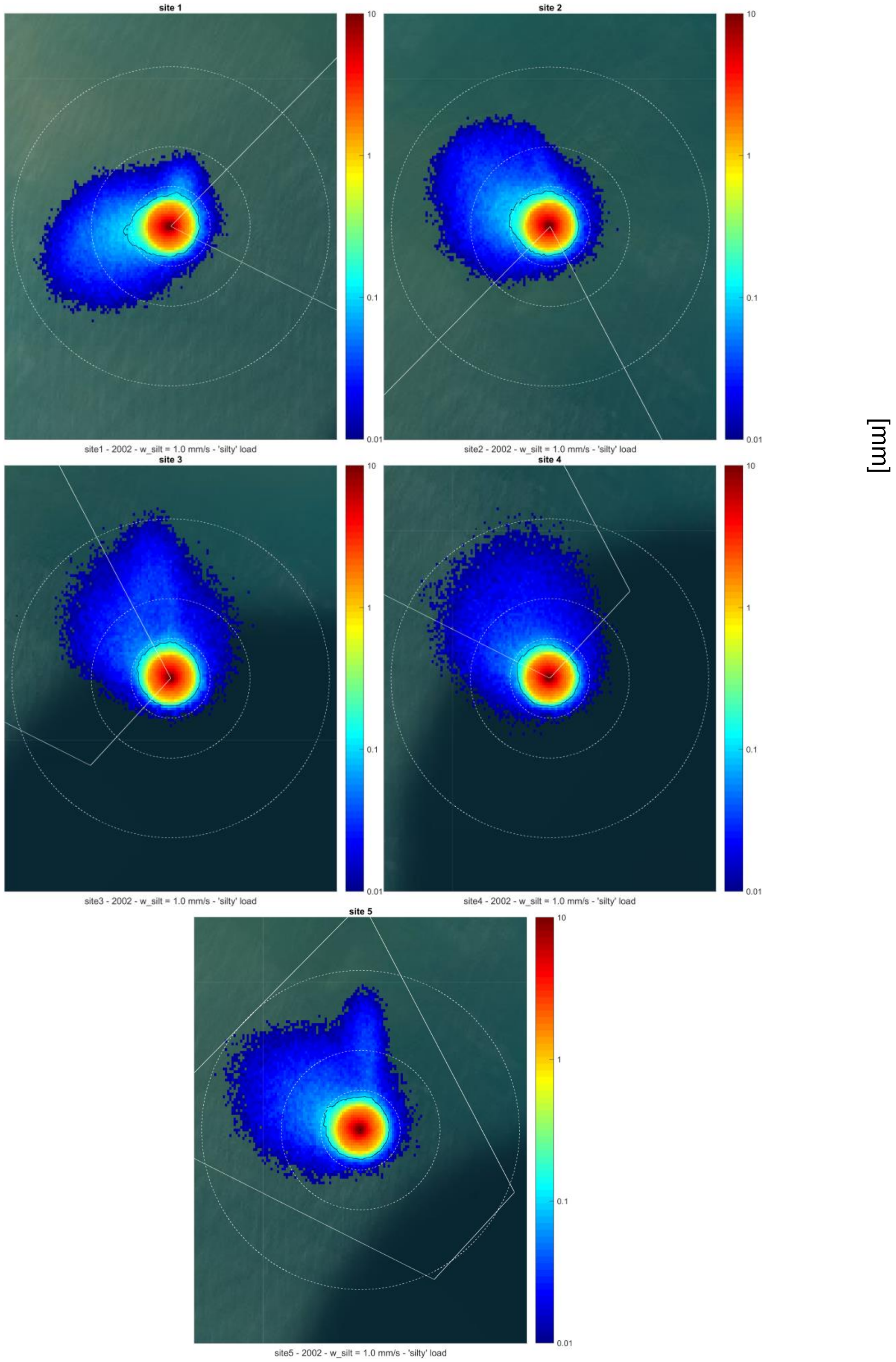

Figure 3.48 Probabilistic sediment deposition fields resulting from the disposal of one hopper load of the Albatros vessel (V=1860 m^3), derived from the annual El Niño period (June 2002-June 2003). The results assumed a settling velocity of 1.0 $mm.s^{-1}$ for the cohesive sediment class. Dashed grey circles have radiuses of 250, 500 and 1000 m. The 0.1 mm contour is shown in black.

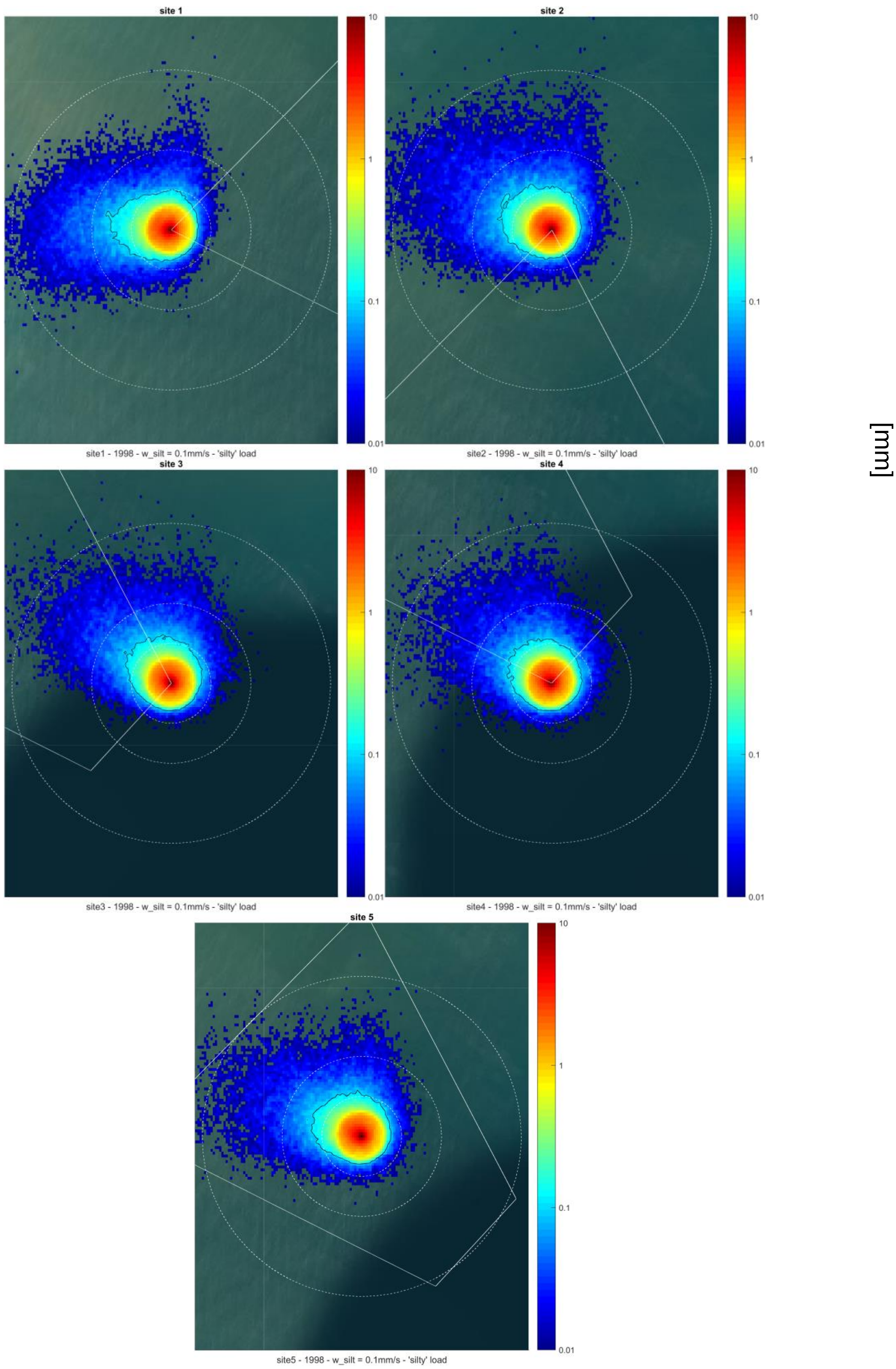

Figure 3.49 Probabilistic sediment deposition fields resulting from the disposal of one hopper load of the Albatros vessel (V=1860 m^3), derived from the annual La Niña period (June 1998-June 1999). The results assumed a settling velocity of 0.1 $mm.s^{-1}$ for the cohesive sediment class. Dashed grey circles have radiuses of 250, 500 and 1000 m. The 0.1 mm contour is shown in black.

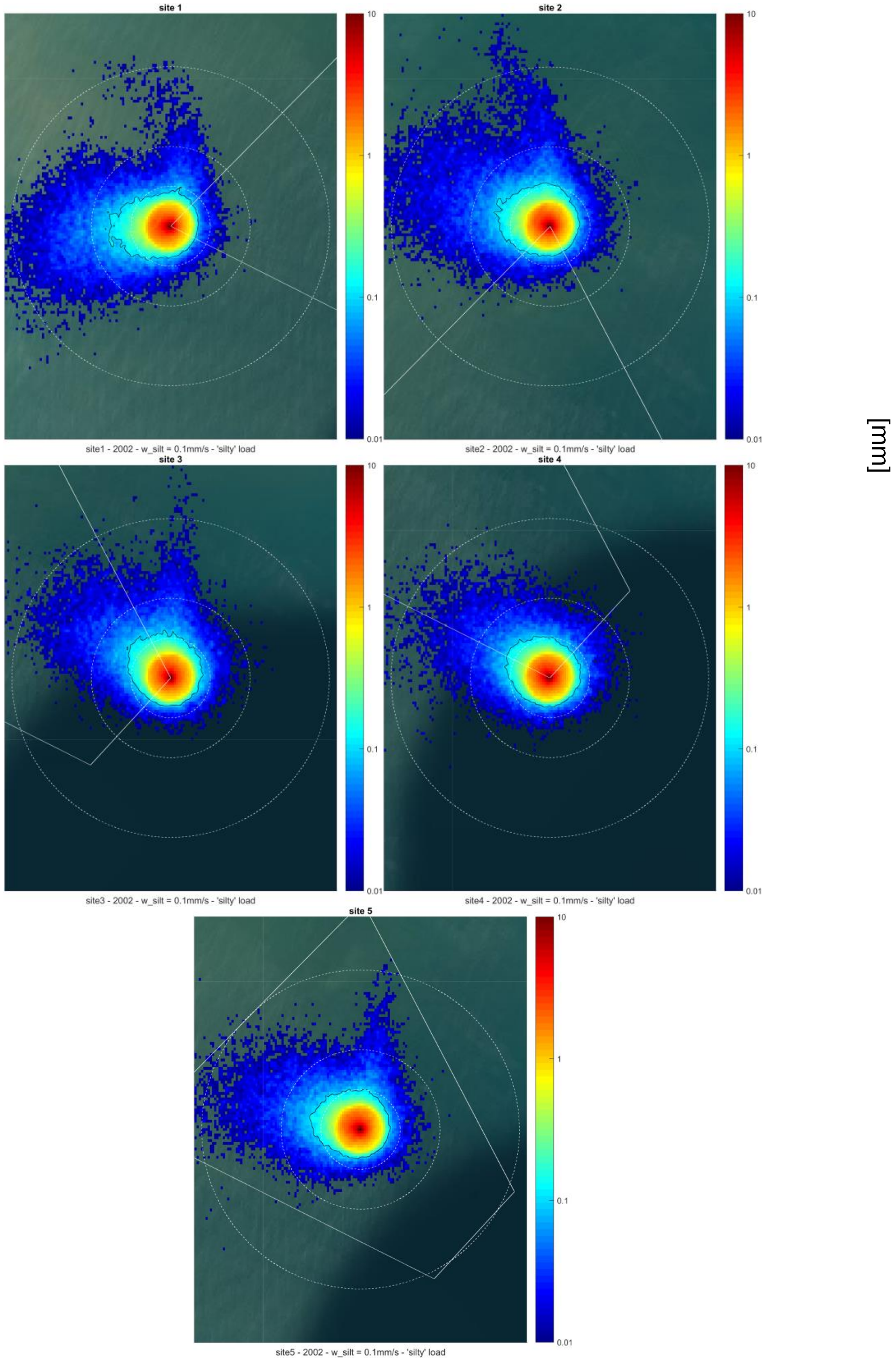

Figure 3.50 Probabilistic sediment deposition fields resulting from the disposal of one hopper load of the Albatros vessel (V=1860 m^3), derived from the annual El Niño period (June 2002-June 2003). The results assumed a settling velocity of 0.1 $mm.s^{-1}$ for the cohesive sediment class. Dashed grey circles have radiuses of 250, 500 and 1000 m. The 0.1 mm contour is shown in black.

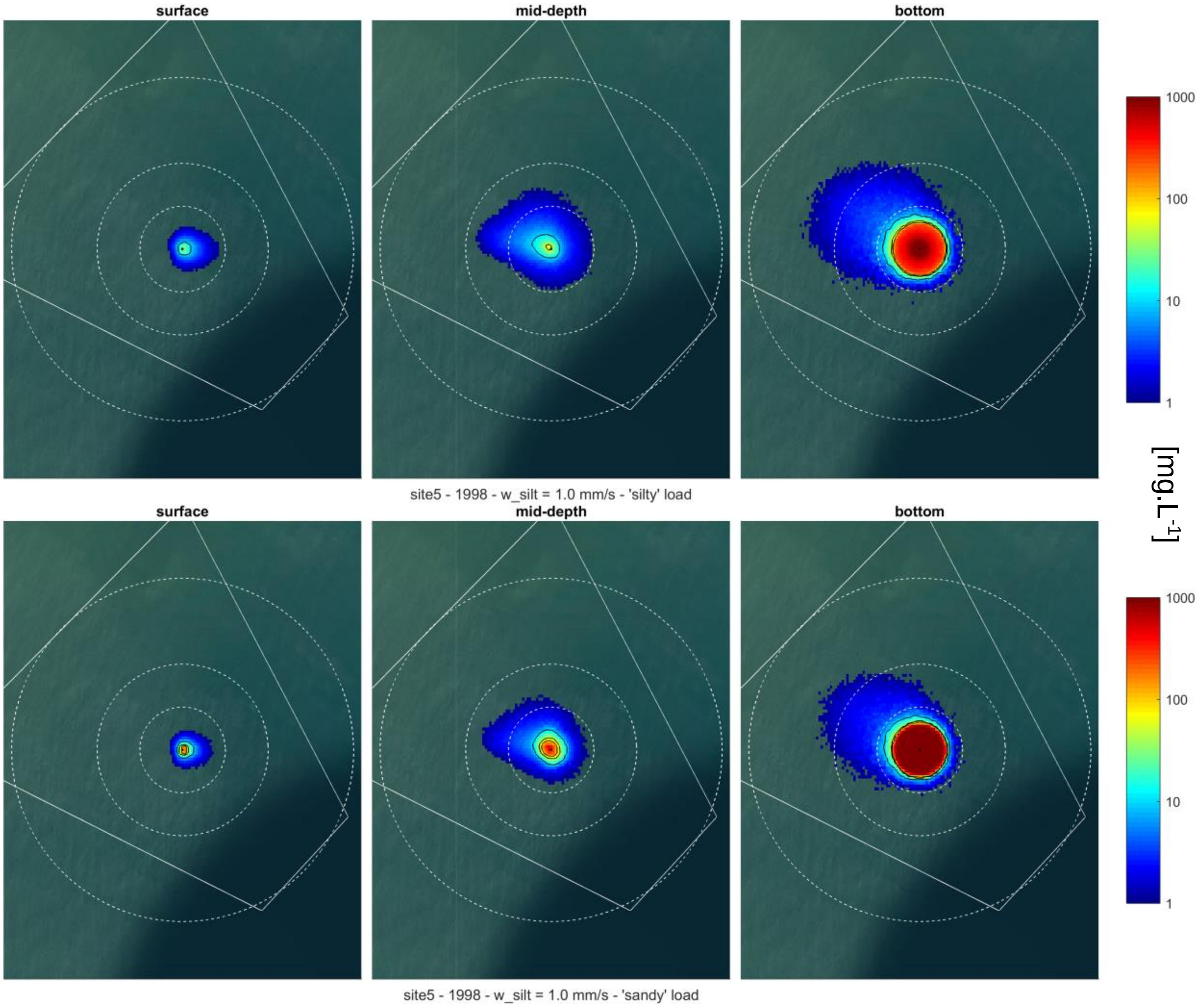

Figure 3.51 Probabilistic *SSC* fields resulting from the disposal of one hopper load of the Albatros vessel (V=1860 m^3), derived from the annual La Niña period (June 1998-June 1999). The results compare the plumes associated with the release of a sediment load composed of 80% silt and 20 % sand (top), and 20% silt 80% sand (bottom). The results assumed a settling a settling velocity of 1.0 mm.s^{-1} for the cohesive sediment class. Dashed grey circles have radiuses of 250, 500 and 1000 m. The 10, 50 and 100 mg.L^{-1} contours are shown in black.

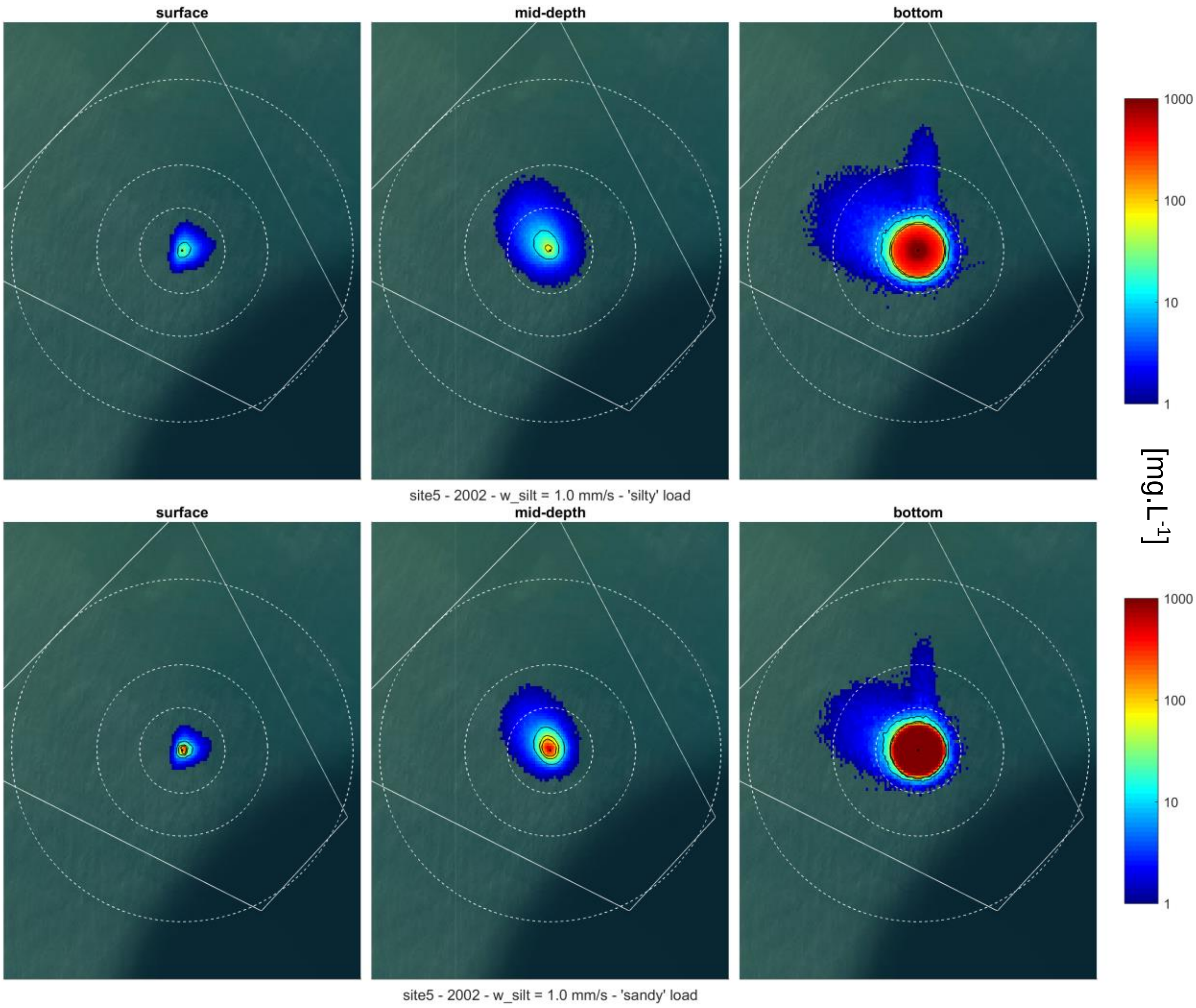

Figure 3.52 Probabilistic *SSC* fields resulting from the disposal of one hopper load of the Albatros vessel (V=1860 m^3), derived from the annual El Niño period (June 2002-June 2003). The results compare the plumes associated with the release of a sediment load composed of 80% silt and 20 % sand (top), and 20% silt 80% sand (bottom). The results assumed a settling a settling velocity of 1.0 $mm.s^{-1}$ for the cohesive sediment class. Dashed grey circles have radiuses of 250, 500 and 1000 m. The 10, 50 and 100 $mg.L^{-1}$ contours are shown in black.

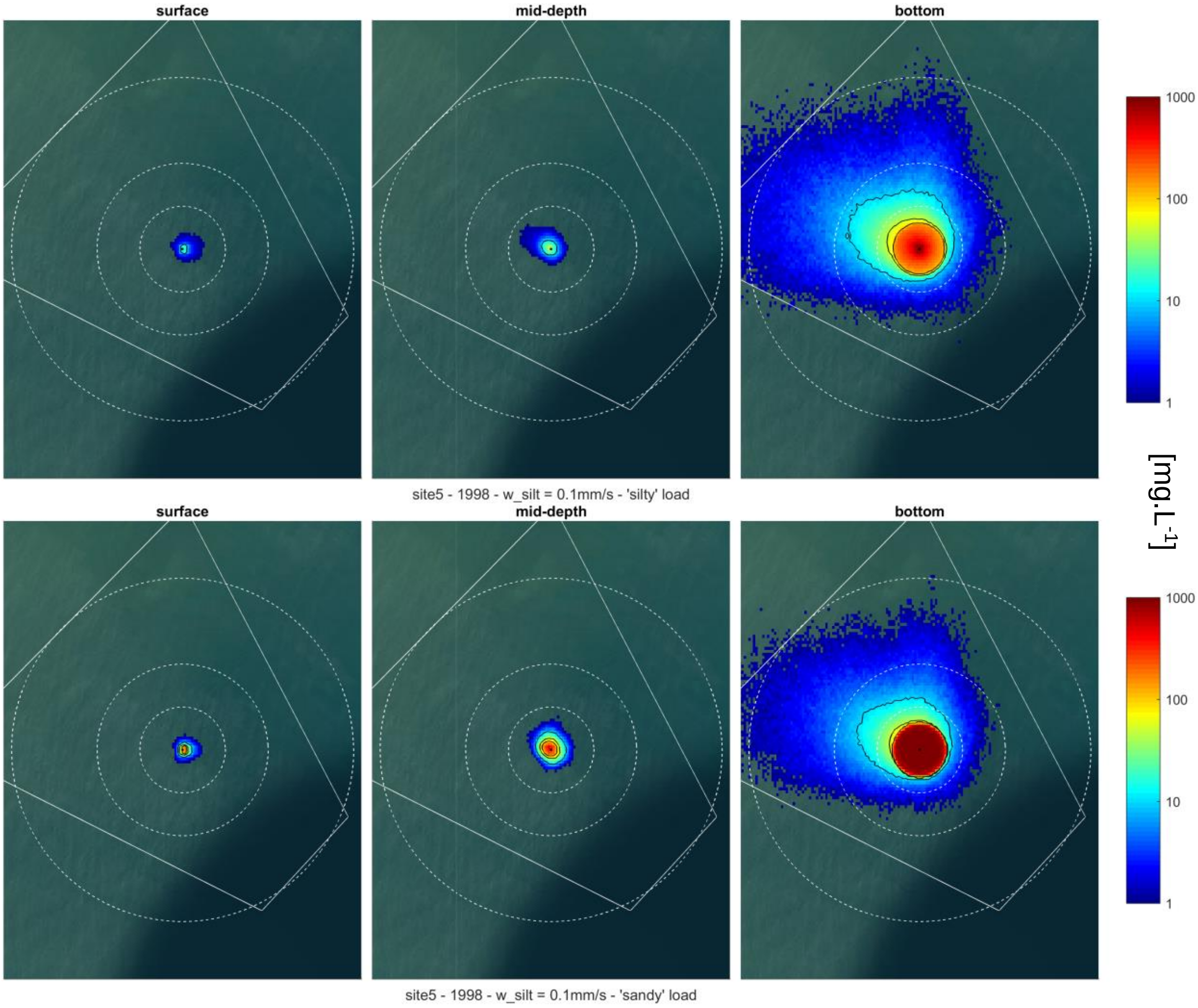

Figure 3.53 Probabilistic *SSC* fields resulting from the disposal of one hopper load of the Albatros vessel (V=1860 m^3), derived from the annual La Niña period (June 1998-June 1999). The results compare the plumes associated with the release of a sediment load composed of 80% silt and 20 % sand (top), and 20% silt 80% sand (bottom). The results assumed a settling a settling velocity of 0.1 $mm.s^{-1}$ for the cohesive sediment class. Dashed grey circles have radiuses of 250, 500 and 1000 m. The 10, 50 and 100 $mg.L^{-1}$ contours are shown in black.

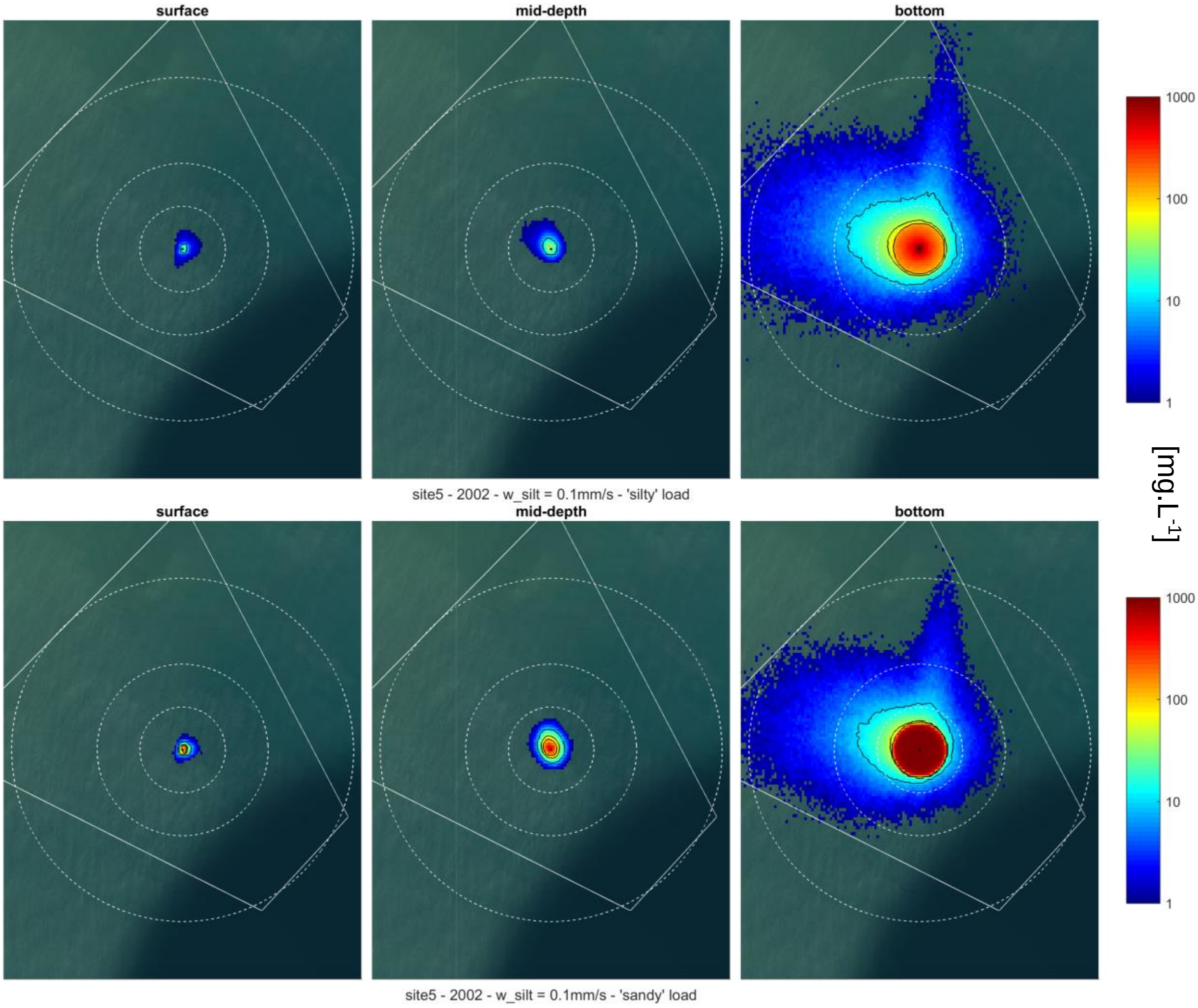

Figure 3.54 Probabilistic *SSC* fields resulting from the disposal of one hopper load of the Albatros vessel (V=1860 m^3), derived from the annual El Niño period (June 2002-June 2003). The results compare the plumes associated with the release of a sediment load composed of 80% silt and 20 % sand (top), and 20% silt 80% sand (bottom). The results assumed a settling a settling velocity of 0.1 $mm.s^{-1}$ for the cohesive sediment class. Dashed grey circles have radiuses of 250, 500 and 1000 m. The 10, 50 and 100 $mg.L^{-1}$ contours are shown in black.

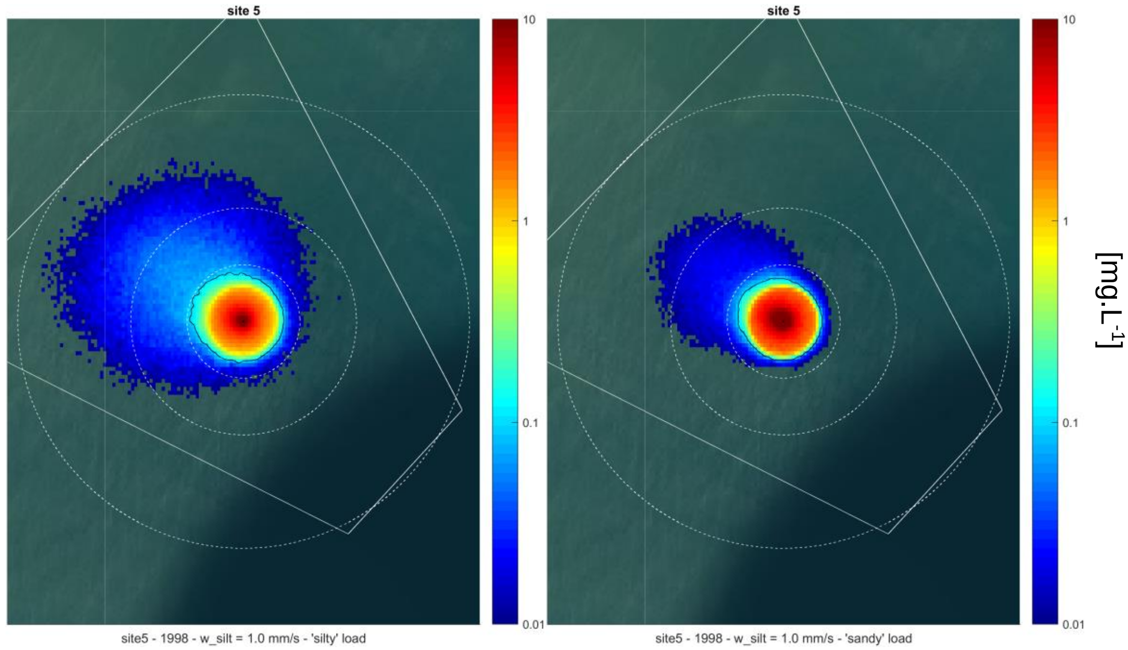

Figure 3.55 Probabilistic sediment deposition fields resulting from the disposal of one hopper load of the Albatros vessel (V=1860 m^3), derived from the annual La Niña period (June 1998-June 1999). The results compare the plumes associated with the release of a sediment load composed of 80% silt and 20 % sand (left), and 20% silt 80% sand (right). The results assumed a settling a settling velocity of 1.0 mm.s^{-1} for the cohesive sediment class. Dashed grey circles have radiuses of 250, 500 and 1000 m. The 10, 50 and 100 mg.L^{-1} contours are shown in black.

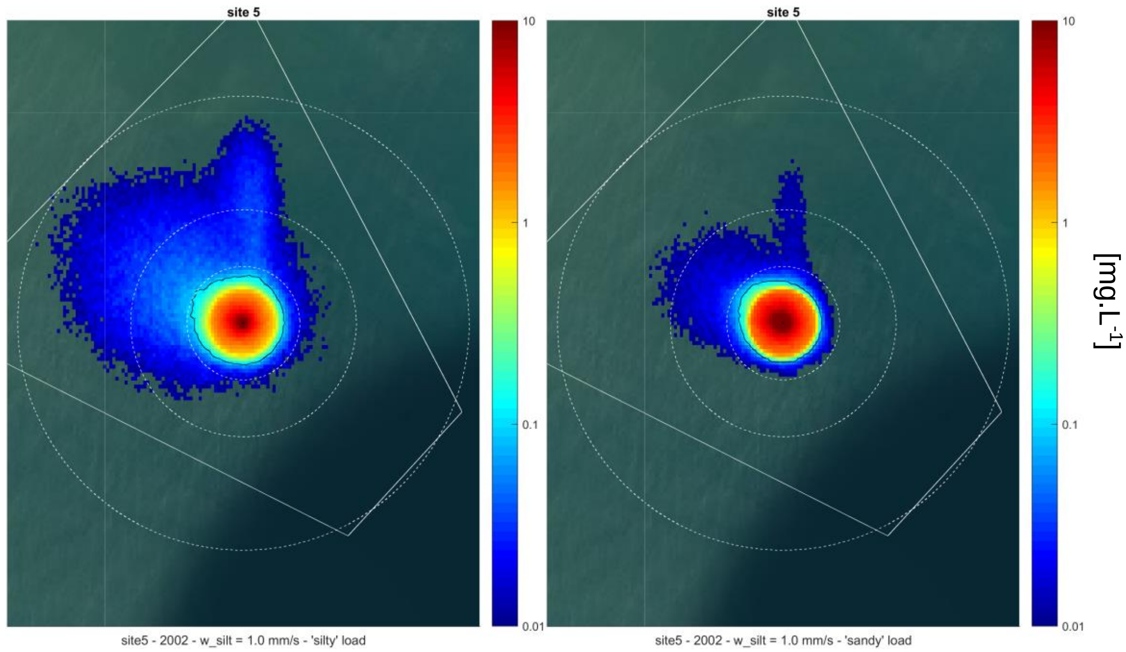

Figure 3.56 Probabilistic sediment deposition fields resulting from the disposal of one hopper load of the Albatros vessel (V=1860 m^3), derived from the annual El Niño period (June 2002-June 2003). The results compare the plumes associated with the release of a sediment load composed of 80% silt and 20 % sand (left), and 20% silt 80% sand (right). The results assumed a settling a settling velocity of 1.0 mm.s^{-1} for the cohesive sediment class. Dashed grey circles have radiuses of 250, 500 and 1000 m. The 10, 50 and 100 mg.L^{-1} contours are shown in black.

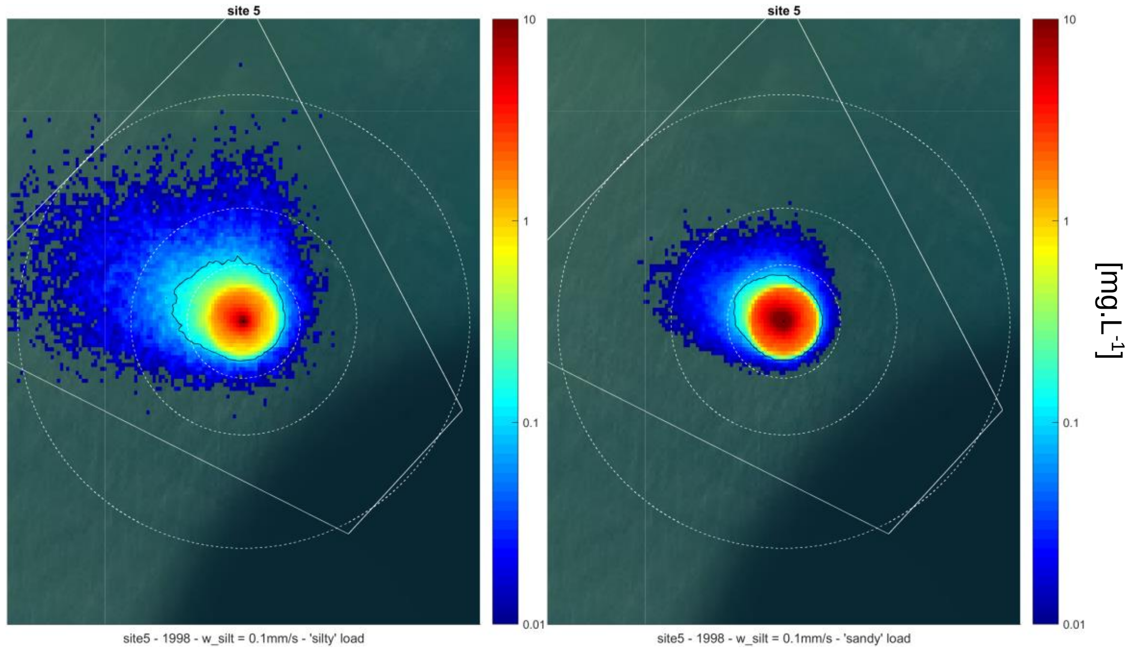

Figure 3.57 Probabilistic sediment deposition fields resulting from the disposal of one hopper load of the Albatros vessel (V=1860 m^3), derived from the annual La Niña period (June 1998-June 1999). The results compare the plumes associated with the release of a sediment load composed of 80% silt and 20 % sand (left), and 20% silt 80% sand (right). The results assumed a settling a settling velocity of 0.1 mm.s^{-1} for the cohesive sediment class. Dashed grey circles have radiuses of 250, 500 and 1000 m. The 10, 50 and 100 mg.L^{-1} contours are shown in black.

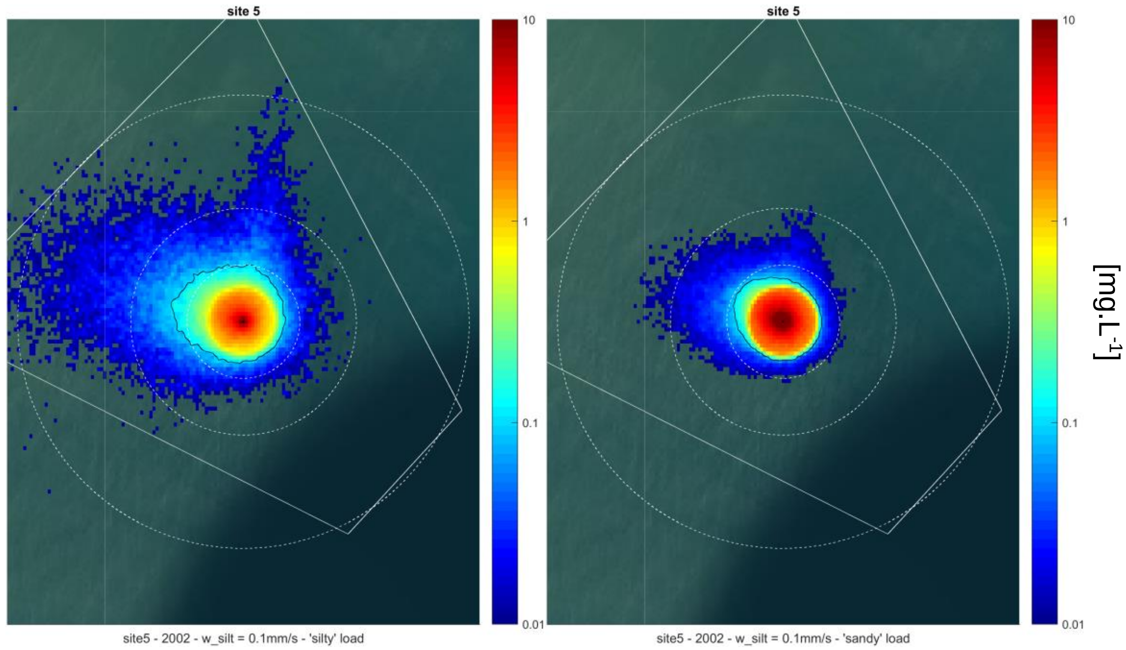

Figure 3.58 Probabilistic sediment deposition fields resulting from the disposal of one hopper load of the Albatros vessel (V=1860 m^3), derived from the annual El Niño period (June 2002-June 2003). The results compare the plumes associated with the release of a sediment load composed of 80% silt and 20 % sand (left), and 20% silt 80% sand (right). The results assumed a settling a settling velocity of 0.1 mm.s^{-1} for the cohesive sediment class. Dashed grey circles have radiuses of 250, 500 and 1000 m. The 10, 50 and 100 mg.L^{-1} contours are shown in black.

3.5. Suspended sediment (*SSC*) plumes and deposition statistics – Albatros vessel

This section supplements the probabilistic results by assessing the plume pattern variability over time in response to the instantaneous forcing. This is done by computing *SSC* and deposition fields at each model time step (i.e. rather than combining all trajectory outputs into one cloud). The approach allows defining statistical properties of the *SSC* plume and deposition fields such as mean and median or extremes (e.g. 90th percentile), as well as information on exceedance times (i.e. percentage of time a given *SSC* threshold is exceeded).

Note these results assume the disposal of a hopper load composed predominantly of silt material (i.e. 80% silt, 20 %); finer sediment will remain much longer in suspension in the water column and are therefore the most problematic with respect to the spatial excursion of the produced sediment plumes.

3.5.1. Mean, median and 90th percentile *SSC* plumes and deposition

Since the computation of the time-varying *SSC* and deposition spatial fields can become very expensive computationally, the two 1-month periods of January and July were selected in each annual simulations (El Niño /La Niña) to capture typical winter and summer forcing conditions. Results are presented for sediment discharged at the centre of the disposal ground.

The mean, median and 90th percentile *SSC* plumes for a summer period, assuming a settling velocity of 1 mm.s^{-1} for the cohesive sediment, are shown in Figure 3.59 and Figure 3.60, while results using a smaller settling velocity of 0.1 mm.s^{-1} are provided in Figure 3.61 and Figure 3.62. Resulting deposition footprints are provided in Figure 3.63 to Figure 3.66. Equivalent results for the winter period are provided in Figure 3.67 to Figure 3.74.

Overall patterns outlined in section 3.3.1 are conserved but the larger amount of sediment disposed expectedly increases the *SSC* and deposition magnitudes, and thus relative excursion of the plumes. For example, while the mean *SSC* plume is contained within 400 m of the release location when using the Pukunui vessel (e.g. Figure 3.19, top, settling 1mm.s^{-1}), this is increased to ~600 m with the larger Albatros vessel (Figure 3.59, top).

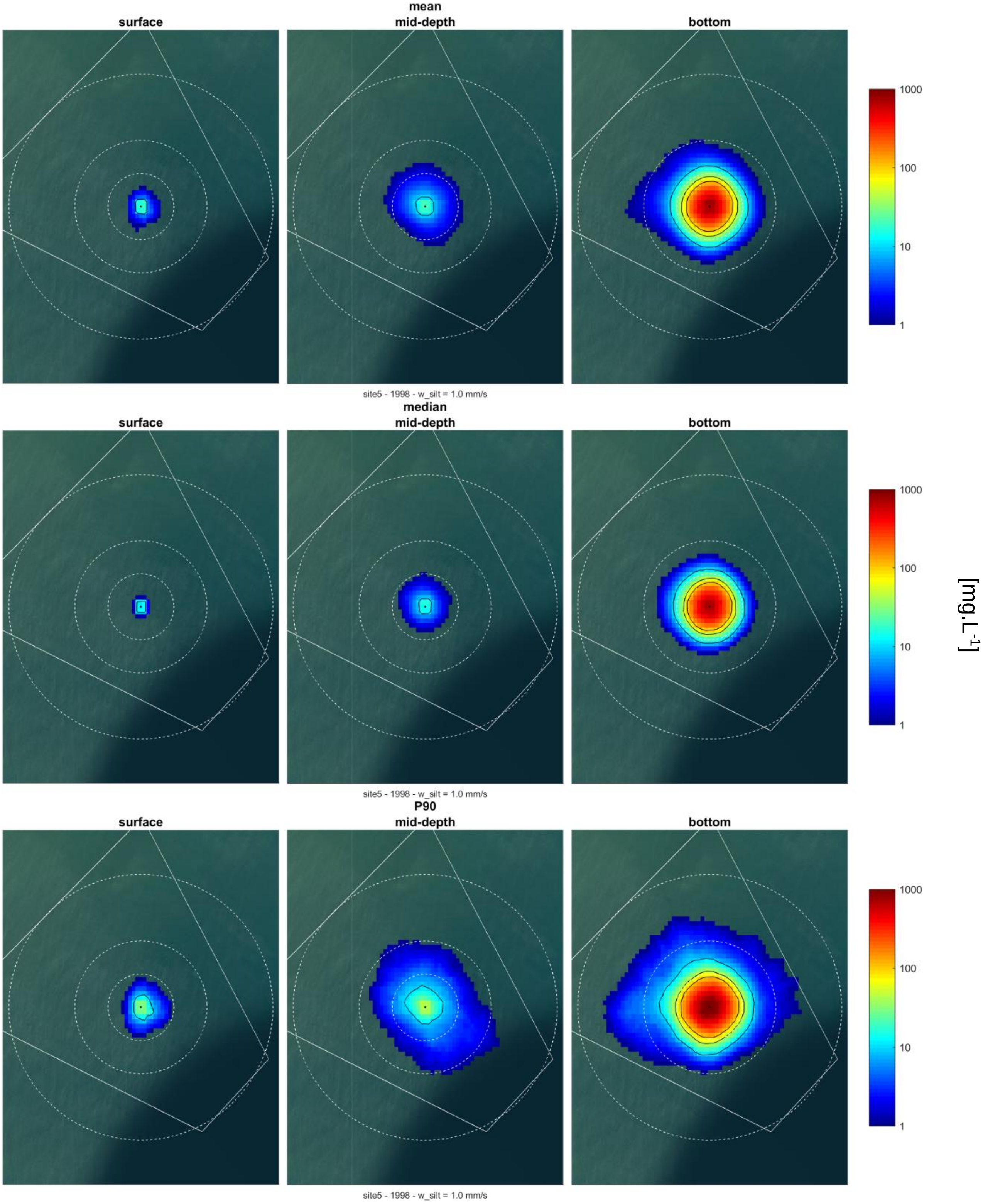

Figure 3.59 Mean, median, and 90th percentile *SSC* fields for disposal at the centre of the disposal ground using the Albatros vessel (V=1860 m^3) computed for January 1999 (during the La Niña episode). The results assumed a settling velocity of 1.0 $mm.s^{-1}$ for the cohesive sediment class. Dashed grey circles have radiuses of 250, 500 and 1000 m. Dashed grey circles have radiuses of 250, 500 and 1000 m. The 10, 50 and 100 $mg.L^{-1}$ contours are shown in black.

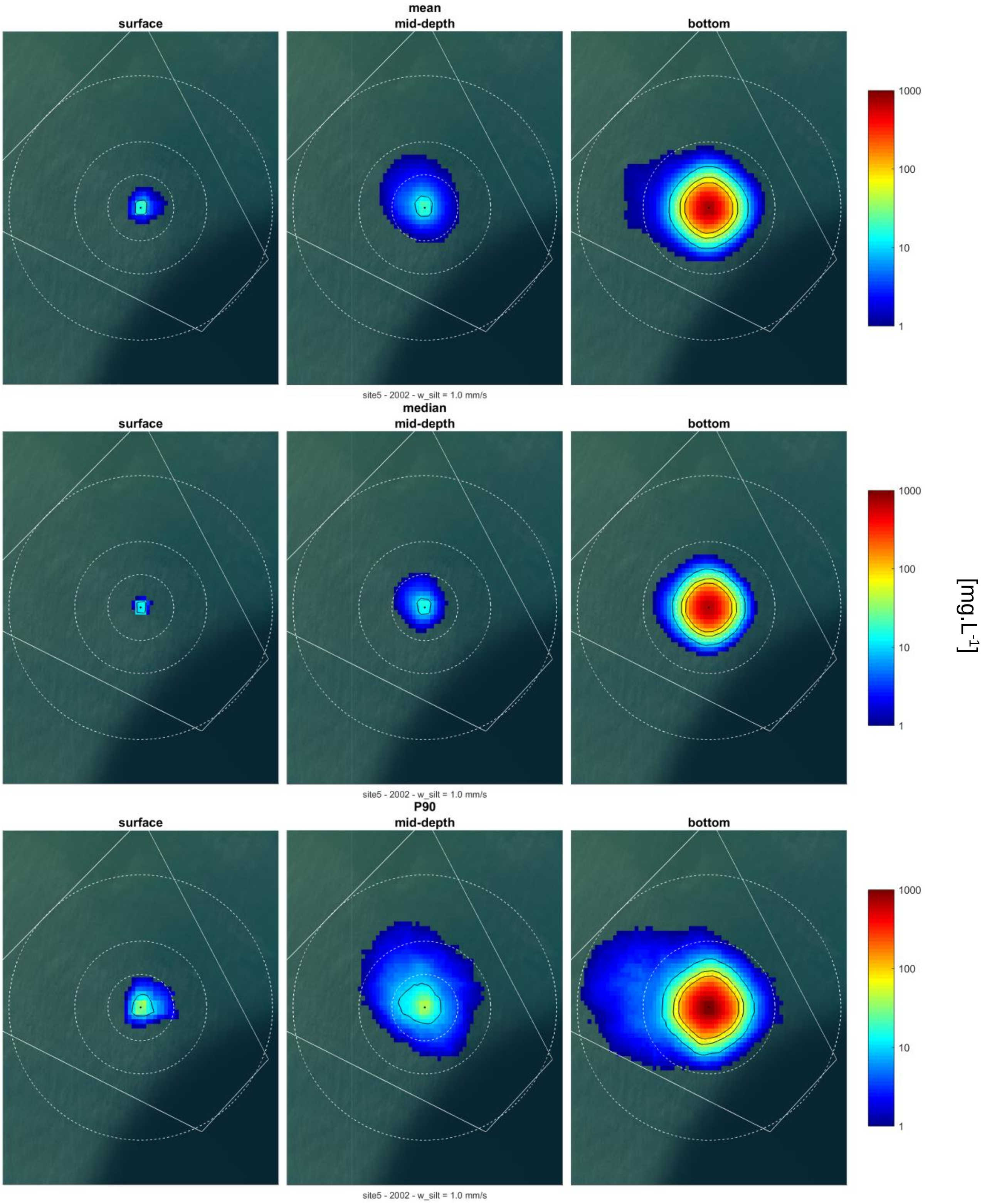

Figure 3.60 Mean, median, and 90th percentile *SSC* fields for disposal at the centre of the disposal ground using the Albatros vessel (V=1860 m^3) computed for January 2003 (during the El Niño episode). The results assumed a settling velocity of 1.0 $mm.s^{-1}$ for the cohesive sediment class. Dashed grey circles have radiuses of 250, 500 and 1000 m. Dashed grey circles have radiuses of 250, 500 and 1000 m. The 10, 50 and 100 $mg.L^{-1}$ contours are shown in black.

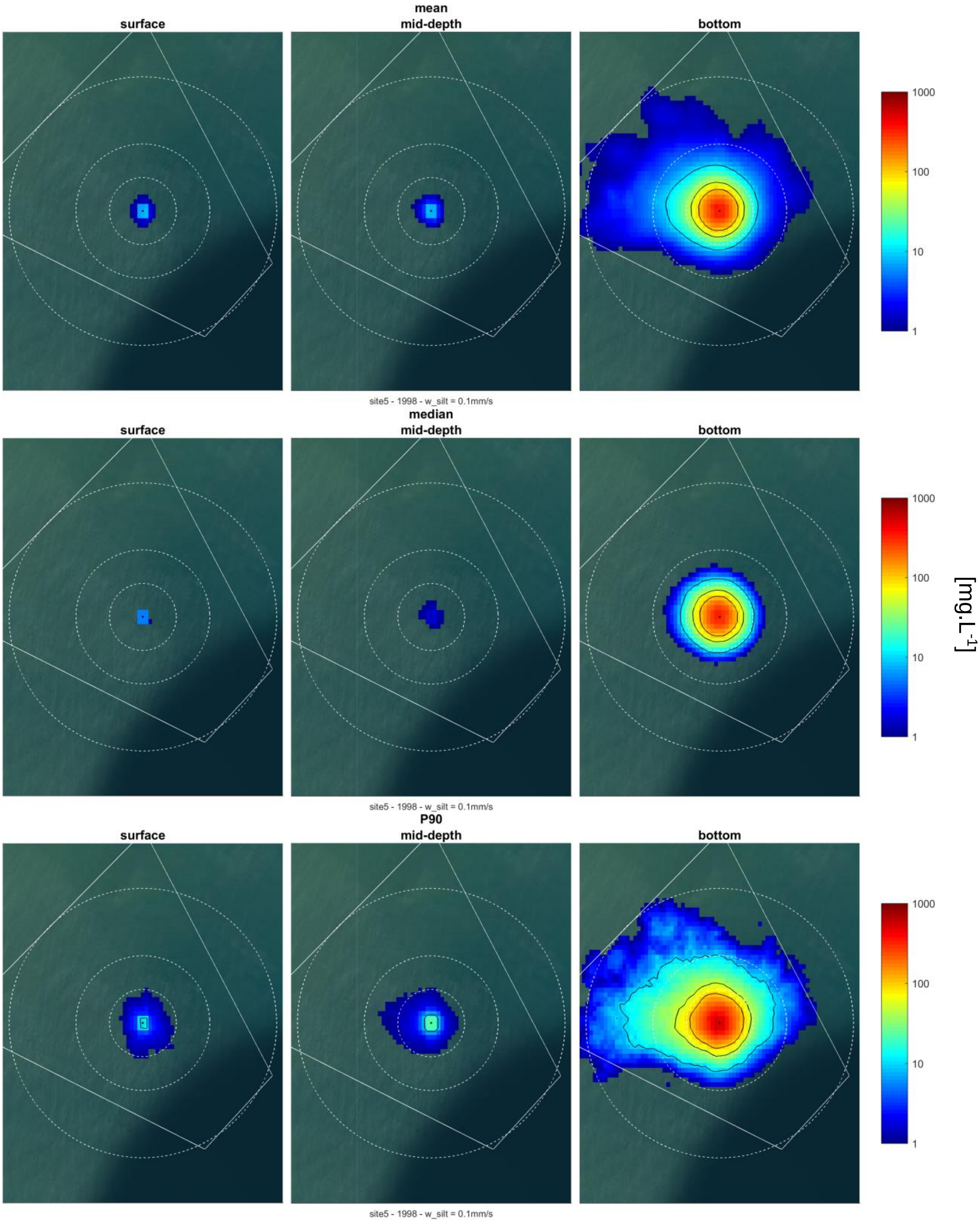

Figure 3.61 Mean, median, and 90th percentile *SSC* fields for disposal at the centre of the disposal ground using the Albatros vessel (V=1860 m^3) computed for January 1999 (during the La Niña episode). The results assumed a settling velocity of 0.1 $mm.s^{-1}$ for the cohesive sediment class. Dashed grey circles have radiuses of 250, 500 and 1000 m. Dashed grey circles have radiuses of 250, 500 and 1000 m. The 10, 50 and 100 $mg.L^{-1}$ contours are shown in black.

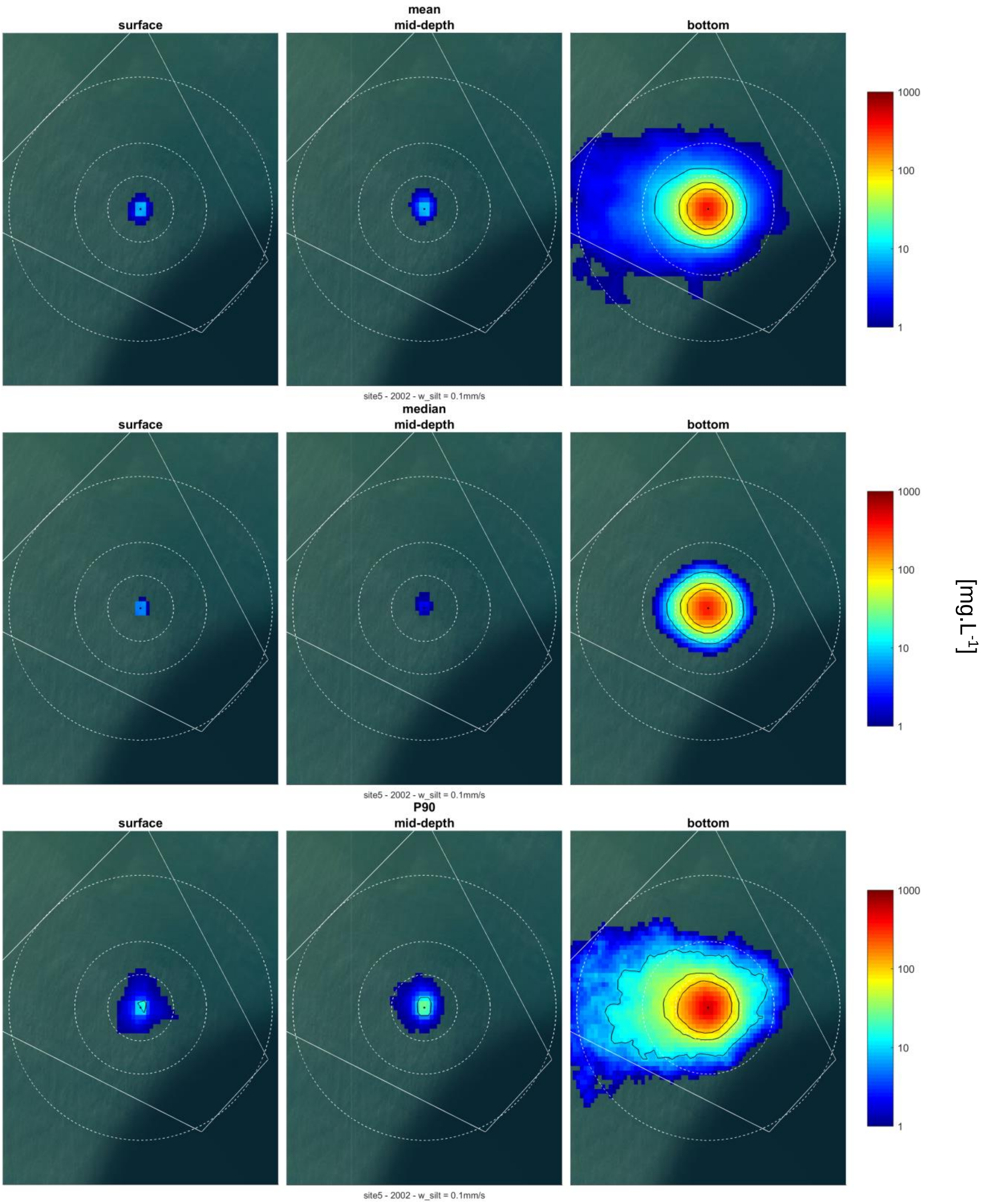

Figure 3.62 Mean, median, and 90th percentile *SSC* fields for disposal at the centre of the disposal ground using the Albatros vessel (V=1860 m^3) computed for January 2003 (during the El Niño episode). The results assumed a settling velocity of 0.1 $mm.s^{-1}$ for the cohesive sediment class. Dashed grey circles have radiuses of 250, 500 and 1000 m. Dashed grey circles have radiuses of 250, 500 and 1000 m. The 10, 50 and 100 $mg.L^{-1}$ contours are shown in black.

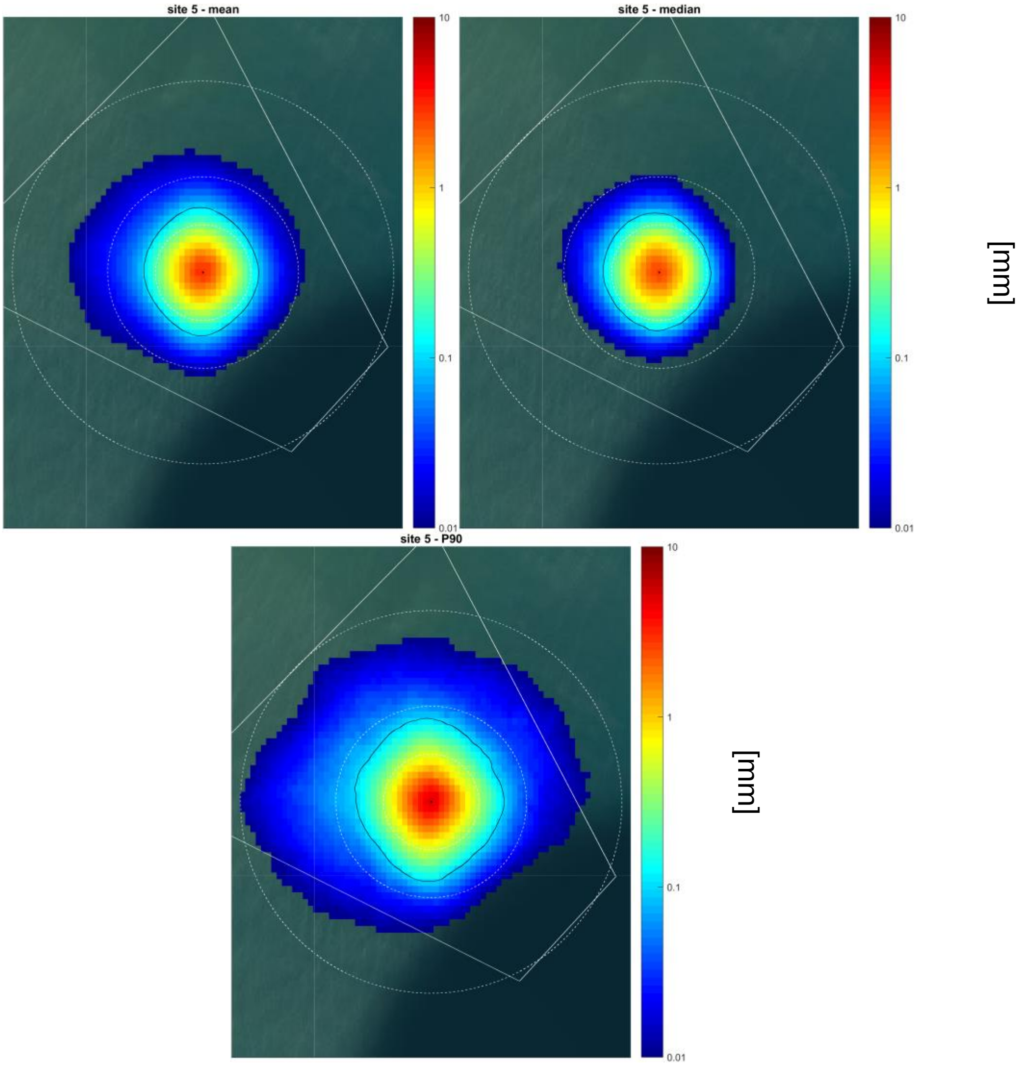

Figure 3.63 Mean, median, and 90th percentile deposition fields for disposal at the centre of the disposal ground using the Albatros vessel (V=1860 m^3) computed for January 1999 (during the La Niña episode). The results assumed a settling velocity of 1.0 $mm.s^{-1}$ for the cohesive sediment class. Dashed grey circles have radiuses of 250, 500 and 1000 m. Dashed grey circles have radiuses of 250, 500 and 1000 m. The 0.1 mm contour is shown in black.

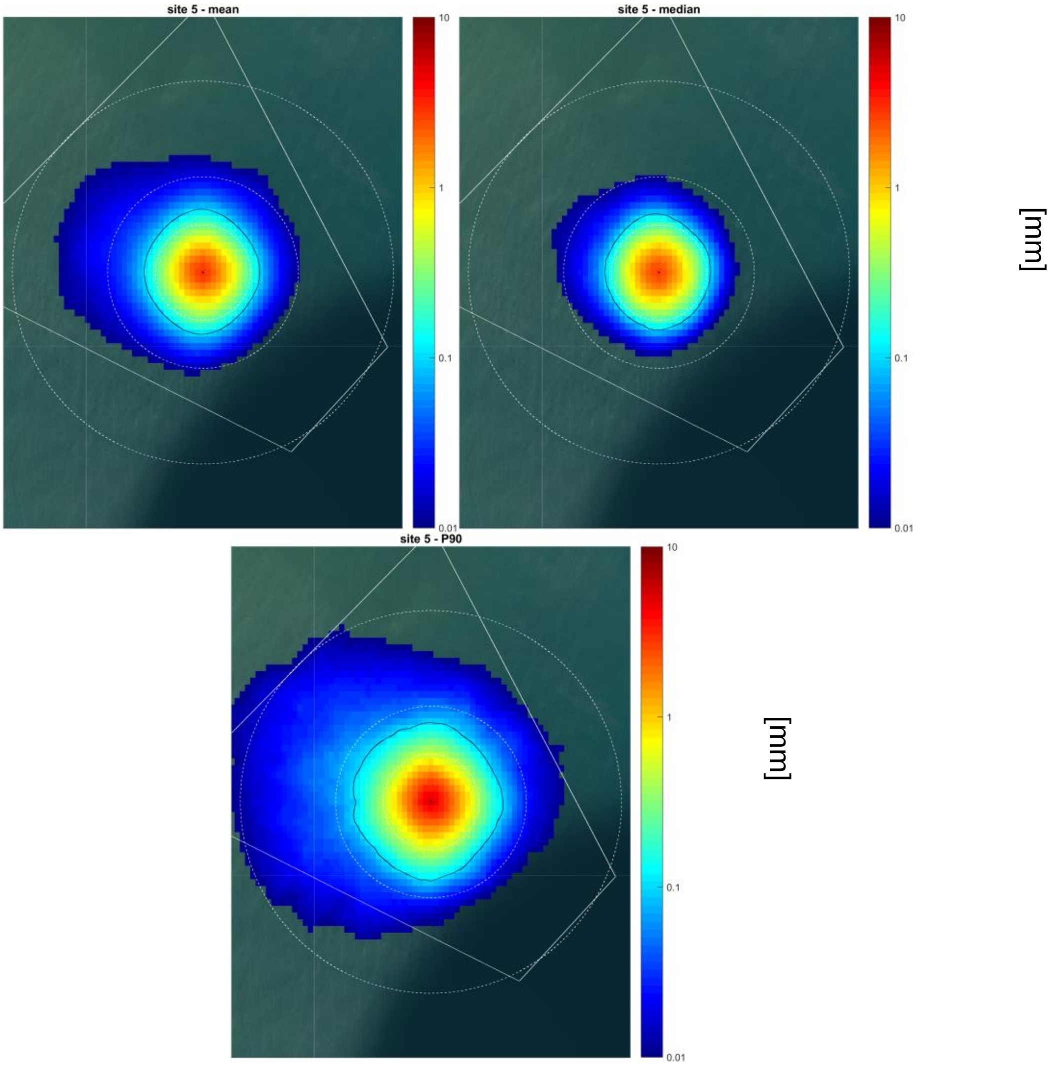

Figure 3.64 Mean, median, and 90th percentile deposition fields for disposal at the centre of the disposal ground using the Albatros vessel (V=1860 m^3) computed for January 2003 (during the El Niño episode). The results assumed a settling velocity of 1.0 mm.s^{-1} for the cohesive sediment class. Dashed grey circles have radiuses of 250, 500 and 1000 m. Dashed grey circles have radiuses of 250, 500 and 1000 m. The 0.1 mm contour is shown in black.

[mm]
[mm]

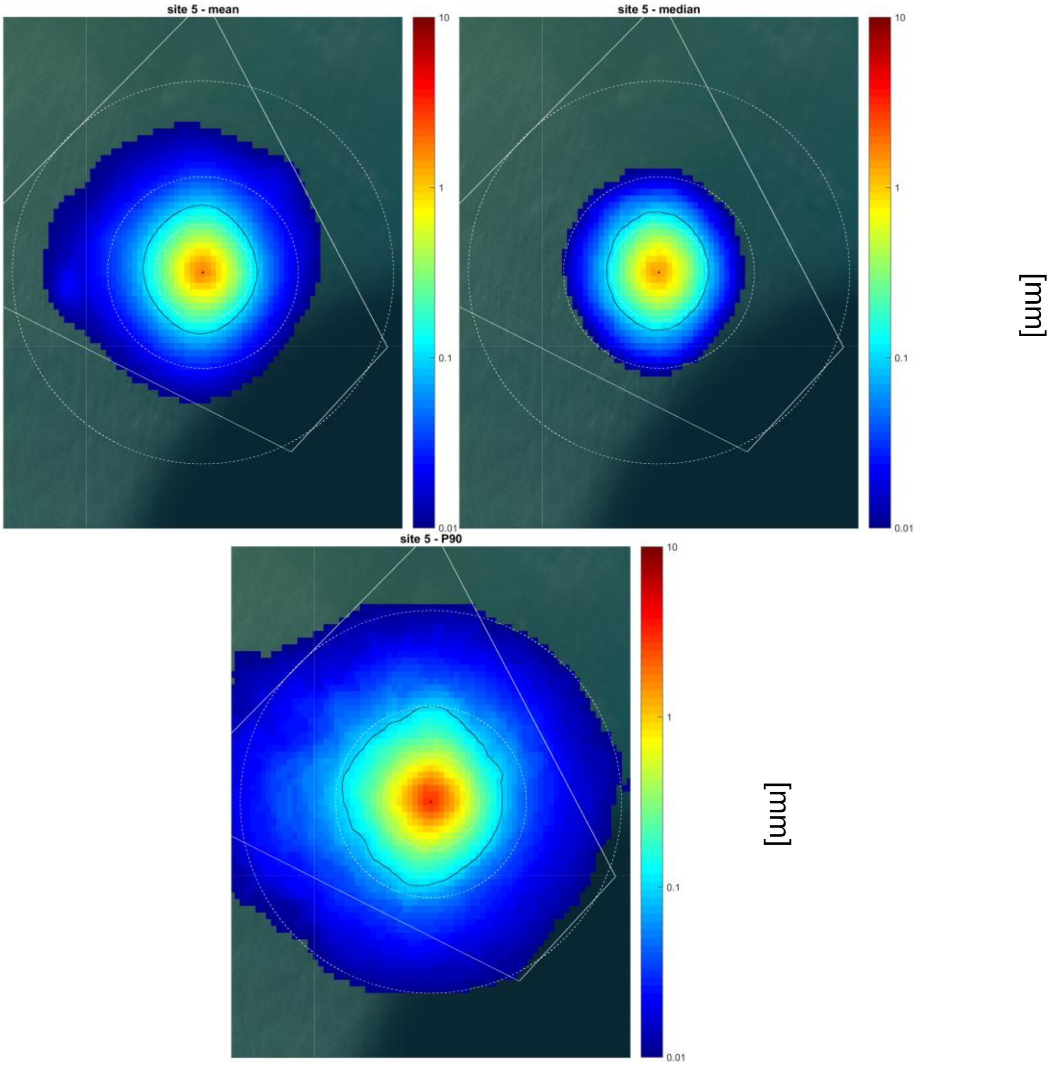

Figure 3.65 Mean, median, and 90th percentile deposition fields for disposal at the centre of the disposal ground using the Albatros vessel (V=1860 m^3) computed for January 1999 (during the La Niña episode). The results assumed a settling velocity of 0.1 $mm.s^{-1}$ for the cohesive sediment class. Dashed grey circles have radiuses of 250, 500 and 1000 m. Dashed grey circles have radiuses of 250, 500 and 1000 m. The 0.1 mm contour is shown in black.

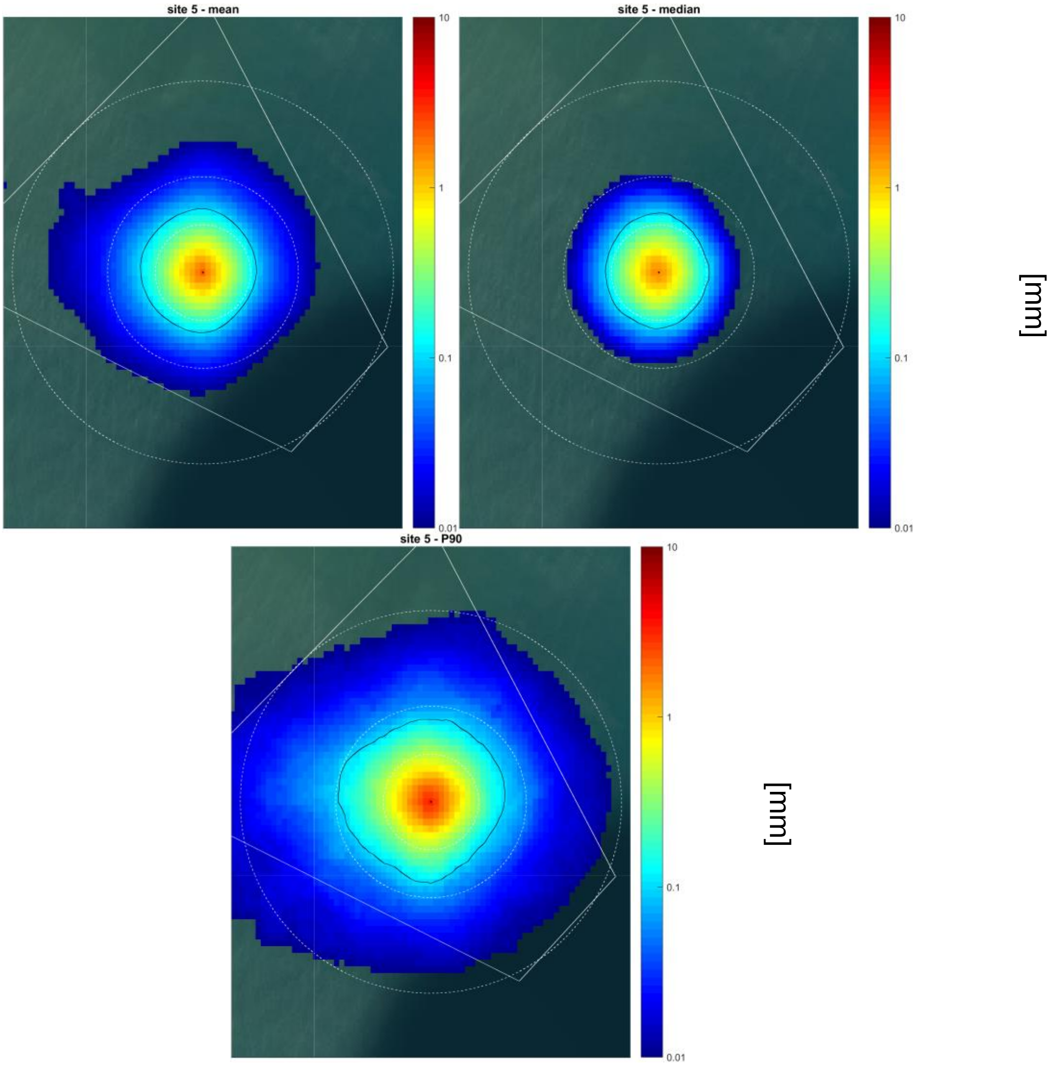

Figure 3.66 Mean, median, and 90th percentile deposition fields for disposal at the centre of the disposal ground using the Albatros vessel (V=1860 m^3) computed for January 2003 (during the El Niño episode). The results assumed a settling velocity of 0.1 $mm.s^{-1}$ for the cohesive sediment class. Dashed grey circles have radiuses of 250, 500 and 1000 m. Dashed grey circles have radiuses of 250, 500 and 1000 m. The 0.1 mm contour is shown in black.

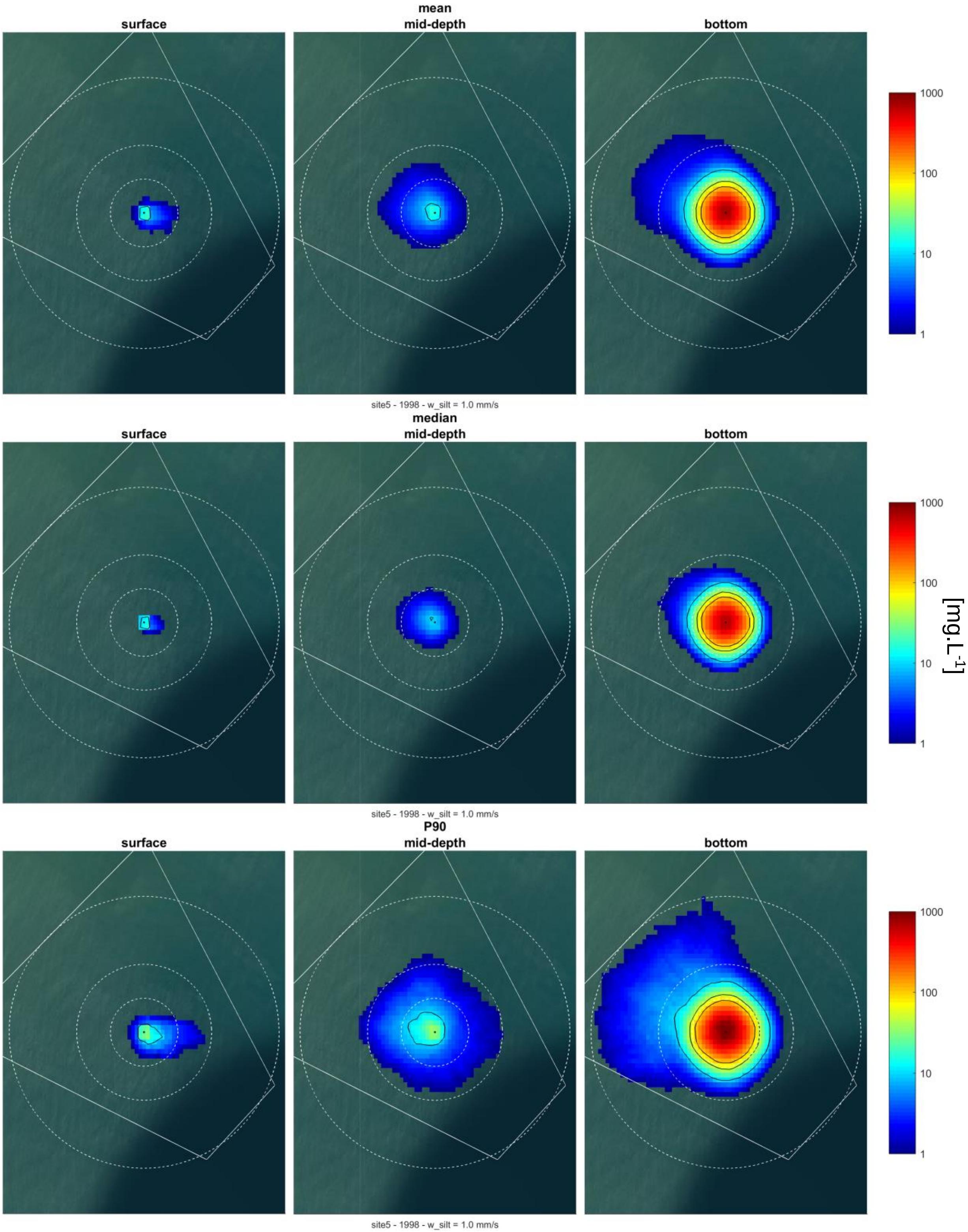

Figure 3.67 Mean, median, and 90th percentile *SSC* fields for disposal at the centre of the disposal ground using the Albatros vessel (V=1860 m^3) computed for July 1998 (during the La Niña episode). The results assumed a settling velocity of 1.0 mm.s^{-1} for the cohesive sediment class. Dashed grey circles have radiuses of 250, 500 and 1000 m. Dashed grey circles have radiuses of 250, 500 and 1000 m. The 10, 50 and 100 mg.L-1 mm contour are shown in black.

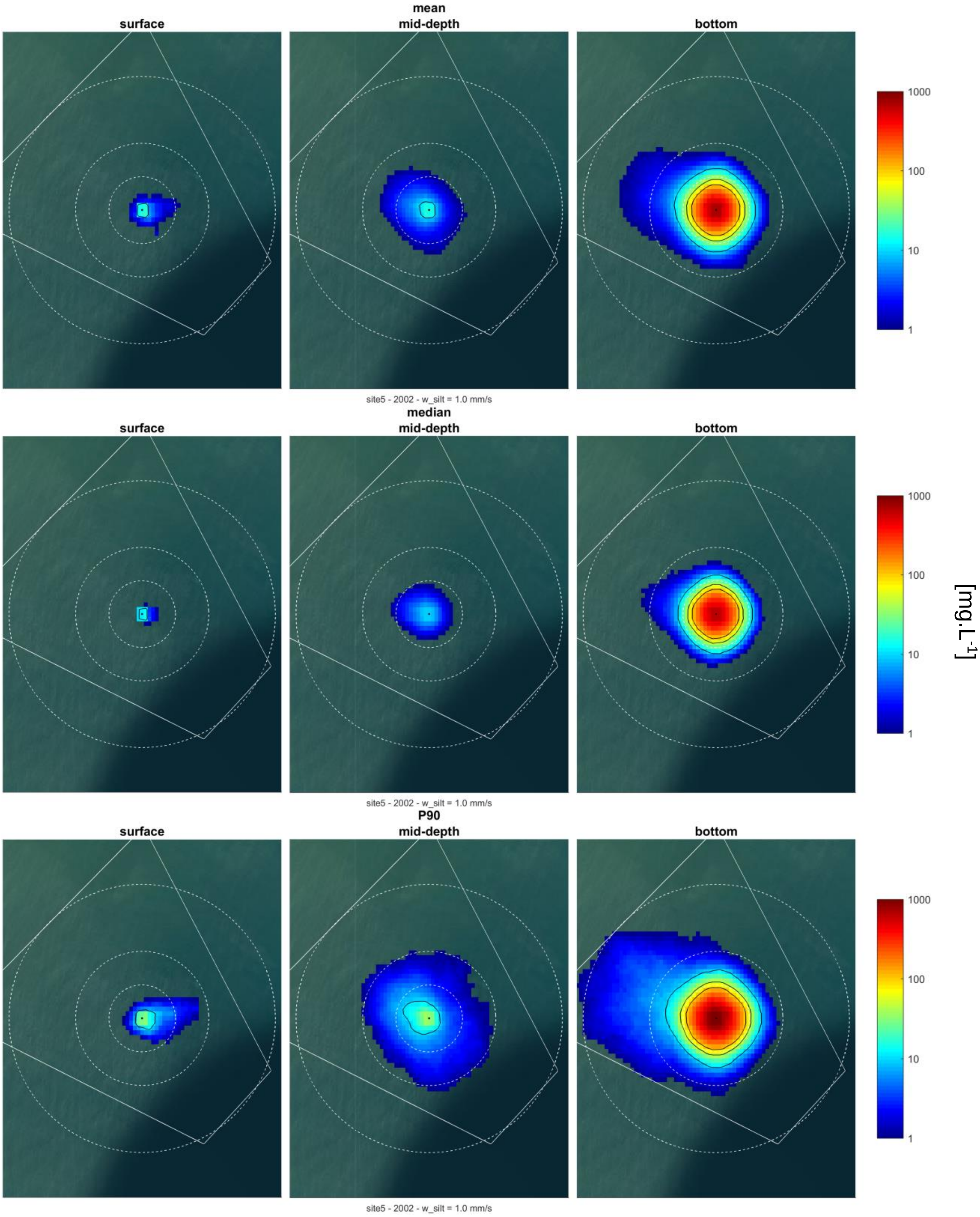

Figure 3.68 Mean, median, and 90th percentile *SSC* fields for disposal at the centre of the disposal ground using the Albatros vessel (V=1860 m^3) computed for July 2002 (during the El Niño episode). The results assumed a settling velocity of 1.0 mm.s^{-1} for the cohesive sediment class. Dashed grey circles have radiuses of 250, 500 and 1000 m. Dashed grey circles have radiuses of 250, 500 and 1000 m. The 10, 50 and 100 mg.L-1 mm contour are shown in black.

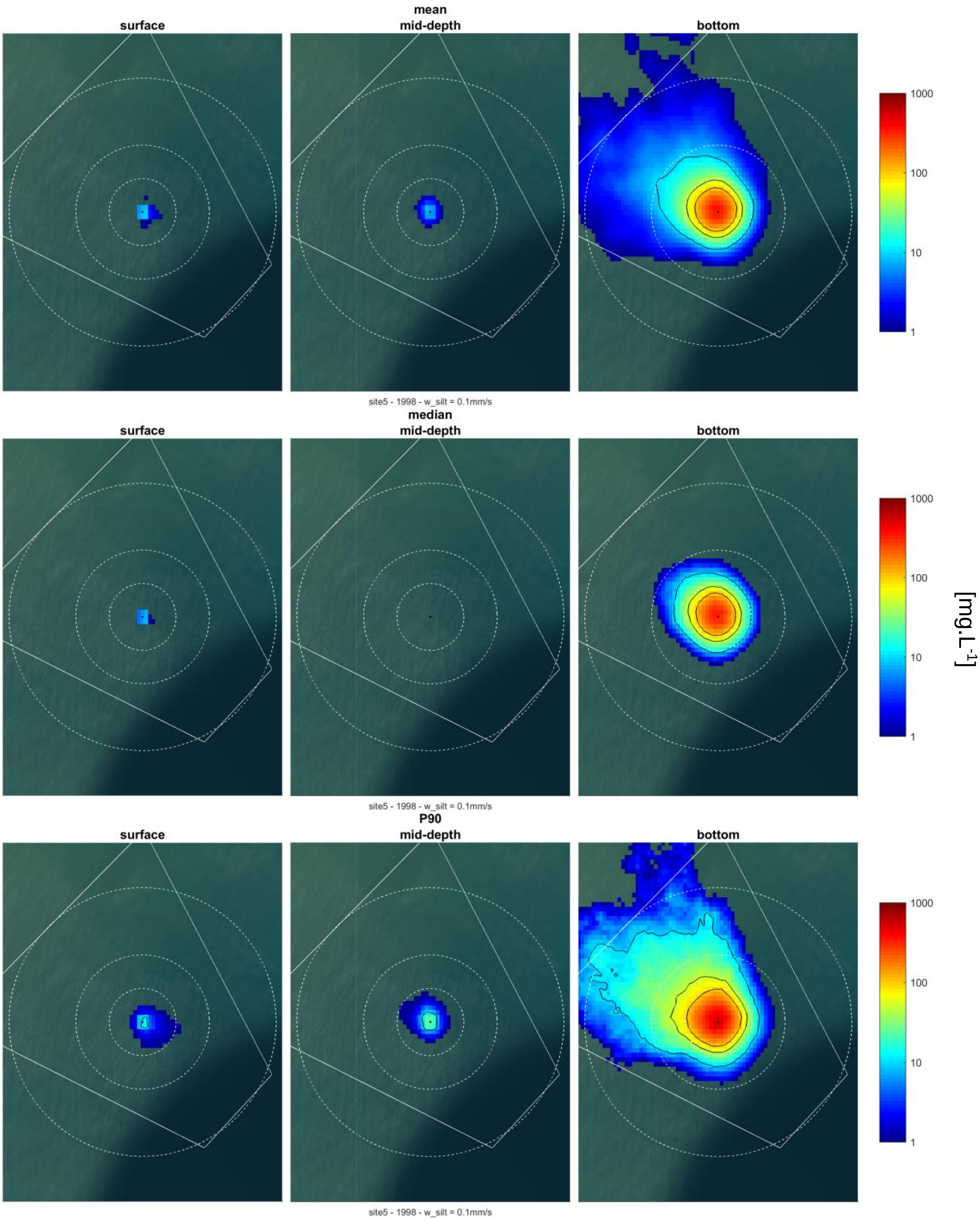

Figure 3.69 Mean, median, and 90th percentile *SSC* fields for disposal at the centre of the disposal ground using the Albatros vessel (V=1860 m^3) computed for July 1998 (during the La Niña episode). The results assumed a settling velocity of 0.1 mm.s^{-1} for the cohesive sediment class. Dashed grey circles have radiuses of 250, 500 and 1000 m. Dashed grey circles have radiuses of 250, 500 and 1000 m. The 10, 50 and 100 mg.L-1 mm contour are shown in black.

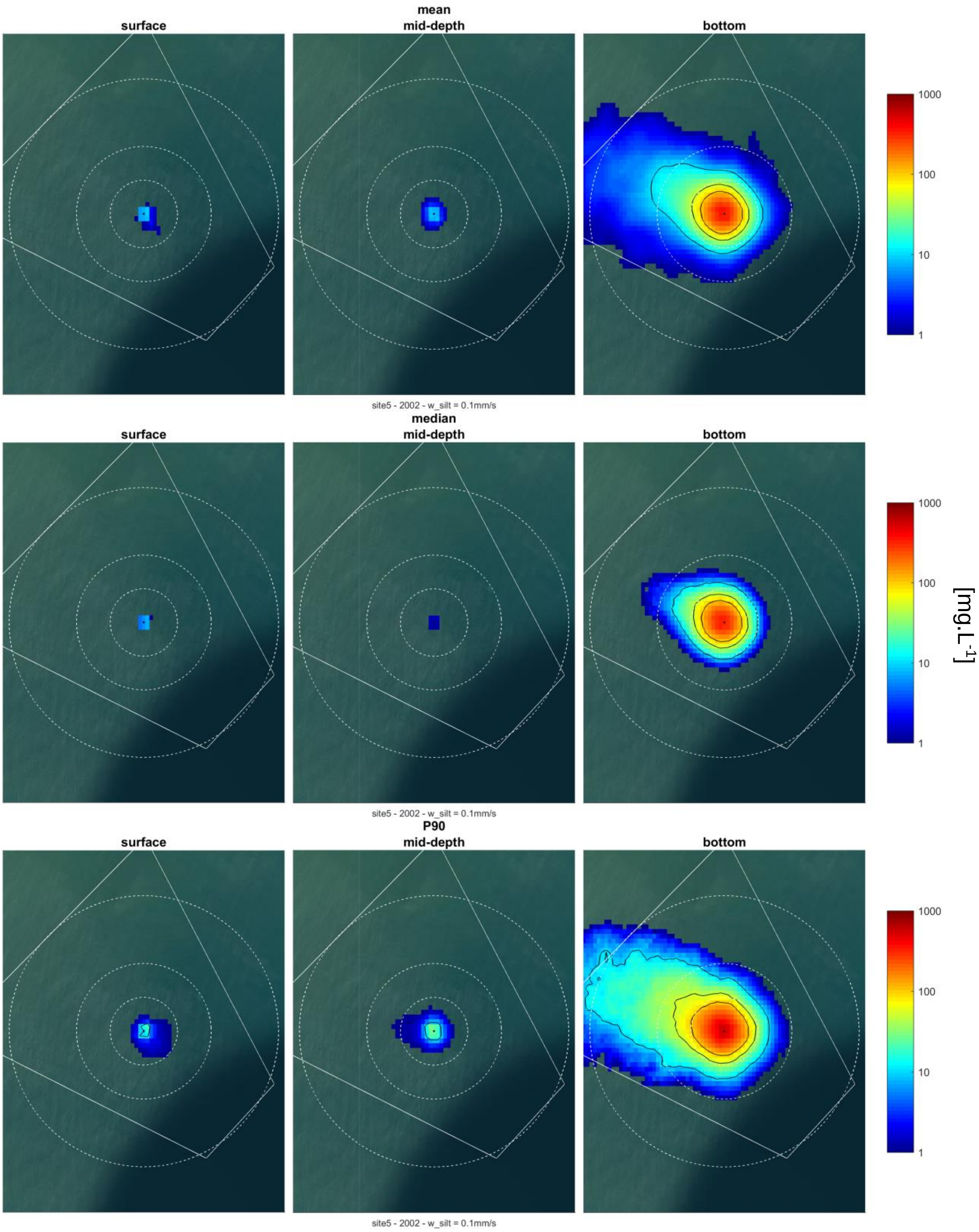

Figure 3.70 Mean, median, and 90th percentile *SSC* fields for disposal at the centre of the disposal ground using the Albatros vessel (V=1860 m^3) computed for July 2002 (during the El Niño episode). The results assumed a settling velocity of 0.1 $mm.s^{-1}$ for the cohesive sediment class. Dashed grey circles have radiuses of 250, 500 and 1000 m. Dashed grey circles have radiuses of 250, 500 and 1000 m. The 10, 50 and 100 mg.L-1 mm contour are shown in black.

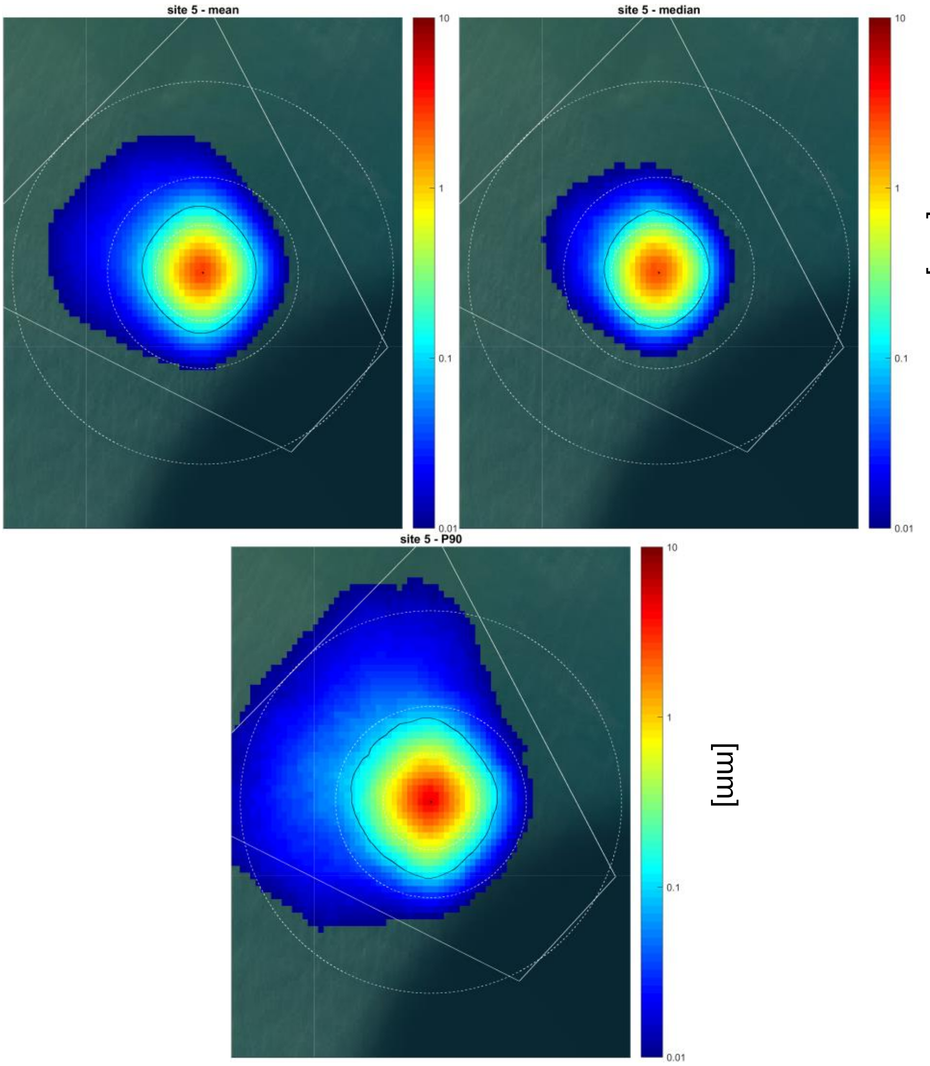

Figure 3.71 Mean, median, and 90th percentile deposition fields for disposal at the centre of the disposal ground using the Albatros vessel (V=1860 m^3) computed for July 1998 (during the La Niña episode). The results assumed a settling velocity of 1.0 mm.s^{-1} for the cohesive sediment class. Dashed grey circles have radiuses of 250, 500 and 1000 m. Dashed grey circles have radiuses of 250, 500 and 1000 m. The 0.1 mm contour is shown in black.

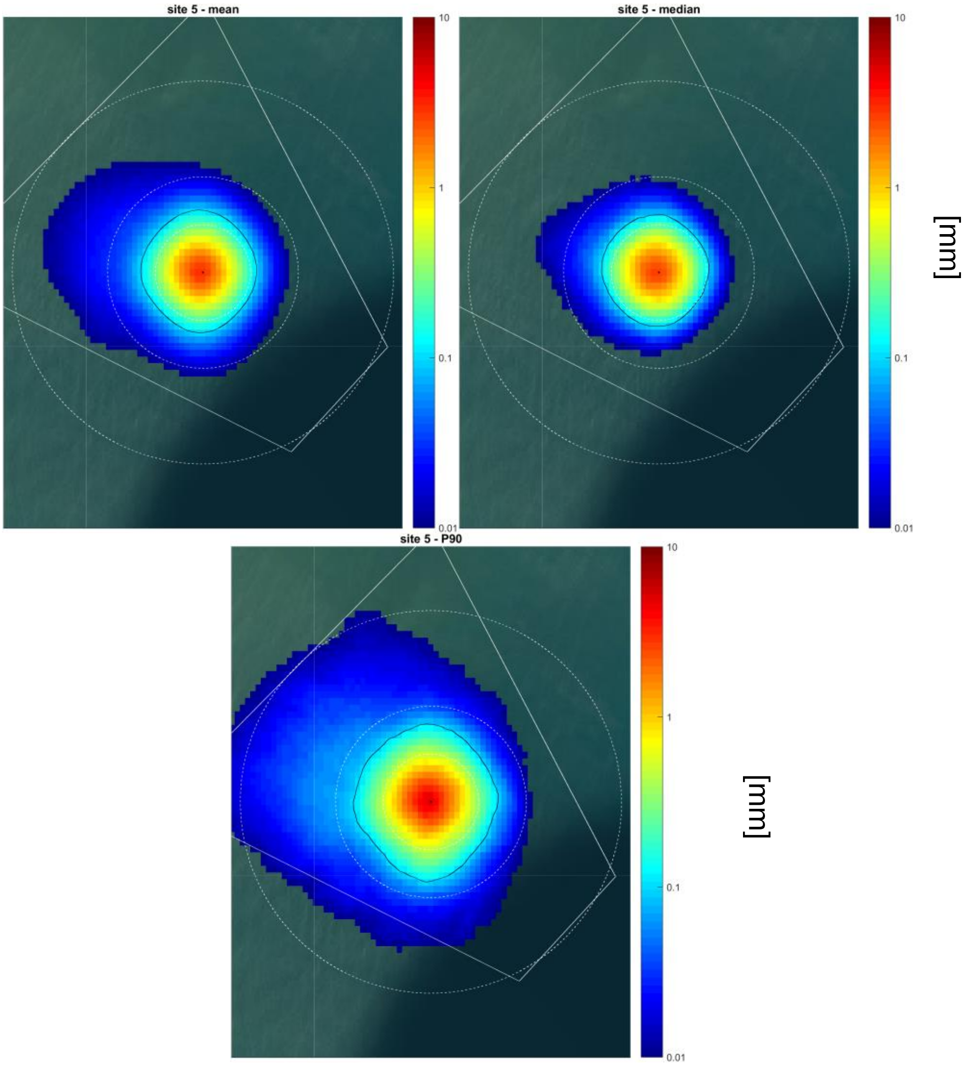

Figure 3.72 Mean, median, and 90th percentile deposition fields for disposal at the centre of the disposal ground using the Albatros vessel (V=1860 m^3) computed for July 2002 (during the El Niño episode). The results assumed a settling velocity of 1.0 $mm.s^{-1}$ for the cohesive sediment class. Dashed grey circles have radiuses of 250, 500 and 1000 m. Dashed grey circles have radiuses of 250, 500 and 1000 m. The 0.1 mm contour is shown in black.

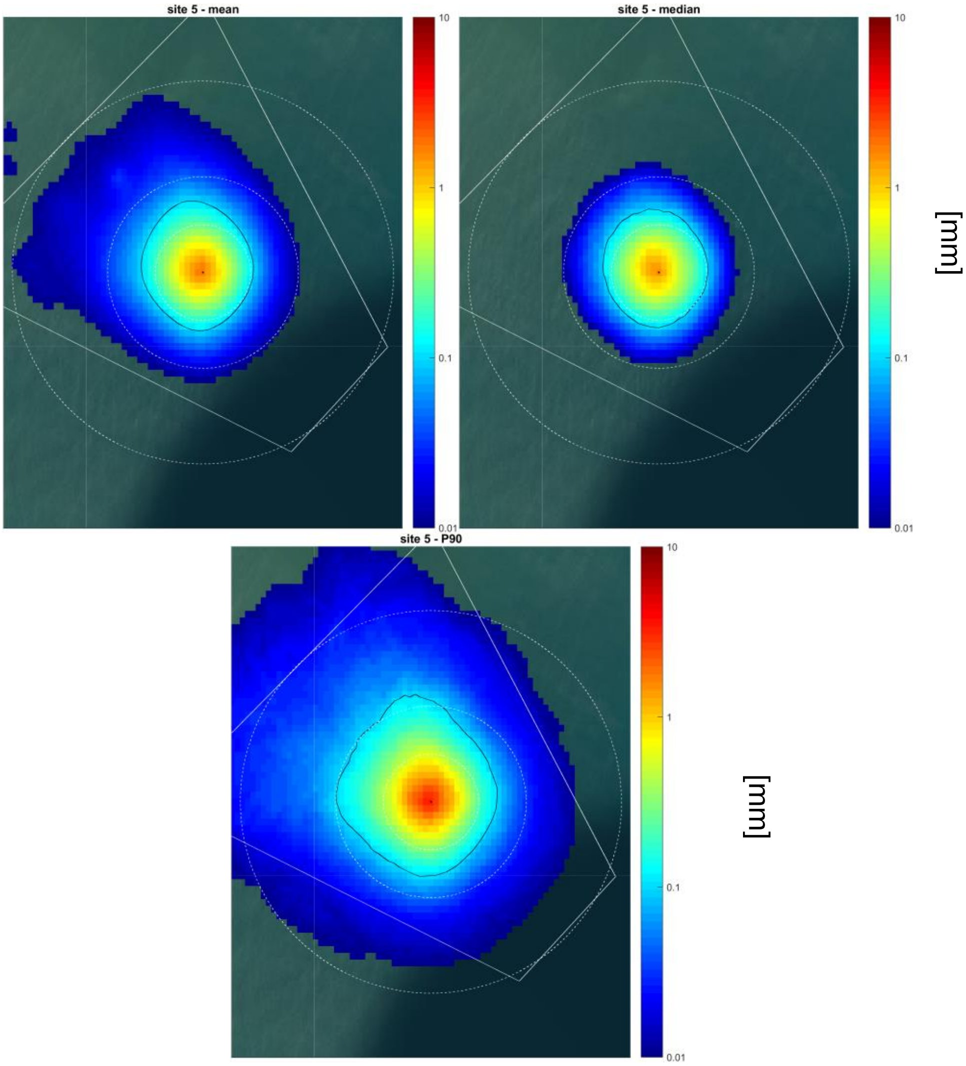

Figure 3.73 Mean, median, and 90th percentile deposition fields for disposal at the centre of the disposal ground using the Albatros vessel (V=1860 m^3) computed for July 1998 (during the La Niña episode). The results assumed a settling velocity of 0.1 mm.s^{-1} for the cohesive sediment class. Dashed grey circles have radiuses of 250, 500 and 1000 m. Dashed grey circles have radiuses of 250, 500 and 1000 m. The 0.1 mm contour is shown in black.

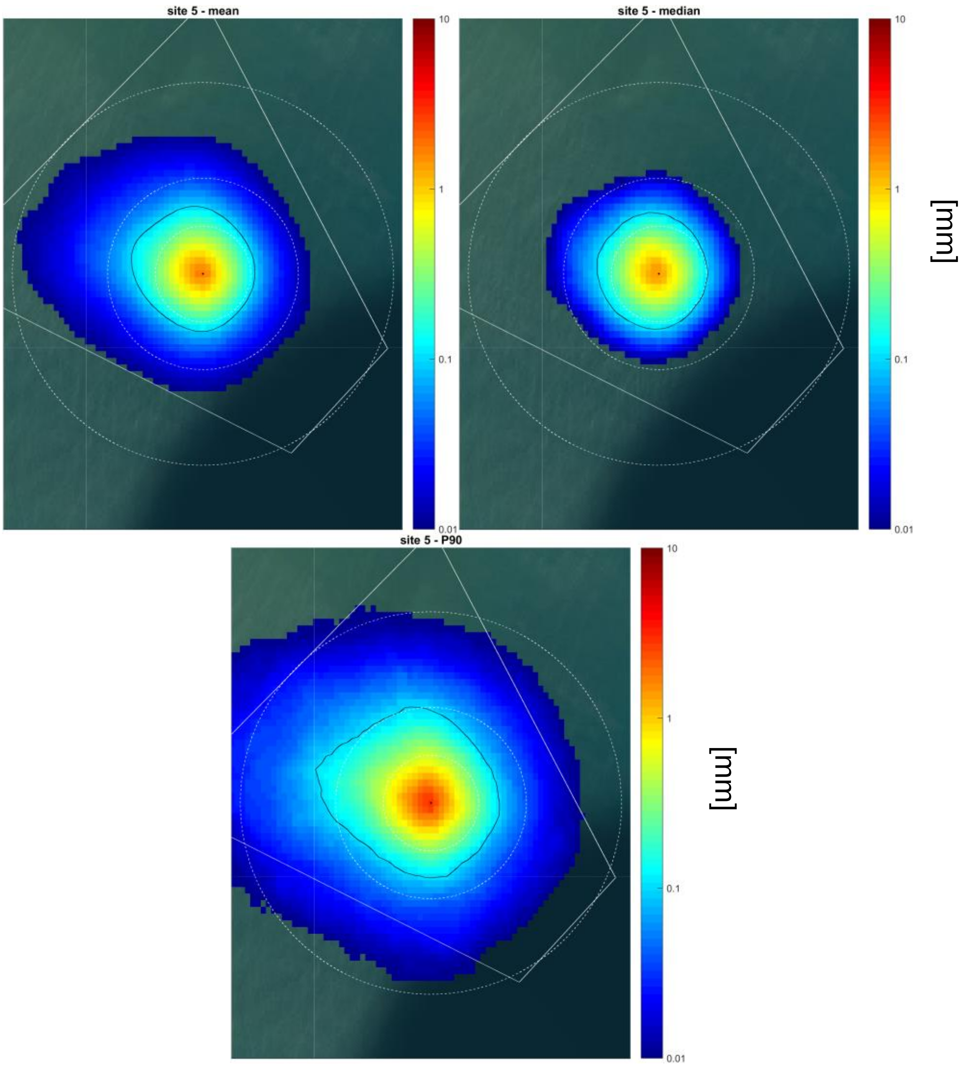

Figure 3.74 Mean, median, and 90th percentile deposition fields for disposal at the centre of the disposal ground using the Albatros vessel (V=1860 m^3) computed for July 2002 (during the El Niño episode). The results assumed a settling velocity of 0.1 mm.s^{-1} for the cohesive sediment class. Dashed grey circles have radiuses of 250, 500 and 1000 m. Dashed grey circles have radiuses of 250, 500 and 1000 m. The 0.1 mm contour is shown in black.

3.5.2. Exceedance time

Exceedance times represent the percentages of time a given *SSC* threshold is exceeded. This is often a useful metric in the context of ecological impact assessment. The exceedance times presented are computed relative to three *SSC* threshold of 10, 50, and 100 $mg.L^{-1}$, and assume a disposal cycle of 4 hours, sustained continuously throughout the 1-month simulations periods. We note that in reality it is most likely that disposal will be discontinued overnight, and disposal is not expected to be repeated at a single location repeatedly; therefore presented results can be considered conservative.

Results for the <u>summer</u> period (January), assuming a settling velocity of 1 $mm.s^{-1}$ for the cohesive sediment, are shown in Figure 3.75 and Figure 3.76 for the La Niña and El Niño context respectively. Results from the simulations using a smaller settling velocity are shown in Figure 3.77 and Figure 3.78. The equivalent results for the winter monthly period (July) are shown in Figure 3.79 to Figure 3.82.

The larger amount of sediment released by the Albatros vessel expectedly raises the percentages of time the considered threshold are exceeded. For example, considering the scenarios using a smaller settling velocity of 0.1 $mm.s^{-1}$, the *visible* footprint of exceedance times in the bottom layer for the smallest *SSC* threshold considered (10$mg.L^{-1}$) expands from a radius of 500 m when operating the Pukunui vessel (Figure 3.41) to ~1000 m when using the Albatros vessel (Figure 3.81).

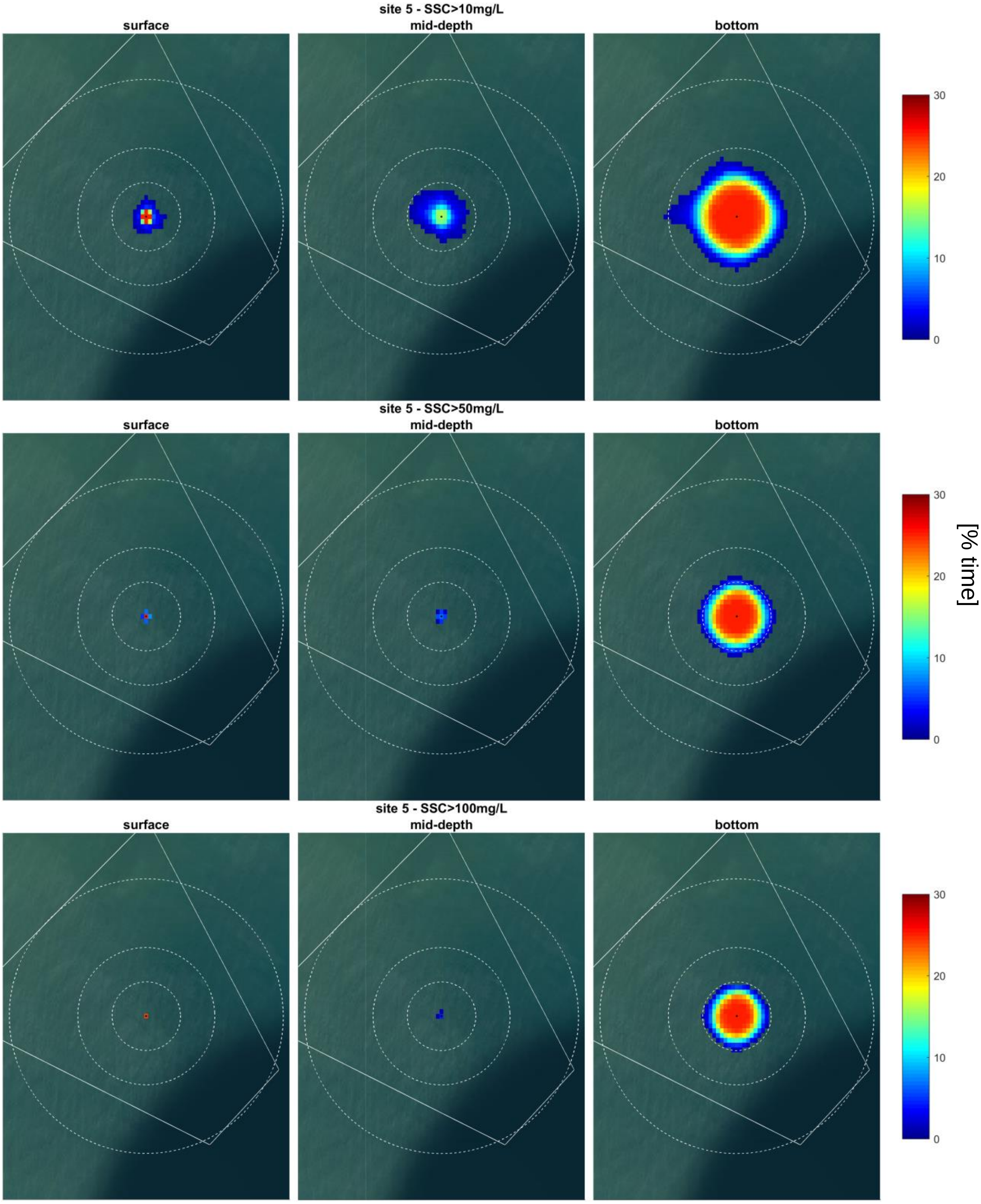

Figure 3.75 *SSC* exceedance for disposal at the centre of the disposal ground using the Albatros vessel (V=1860 m^3) computed for January 1999 (during the La Niña episode), for three *SSC* thresholds, 10, 50 and 100 mg.L^{-1}. The results assumed a settling velocity of 1.0 mm.s^{-1} for the cohesive sediment class. Dashed grey circles have radiuses of 250, 500 and 1000 m. Dashed grey circles have radiuses of 250, 500 and 1000 m.

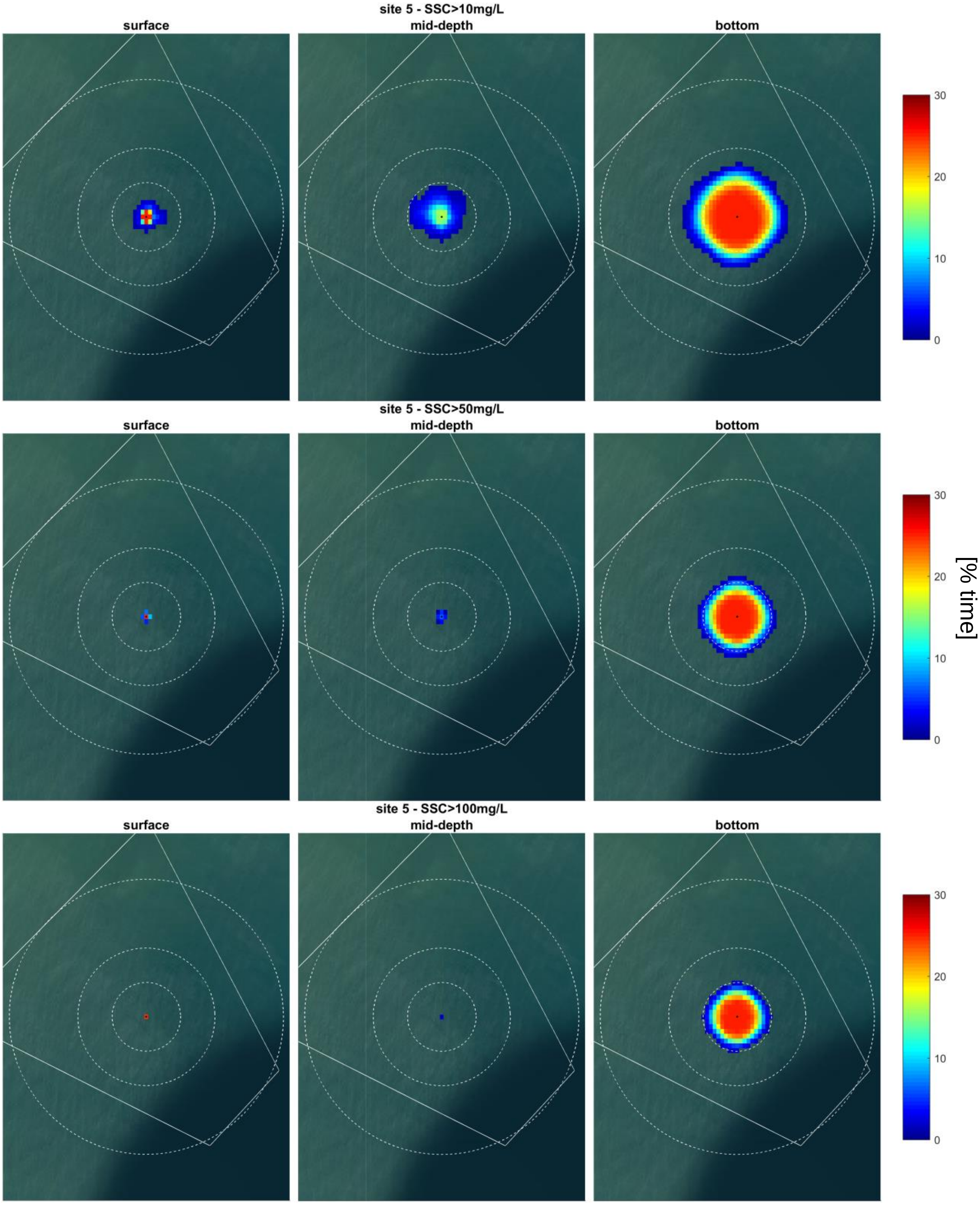

Figure 3.76 *SSC* exceedance for disposal at the centre of the disposal ground using the Pukunui vessel (V=480 m^3) computed for January 2003 (during the El Niño episode) , for three *SSC* thresholds, 10, 50 and 100 mg.L^{-1}. The results assumed a settling velocity of 1.0 mm.s^{-1} for the cohesive sediment class. Dashed grey circles have radiuses of 250, 500 and 1000 m. Dashed grey circles have radiuses of 250, 500 and 1000 m.

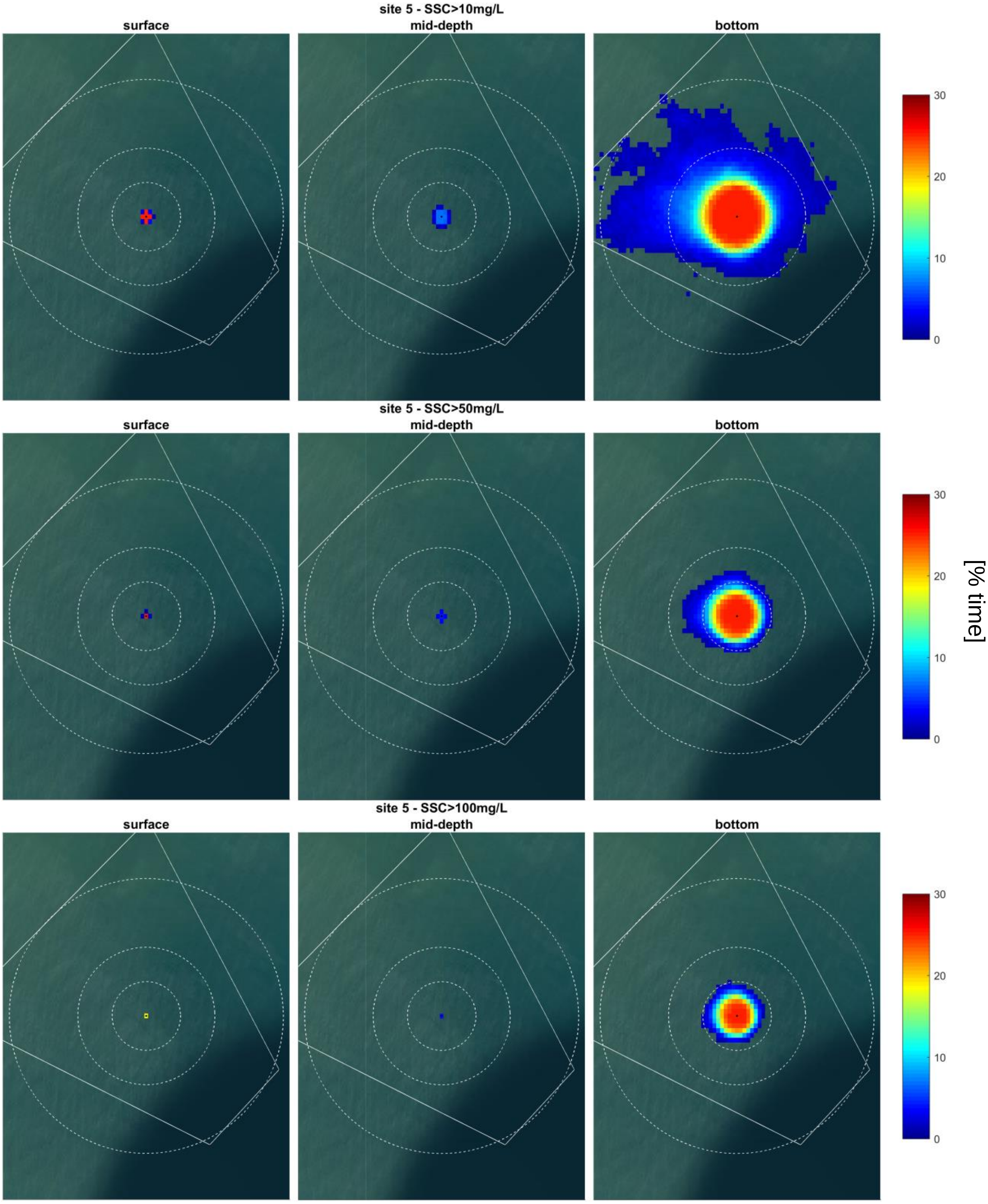

Figure 3.77 *SSC* exceedance for disposal at the centre of the disposal ground using the Albatros vessel (V=1860 m^3) computed for January 1999 (during the La Niña episode) , for three *SSC* thresholds, 10, 50 and 100 $mg.L^{-1}$. The results assumed a settling velocity of 0.1 $mm.s^{-1}$ for the cohesive sediment class. Dashed grey circles have radiuses of 250, 500 and 1000 m. Dashed grey circles have radiuses of 250, 500 and 1000 m.

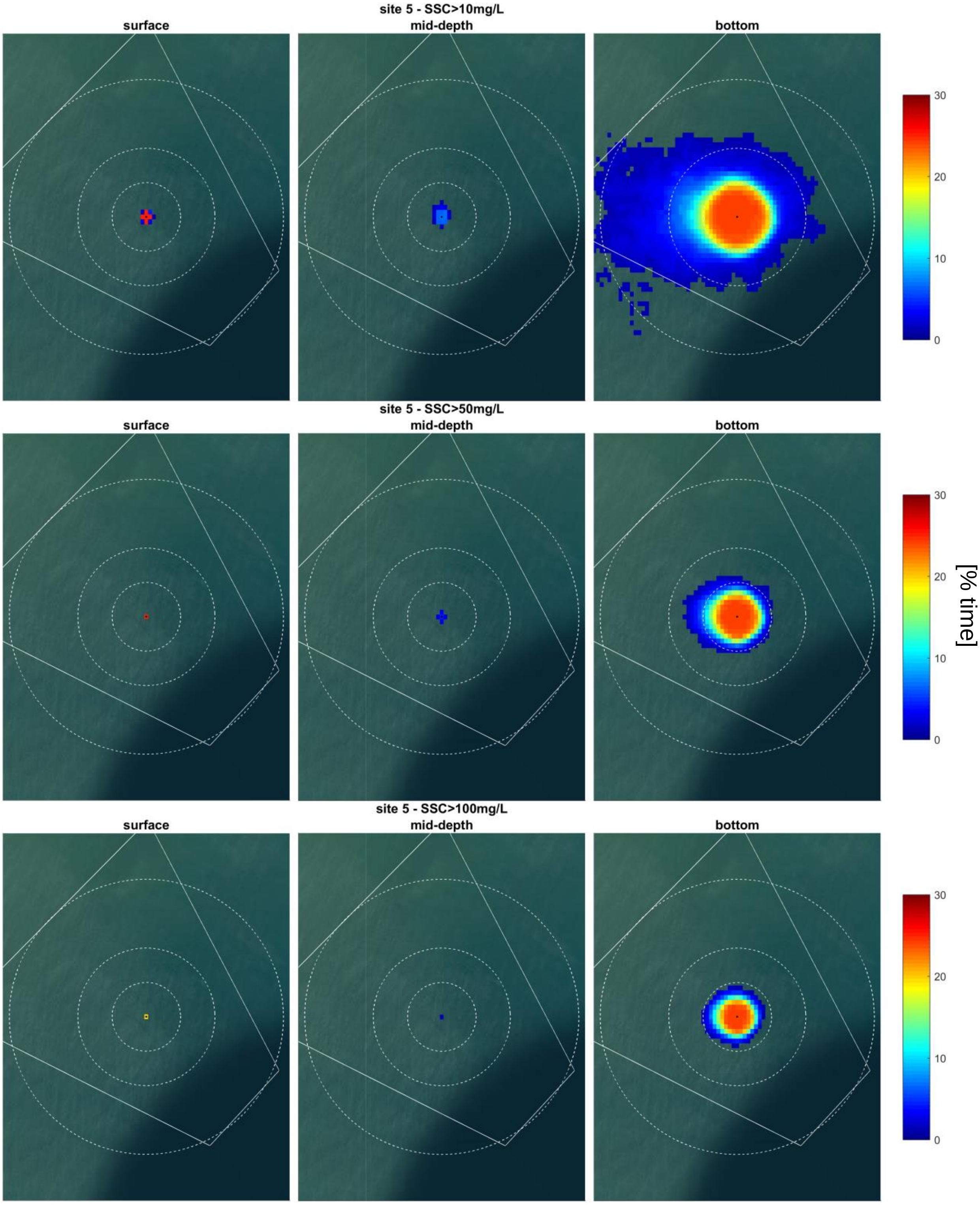

Figure 3.78 *SSC* exceedance for disposal at the centre of the disposal ground using the Albatros vessel (V=1860 m^3) computed for January 2003 (during the El Niño episode) , for three *SSC* thresholds, 10, 50 and 100 mg.L^{-1}. The results assumed a settling velocity of 0.1 mm.s^{-1} for the cohesive sediment class. Dashed grey circles have radiuses of 250, 500 and 1000 m. Dashed grey circles have radiuses of 250, 500 and 1000 m.

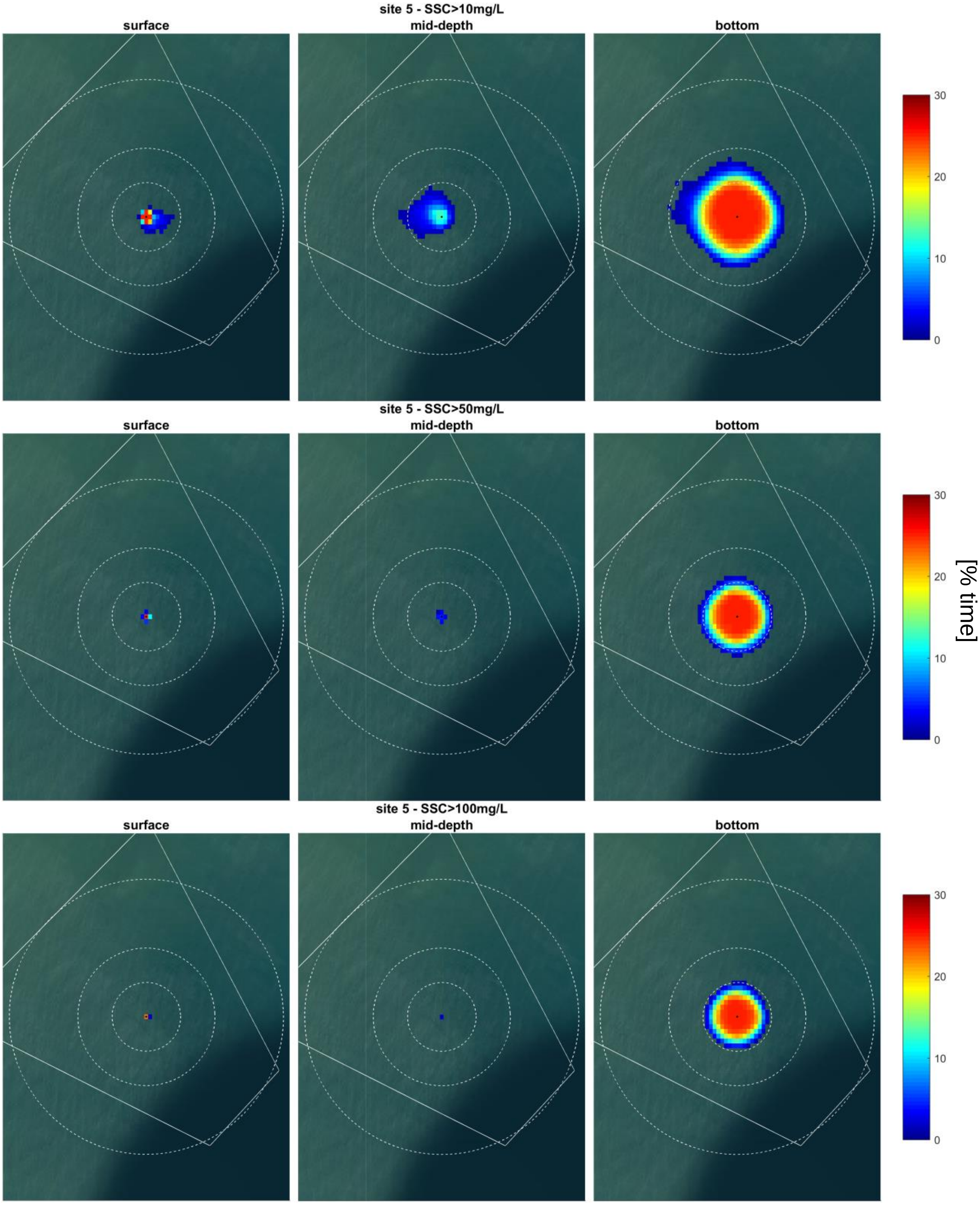

Figure 3.79 *SSC* exceedance for disposal at the centre of the disposal ground using the Albatros vessel (V=1860 m^3) computed for July 1998 (during the La Niña episode), for three *SSC* thresholds, 10, 50 and 100 mg.L^{-1}. The results assumed a settling velocity of 1.0 mm.s^{-1} for the cohesive sediment class. Dashed grey circles have radiuses of 250, 500 and 1000 m. Dashed grey circles have radiuses of 250, 500 and 1000 m.

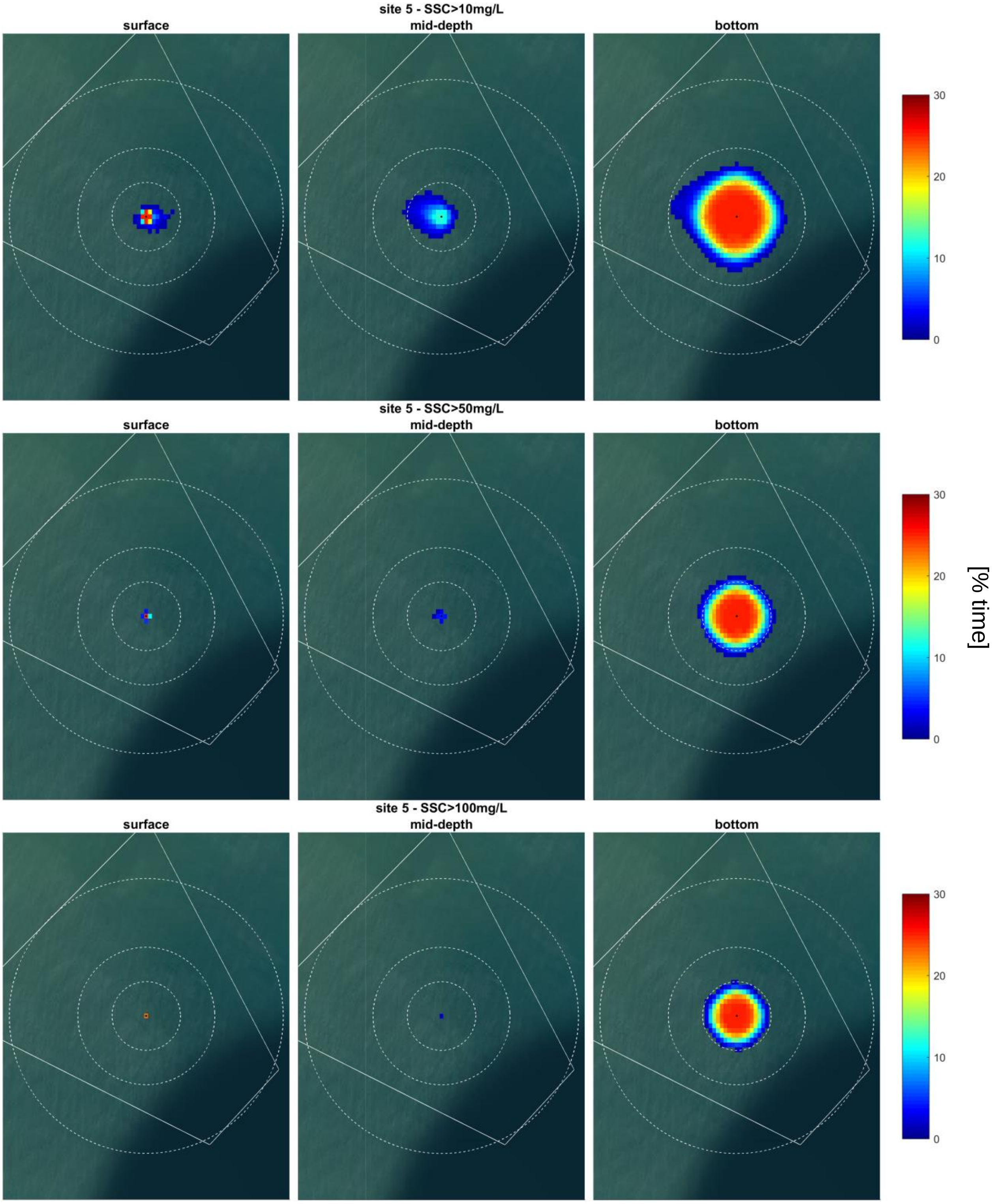

Figure 3.80 *SSC* exceedance for disposal at the centre of the disposal ground using the Albatros vessel (V=1860 m^3) computed for July 2002 (during the El Niño episode), for three *SSC* thresholds, 10, 50 and 100 $mg.L^{-1}$. The results assumed a settling velocity of 1.0 $mm.s^{-1}$ for the cohesive sediment class. Dashed grey circles have radiuses of 250, 500 and 1000 m. Dashed grey circles have radiuses of 250, 500 and 1000 m.

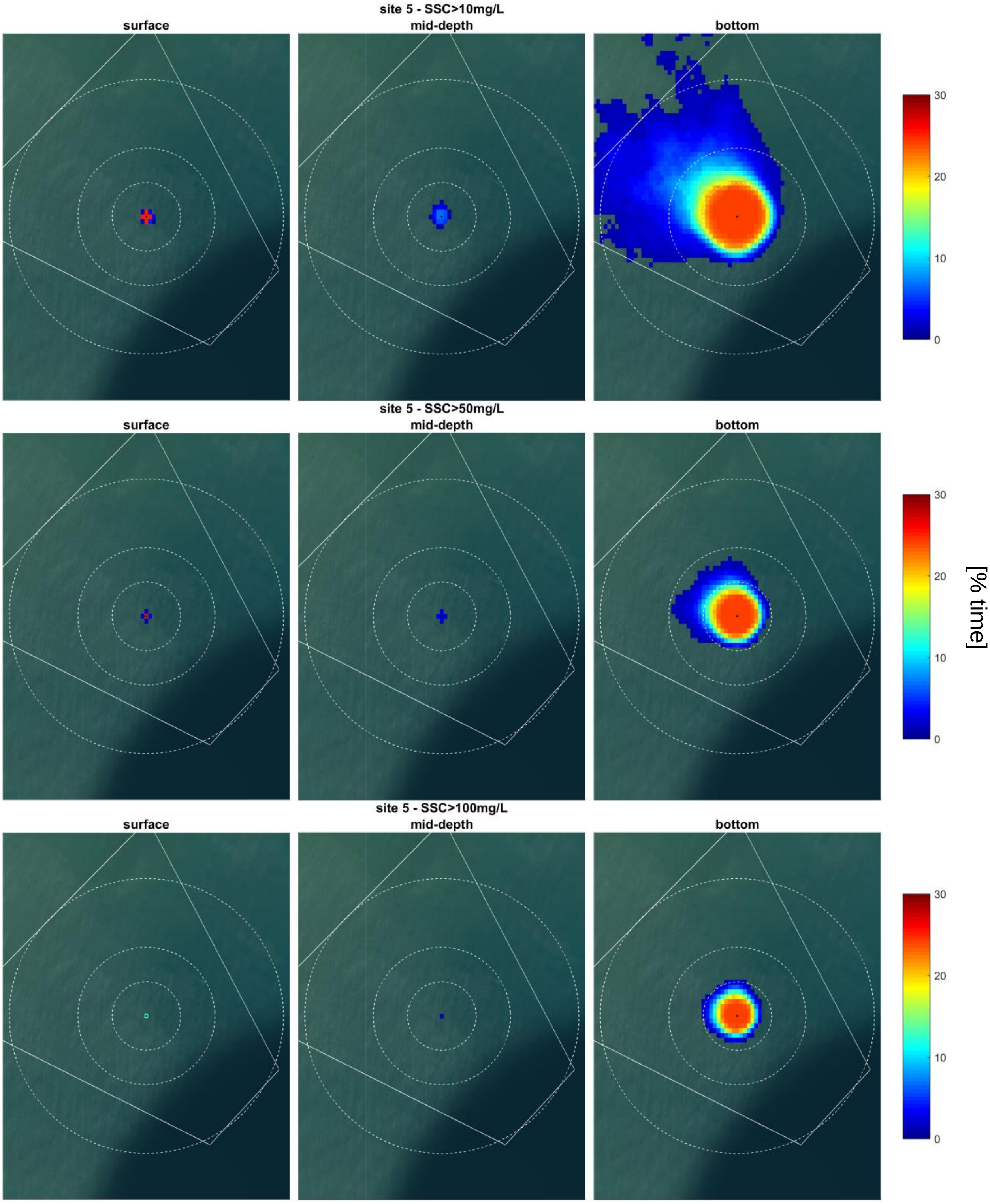

Figure 3.81 *SSC* exceedance for disposal at the centre of the disposal ground using the Albatros vessel (V=1860 m^3) computed for July 1998 (during the La Niña episode) , for three *SSC* thresholds, 10, 50 and 100 mg.L^{-1}. The results assumed a settling velocity of 0.1 mm.s^{-1} for the cohesive sediment class. Dashed grey circles have radiuses of 250, 500 and 1000 m. Dashed grey circles have radiuses of 250, 500 and 1000 m.

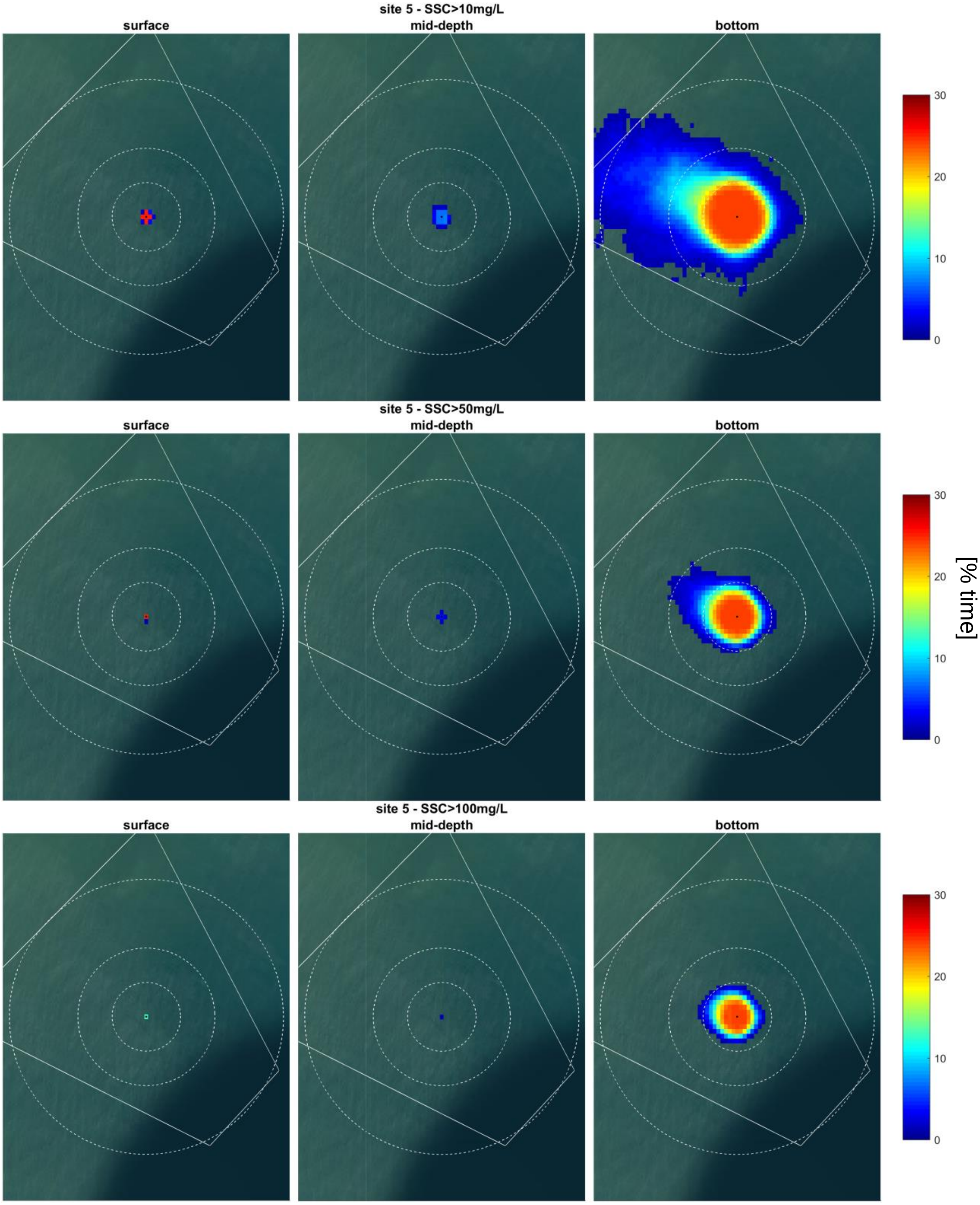

Figure 3.82 *SSC* exceedance for disposal at the centre of the disposal ground using the Albatros vessel (V=1860 m^3) computed for July 2002 (during the El Niño episode) , for three *SSC* thresholds, 10, 50 and 100 $mg.L^{-1}$. The results assumed a settling velocity of 0.1 $mm.s^{-1}$ for the cohesive sediment class. Dashed grey circles have radiuses of 250, 500 and 1000 m. Dashed grey circles have radiuses of 250, 500 and 1000 m.

4. SUMMARY

The objective of the present report is to characterise the dispersion patterns of the sediment plumes and deposition footprints produced during the disposal of sediment dredged from the channel and port basins.

Sediment plume dispersal and settling was simulated using particle-tracking simulations during two different 1-year periods with contrasting historical climatic contexts, namely El Niño/La Niña episodes. The disposal operations are simulated in the particle-tracking model using different source terms representing processes by which sediment is suspended into the water column, where they become subject to advection and diffusion by the ambient current forcing i.e. passive plume. This includes sediment de-entrainment from the dense dynamic plume descending to the seabed immediately after the hopper door opens, as well as sediment suspended through the formation of a density current following dynamic plume collapse on the seabed. Two different vessels with different hopper capacities are considered; i.e. the Pukunui (V= 480 m^3) and Albatros TSHD (V=1860 m^3).

Given the uncertainties associated with the effective timing of the operations, as well as the in-situ characteristics of the disposed sediment, a probabilistic approach was followed whereby the long-term annual simulations are post processed to provide robust statistical metrics on the *SSC* plume dispersion and expected depositional thicknesses. For sensitivity purposes, two different sediment settling velocity were considered for the cohesive fraction to account for uncertainties in the flocculation effects.

The general *SSC* plume pattern consists of relatively contained *SSC* plume in the surface and mid-depth layers, becoming more dispersed (radius of order ~200 m) in the bottom layer due to the formation of a density current. Predicted deposition patterns are predominantly circular, with thinner northwest-directed features resulting from the deposition of the passive plumes. Predictions for the Pukunui vessel (hopper volume = 480 m^3) suggest *SSC* levels will generally fall below the 10 $mg.L^{-1}$ threshold within 0-50 m of the release in the surface and mid-depth levels and within 150 m of the release in the bottom levels. Predictions for the Albatros vessel (hopper volume = 1860 m^3) suggest *SSC* levels will generally fall below the 10 $mg.L^{-1}$ threshold within 50-200 of the release in the surface and mid-depth levels and within 250 m of the release in the bottom levels.

5. REFERENCES

Aarninkhof, S., Luijendijk, A., 2010. Safe disposal of dredged material in an environmentally sensitive environment.

Beamsley, B.J., 2003. Nearshore sediment dynamics in a mixed sand/mud environment (D Phil Earth Sciences). University of Waikato, Hamilton, N.Z.

Bellasio, R., Bianconi,R, Mosca, S., Zannetti, P., 2017. Formulation of the Lagrangian particle model LAPMOD and its evaluation against Kincaid SF6 and SO2 datasets. Atmos. Environ. 163, 87–98.

Bokuniewicz, H., Gordon, R, 1980. Deposition of dredged sediment at open water sites. Estuar. Coast. Mar. Sci. 10(3), 289–303.

Bokuniewicz, H. J., Gilbert, J., Gordon, R. B., Higgins, J. L., Kaminsky, P., Pilbeam, C. C., et al., 1978. Field study of the mechanics of the placement of dredged material at open-water disposal sites (No. D-78-7). US Army Engineer Waterways Experiment Station., Vicksburg, MS.

Botev, Z. I, Grotowski, J. F, Kroese, D.P, 2010. Kernel density estimation via diffusion. Ann. Stat. 38, 2916–2957.

De Haan, P., 1999. On the use of density kernels for concentration estimations within particle and puff dispersion models. Atmos. Environ. 33, 2007–2021.

Drapeau G., Lavallee D., Dumais J.F., Walsh G., 1992. Dispersion model of dredge spoil dumped in coastal waters. Presented at the International Conference on Coastal Engineering 1992, American Society of Civil Engineers, New York., Venice, Italy, pp. 3054–3067.

Elder, J.W., 1956. The dispersion of marked fluid in turbulent shear flow. J. Fluid Mech. 5, 544–560.

Fischer, H.B., Koh, R.C.Y., Imberger, J., Brooks, N.H., 1979. Mixing in Inland and Coastal Waters. Academic Press, San Diego, Califonia USA.

Gordon, R., 1974. Dispersion of dredge spoil dumped in near-shore waters. Estuar. Coast. Mar. Sci. 2, 349–358.

HR Wallingford, 2010. TASS Software - Trailer suction hopper dredger, User guide for TASS version 3.2.1. Report prepared by HR Wallingford for the EcoShape Projcct (No. Rev. 7).

Lee J.H., Cheung V., 1990. GENERALIZED LAGRANGIAN MODEL FOR BUOYANT JETS IN CURRENT. J. Environ. Eng. 116, 1085–1106.

MetOcean Solutions, 2017. Eastland Port Maintenance Dredging and Disposal Project. Hydrodynamic hindcast validation (No. P0331- 01).

MetOcean Solutions Ltd., 2016. LYTTELTON HARBOUR/WHAKARAUPŌ CHANNEL DEEPENING PROJECT. Simulations of suspended sediment plumes and associated deposition from offshore disposal (Technical report prepared for Lyttelton Port Company Limited No. P0201- 02).

Okubo, A., 1971. Oceanic diffusion diagrams. Deep-Sea Res. 18, 789–802.

Silverman, B.W, 1986. Density Estimation for Statistics and Data Analysis, Chapman and Hall Ltd. ed. London.

Smith, S.J., Friedrichs, C.T., 2011. Size and settling velocities of cohesive flocs and suspended sediment aggregates in a trailing suction hopper dredge plume. Cont. Shelf Res., Proceedings of the 9th International Conference on Nearshore and Estuarine Cohesive Sediment Transport Processes 31, S50–S63. https://doi.org/10.1016/j.csr.2010.04.002

Spearman, J., Bray, R.N., Land, J., Burt, T.N., Mead, C.T., Scott, D., 2007. Plume dispersion modelling using dynamic representation of trailer dredger source terms, in: J.P.-Y. Maa, L.P.S. and D.H.S. (Ed.), Proceedings in Marine Science, Estuarine and Coastal Fine Sediments DynamicsIntercoh 2003. Elsevier, pp. 417–448.

Truitt, C., 1988. Dredged Material Behavior During Open-Water Disposal. J. Coast. Res. 4, 489–497.

USACE-EPA, 1998. Evaluation of Dredged Material Proposed For Discharge in Waters of the U.S. - Testing Manual. Enviroment Protection Agency and and United States Army Corps of Engineers, Washington.

Van Rijn, L.C., 2007. A unified view of sediment transport by current and waves, Part II. J. Hydraul. Eng. ASCE.

Vitali, L., Monforti, F., Bellasio, R., Bianconi, R., Sachero, V., Mosca, S., Zanini, G., 2006. Validation of a Lagrangian dispersion model implementing different kernel methods for density reconstruction. Atmos. Environ. 40, 8020–8033.

Whitehouse R., Soulsby R., Robert W., Mitchener H., 2000. Dynamics of estuarine muds, Thomas Telford, London. ed.

Zhang, Y.J., Ateljevich, E., Yu, H.-C., Wu, C.H., Jason, C.S., 2015. A new vertical coordinate system for a 3D unstructured-grid model. Ocean Model. 85, 16–31.

Zhang, Y.L., Baptista, A.M., 2008. A semi-implicit Eulerian-Lagrangian finite element model for cross-scale ocean circulation. Ocean Model. 21, 71–96.